LAND AND WATER
www.csiro.au

Groundwater contamination risks from conventional gas in the southeast SA: Pathways, vulnerability and modelling analysis

David Rassam, J Sreekanth, Dennis Gonzalez, Dirk Mallants, Rebecca Doble

27 May 2020

GISERA

Citation

David Rassam, J Sreekanth, Dennis Gonzalez, Dirk Mallants, Rebecca Doble (2020) Groundwater contamination risks from conventional gas in the southeast SA: Pathways, vulnerability and modelling analysis, CSIRO Land and Water.

Copyright

Important disclaimer

Contents

Figures

Tables

Acknowledgments

The authors acknowledge the funding provided by the CSIRO Gas Industry Social and Environmental Research Alliance (GISERA) for undertaking this study. We acknowledge the South Australia Department of Energy and Mining (SA DEM) for providing support and advice in designing the scenarios analysed in this study for contamination risk assessment. We acknowledge SA Department of Environment and Water for the provision of the regional scale groundwater model, pertaining data sets for the child model used in this study. We also acknowledge the co-operation of Beach Energy in this study by providing relevant data and reports from their EIS studies. Representatives from SA DEM, DEW, Beach Energy, CSIRO Energy, CSIRO Land and Water contributed to the initial stakeholder workshop of this study and their contributions are also greatly acknowledged.

Executive summary

An onshore conventional gas drilling program is being undertaken in the Otway Basin near the Penola area, southeast of South Australia. Conventional gas development involves activities and substances that can potentially lead to groundwater contamination due to incidents and through various pathways. This study, which was commissioned by the Gas Industry Social and Environmental Research Alliance (GISERA), employed spatial and process modelling tools to evaluate the likelihood of potential contamination of groundwater resources and receptors associated with the likely causal pathways for three conventional gas wells, namely, Haselgrove 4, Nangwarry 1 and Dombey 1, located around the Penola region.

Independent of the causal pathways and hazards, the physiography and groundwater system characteristics affect groundwater vulnerability to contamination. We used 6 different physiographic and groundwater characteristics to estimate the vulnerability of groundwater in the vicinity of the three gas wells under consideration. The distribution of water-dependent risk receptors in these areas is an important factor that determines the level of contamination risk; hence, an asset density analysis was undertaken. The analysis has indicated that a contamination risk assessment using flow and transport modelling was warranted, given the presences of relatively high vulnerability areas within the region due to shallow water table and other confounding factors. The vulnerability was deemed to be relatively low around areas north of the Haselgrove 4 gas well, moderate to high around the Dombey 1 gas well, and relatively high in areas around the Nangwarry 1 gas well. It is important to note that groundwater vulnerability as quantified using this approach represented the relative sensitivity of areas based on the natural physiographic factors and thus was not indicative of contamination risk from any specific point, or non-point source.

The contamination risk was explicitly quantified by considering three plausible contamination scenarios: (1) leakage from a drilling sump liner, (2) compromised well integrity, and (3) spills. Scenarios (1) and (3) are broadly classified as surface-based pathways that relate to contaminations associated with surface handling and storage of drilling fluid and/or other contaminants; they involve the risk of contaminants migrating through the unsaturated and saturated zones before potential interception with water-dependent receptors. On the other hand, Scenario (3) is a deep groundwater pathway that relates to accidental release of materials directly into the aquifer as a result of well-integrity loss that may lead to leakage of small volumes of fluids through the micro-annulus developed between cement and casing/formation. For each scenario, water flow and solute transport modelling was carried out to estimate peak concentrations at risk receptors reported as a fraction of the input concentration at the source. A coupled modelling approach was adopted with the flow path segmented into two stages to model flow and transport processes in the unsaturated and saturated zones, respectively. A one-dimensional numerical model was used to simulate flow and solute transport in the unsaturated zone to define a time-series of solute flux at the aquifer interface. An analytical one-dimensional solution for solute transport under steady state flow was used to estimate peak concentrations at locations where groundwater dependent receptors intercept the flow path. The analytical solution requires prior knowledge of the flow path length and the flow rate. The particle tracking program MODPATH was used to identify all plausible travel paths (tracks) starting from the three gas well

sites considered in this study. A spatial analysis identified groundwater dependent receptors that can potentially intercept these tracks, subsequently, the length of each individual track and the flow rate along it was defined.

This novel coupled modelling approach is conducive to implementing a Monte-Carlo simulation framework to probabilistically estimate concentrations without the need to run computationally complex three-dimensional contaminant transport models. The probabilistic modelling approach accounted for uncertainties along the entire flow path from source to receptor. Flow and solute transport parameters such as hydraulic conductivity, dispersion and attenuation coefficients were sampled from plausible ranges reported in the literature and were further constrained by model calibration where possible. The stochastic model runs were then used to simulate the relative concentration changes at risk receptors groundwater bores and surface water courses given a unit solute concentration is released into the unsaturated or saturated zone corresponding to the three scenarios considered. The key findings for the three scenarios are provided in the following:

Scenario 1 (leakage from a drilling sump liner): Coupled unsaturated-saturated solute transport modelling for the Dombey 1 site has shown a significant reduction in solute concentration along the flow path towards receptor locations. Analyses of the stochastic modelling results shows that it is highly likely that the maximum concentration at any receptor location would be less than 1% of the concentration at the source (drilling sump). This is deduced from the stochastic simulations which showed that 91.2% and 79.8% of the simulations had concentration of less than 1% of the input concentration with and without solute degradation, respectively. The highest concentrations (close to 1% of the input) are predicted at receptors in the proximity of the gas wells. Receptors located farther away from the facilities would have much lesser or zero concentrations. Coupled unsaturated-saturated solute transport modelling for Haselgrove 4 site has shown a similar reduction in solute concentration. In this case, analyses of the stochastic modelling results has shown that 91.6% and 85.7% of the simulations had concentration of less than 1% of the input concentration with and without solute degradation, respectively. The Haselgrove 4 site exhibited slightly higher maximal concentrations due to a closer proximity to one receptor bore compared to Dombey 1. The spatial analysis for Nangwarry 1 well has shown that the closest bore that intersected with the particle tracks was more than four kilometres away. Based on the very low concentrations for the Dombey 1 well at such distances, no further analysis was deemed necessary for this and the other scenarios.

Scenario 2a (compromised well integrity): Analyses of the stochastic modelling results for Dombey 1 well for this scenario has shown that with solute degradation, 87.9% of the simulations had maximum concentration of less than 1% of the input concentration; without solute degradation, 73.5% of the simulations had maximum concentration of less than 5% of the input concentration. Analyses of the stochastic modelling results for the Haselgrove 4 well for this scenario has shown that with solute degradation, 84% of the simulations had concentration of less than 1% of the input concentration; without solute degradation, 68.8% of the simulations had concentration of less than 5% of the input concentration. The Haselgrove 4 site exhibited higher maximal concentrations due to a groundwater receptor bore that is located very close (88 m) from the gas well was considered in the analysis. The concentrations at receptors farther from the gas well would be much smaller.

Scenarios 3a (surface spill) and 3b (subsurface flow line leakage): Unsaturated flow and transport modelling for both scenarios has shown that when a unit concentration is applied at the source, solute concentrations observed at the water table interphase were equal to 0.0017 and 0.0028, for scenarios 3a and 3b, respectively. This attributable to the dilution effect of rainwater infiltrating the exposed soil surface. Hence, further modelling in the saturated zone was deemed unnecessary.

The probabilistic modelling presented here has shown that it is very unlikely that plausible contamination events would result in high contaminant concentrations at groundwater receptors in the vicinity of the gas development considered in this study. This modelling approach enables the regulator to quantify the residual contamination given any concentration of contaminant at the source; the results presented here were based on an initial unit concentration at the source and can be linearly scaled by any other input concentration.

This generic approach has potential applicability in informing regulatory and management decisions. For example, it can be used to infer distances for attaining safe levels of natural attenuation for potable water quality or to avoid aquatic toxicity for target organisms or inform management measures to ensure safety at target distances. We illustrated the applicability of this method for such purposes by an example. In this example, we computed distances beyond which aquatic toxicity is unlikely to occur from one each of the organic and inorganic chemicals used in the drilling fluid (considering the composition used at the Haselgrove-3 well site) and aquatic toxicity levels for an indicator aquatic crustacean genus, Daphnia. The example application for one organic (citric acid) and one inorganic (Potassium Chloride) chemicals considering the concentrations used for drilling one of the wells in the region showed that median distances of 67 m and 156 m respectively from the Dombey 1 well could ensure that the concentrations of these chemicals are below the chronic aquatic toxicity levels for the indicator crustacean genus of daphnia. The corresponding 95th percentile values of the distances are 488 m and 189 m respectively. Similar values were calculated for the Haselgrove 4 well as well. Alternatively, the simulated dilution levels can also be used to inform the concentration levels used at the source to ensure that concentrations are below prescribed levels within target distances.

While the integrated modelling method presented in this study is generic and can be applied for computing attenuation levels for such applications as described above, the model scales and parameters should be tailored to suit the individual application, source-receptor combinations and chemical species of interest. The saturated zone models we developed in this study has a regional focus with the objective of simulating concentration changes and attenuation levels for a broad range of plausible parameter combinations and considering three gas wells and potential receptors across the region. This study is a screening analysis that identified the risks associated with gas development for plausible contamination scenarios considering probable characteristics of leakage, spill (flux, duration) and a probable range of hydraulic and solute transport parameters of soils and aquifer media. Predictive assessment of concentration changes at specific receptors in the vicinity of the facilities would need to account for the actual characteristics (flux, duration) should a contamination event actually happen, and would need to incorporate the local site-specific hydrogeological characteristics using finer spatial and temporal modelling of the flow and transport processes.

1 Introduction

Drilling fluids used in onshore gas activities including conventional gas consist of a mixture of water and various chemical additives. While industry and regulatory standard procedures ensures minimal likelihood of environmental hazards occurring, these activities and causal pathways associated with onshore gas developments may lead to water contamination risks. This study was commissioned by the Gas Industry Social and Environmental Research Alliance (GISERA) to identify broad and likely pathways that can lead to contamination events and to develop and apply vulnerability and modelling analyses for selected plausible pathways to undertake a screening analysis of contamination risks. In doing so, a probabilistic modelling method was developed to account for uncertainties in the characteristics of aquifers and flow and transport parameters to probabilistically quantify solute concentration changes in the aquifer at the risk receptors for plausible scenarios of contamination. The method was applied to quantify contamination risks in the vicinity of three gas wells, Haselgrove 4, Nangwarry 1 and Dombey 1 in the southeast SA (Figure 1). The three gas well locations are shown in Figure 1 together with the extent of the child groundwater model used for the saturated zone transport modelling analysis.

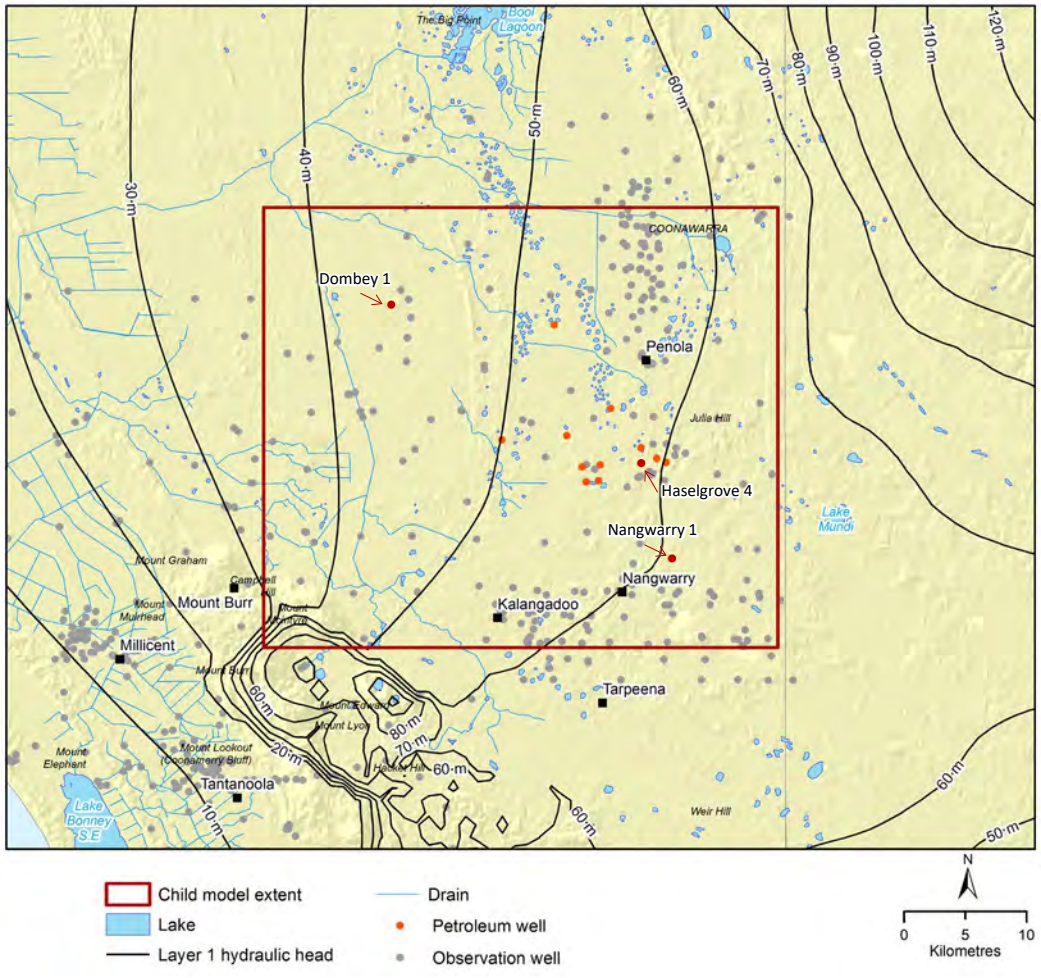

Figure 1: Study area showing the location of the three gas wells considered for groundwater contamination risk assessment

The study focuses on plausible contamination pathways from conventional gas development in within the study area in the southeast SA only. Pathways associated with unconventional gas activities like hydraulic fracturing are not considered, as unconventional gas development is not considered in the region. The study focuses on plausible pathways of contamination accounting for the gas development activities that could potentially result in a leakage or spill event and modelling realistic scenarios of transport through the porous media considering broad range of transport characteristics of the soluble constituents that could leak or spill. However, this study is not an assessment of individual chemicals used the conventional gas development per se, nor does it assess the toxicity and hazard associated with chemicals, although an example is provided to demonstrate the potential applicability of the generic method for such purposes. A companion project in GISERA SA (Schiteie et al., 2019; Tran-Dinh et al., 2019) comprehensively assessed the chemical compound concentrations and degradation characteristics of chemicals used in onshore gas production.

Recently, Jacobs (2016) undertook a similar study for hydrogeological risk assessment for southeast SA, focussing on unconventional gas development. That study used a two step-approach where aquifer vulnerability was first quantified spatially by considering groundwater occurrence and depth to groundwater as the two important variables. In the second step, the study calculated groundwater travel times in the Upper Tertiary Limestone aquifer and Lower Tertiary Confine aquifer. Then, the contamination risk was evaluated by considering both the vulnerability of aquifer and likelihood of contaminant particles reaching the stratigraphic location for the aquifer relative to the likely source/origin of contamination.

Similar principles were used in our study to assess contamination risk. In this study a comprehensive risk assessment was undertaken by doing:

- An assessment of aquifer vulnerability using spatial characteristics comprising depth to groundwater, recharge, aquifer type, soil type, topography, impact of vadose zone and hydraulic conductivity.
- Integration of vulnerability characteristics in risk assessment by spatial and temporal modelling of travel times and contaminant transport in unsaturated (soil column) and saturated zones (aquifer)
- Spatially explicit assessment of assets and receptors in the gas development area for proximity and contamination risks
- Accounting for the predictive uncertainty of flow and transport in soil and aquifer media by considering plausible ranges of soil/aquifer flow and transport characteristics.

Chapter 2 of this report describes the pathways of contamination risk in conventional gas development. Chapter 3 describes vulnerability and proximity analysis for the selected region in southeast SA. Chapter 4 describes the modelling methods used for transport modelling in the soil and aquifer media and Chapter 5 presents the results of contamination risk assessment for selected scenarios. The scenarios assessed in this study were designed to understand the residual risks of contamination when standard procedures for storage, handling and management of liquids and contaminant substances as stipulated by the South Australia Environmental Protection Agency (SA EPA) are followed. Hence, the findings of this study indicating low contamination risks for most scenarios analysed does not preclude the requirement for following the stringent procedures and management practices as imposed by these regulations.

2 Conventional gas development – pathways of contamination risk

There are several activities and associated causal pathways associated with onshore gas developments that can lead to water contamination risks. Recent CSIRO studies (Mallants et al., 2017a, b, 2018) have identified two broad categories of contamination migration pathways that are relevant for onshore gas development. The two broad pathways that are relevant to conventional gas development are: 1) surface-based pathways: i.e., pathways related to surface handling of drilling fluids including surface pathways (surface runoff), soil and shallow groundwater pathways and 2) deep groundwater pathways: i.e., pathways related to drilling, and well decommissioning involving deeper groundwater pathways. Also, it is noteworthy that since the gas development in South East SA focuses only on conventional sources, there will be a much smaller number of chemical contamination sources and pathways that need consideration.

The contamination events resulting from these two categories can include accidental or flood-induced surface spillage of contaminants, vertical leakage of poor quality water from holding ponds, loss of drilling fluids in groundwater formations during drilling, migration of groundwater and dissolved chemicals through leaky wells, poor-integrity water bores, leaks in underground seals, natural or reactivated faults, and migration of geogenic contaminants up a poor-integrity wellbore (Mallants et al., 2018; Wu et al., 2016; Jacobs 2016). Based on a review of international literature and data from unconventional gas industry in Australia, the likelihood of these contamination events was previously determined to be unlikely (for surface handling events) to extremely unlikely (for events related to deeper groundwater). After considering the nature of causal pathways of contamination from onshore conventional gas activities in the study area located within the southeast SA region, appropriate spatial and process modelling tools were developed for the probabilistic evaluation of impacts to groundwater resources and receptors associated with the likely causal pathways in the selected study area where onshore gas activities are current or planned for the near future.

2.1 Developing the gas well: Comparison between conventional gas and coal seam gas

Prior to developing conceptual models of potential chemical migration pathways, it is important to highlight the fundamental differences between conventional gas production and coal seam gas production. These difference in production processes have considerable impact on the plausible contamination events and pathways that need consideration in an impact assessment.

The fundamental difference between conventional gas and coal seam gas (and by extension shale and tight gas) lies in the geology of the gas resource. Unconventional gas resources are regionally pervasive and located within underground formations, such as coal, shale and low permeability sand. Coal seam gas is trapped in coal beds by adsorption of the gas molecules to the internal surfaces of coal. It cannot migrate to a trap and form a conventional gas deposit. This distinguishes it from conventional gas resources, which occur as discrete accumulations in traps formed by folds

and other structures in porous and permeable sedimentary layers (Figure 2). Coal seam gas remains adsorbed onto the coal surfaces mainly within the micropores of coal seam layers in saturated groundwater, where it was formed (Moore, 2012). The combined pressure of the sediments and water overlaying the coal seam keeps the gas within the micropores. The porosity and permeability of the conventional gas resources is also much larger than that of the unconventional gas resources. As a result, there is no need to increase the permeability of the rock to allow the gas to flow to the well. Indeed, conventional gas production in the South East of South Australia has been going on for at least 22[1] years without the need for hydraulic fracturing.

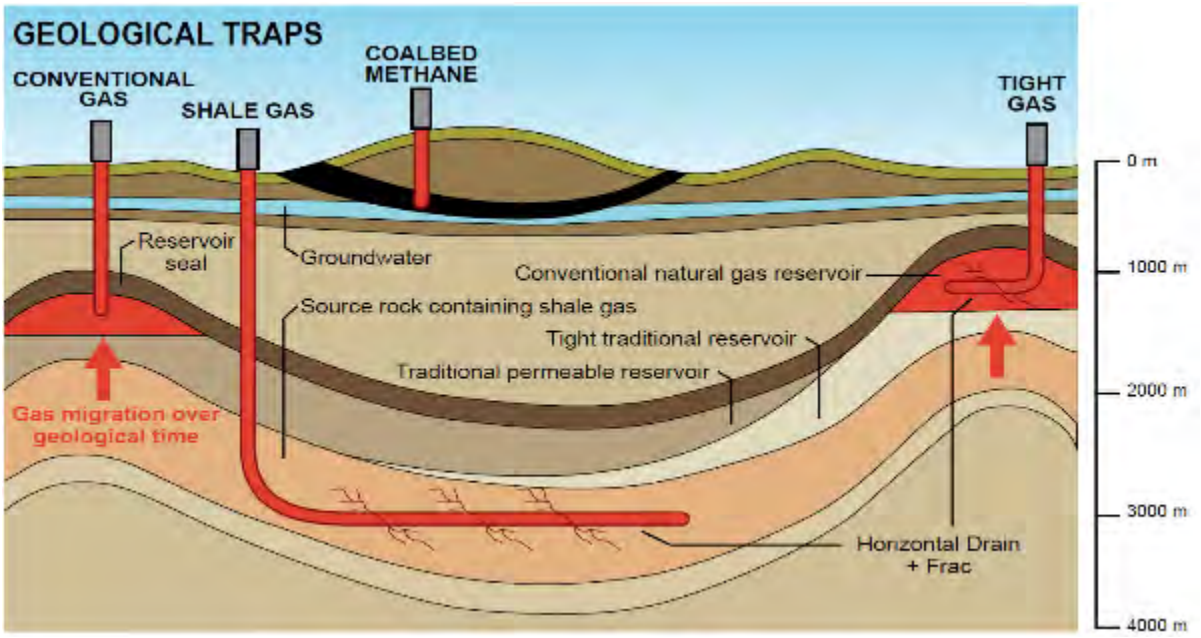

Figure 2 Schematic occurrence of gas resources; unconventional gas includes coal seam gas, shale gas, and tight gas (source: Department of Mines and Petroleum, 2013).

Another important difference between conventional gas and coal seam gas production is the much smaller volume of produced water associated with the former compared to the latter. In the Surat Basin, Queensland, typical water production of coal seam gas wells has been assessed at 0.4 ML/day to 0.8 ML/day during the de-watering stage before decreasing to 0.1 ML/day in the decline stage. In the Sydney Basin (Camden field), the water production is 0.20 ML/day during de-watering and decreases to 0.02 ML/day (RPS 2011). Note that volumes of produced water per well decrease significantly over the lifetime of the well (typically a period of about 25 to 30 years[2]).

[1] The Katnook gas plant that provided natural gas to the south east operated continuously between 1991 and 2013

[2] For gas fields in the Surat Basin (Fairview, Spring Gully) the estimated average well life is 20 to 30 years; in the Surat Basin-Walloons (Talinga, Kenya, Argyle, Orana, Condabri) well life is 15 years (Origin 2008).

In a study conducted by RPS (2011), the ratio of produced water to energy for different basins reveals the following: 50.4 ML/PJ for the Bowen Basin, 192.5 ML/PJ for the Surat Basin and 1.2 ML/PJ for the Sydney Basin. While considerable variations in rates exist between regions, large variability has also been observed within coal seam gas fields. For instance, in the Stratford Pilot area (approximately 70 km north of Newcastle in New South Wales) water production rates per well varied from 0.00475 ML/day to 0.0795 ML/day (Lucas 2008).

Of relevance in this study for the southeast region is the Katnook gas processing facility which was built and commissioned in 1991. The Katnook complex, comprising the Katnook, Haselgrove, Haselgrove South, and Redman gas fields produced gas and condensate from the Katnook processing facilities between 1991 and 2011. It produced over 70 Bcf of gas and 0.4 MMbbls of condensate from the Pretty Hill Sandstone reservoir and supplied to local industry and the adjacent Ladbroke Grove Power Station, which was commissioned in 2000. All Penola Trough fields are currently shut. The plant and fields are owned and operated by Beach Energy (100%). The volume of produced water from the gas wells supplying the Katnook gas plant has been reported to be negligible[3]. The 2006 Operational Review (Taylor et al., 2007) reported a total of 1951 kL of water production from the Katnook gas field during 2006 and a cumulative water production volume of 13,150 kL since start of production in 1991. They also reported water production of respectively 1094, 684 and 2231 kL of water production from the Haselgrove, Redman and Ladbroke Grove fields in the year 2006. The respective cumulative volumes were 8541, 5201 and 18,594 kL of water since start of production. RPS (2011) reported zero (0) produced water for the South Australian section of the Otway Basin. As a result, the required water management infrastructure and associated risks were much smaller for conventional gas compared to coals seam gas.

2.2 Lifecycle phases of gas well development

To assess what activities might lead to spills and leaks, we first identified all activities and processes that occur throughout the life-cycle phases of conventional gas operations. Five lifecycle stages are considered: (i) exploration; (ii) appraisal; (iii) development; (iv) production and (v) rehabilitation:

- Exploration (including drilling) phase: develop well pad, establish water supply for drilling fluids, transport of drilling chemicals to pad, drilling exploration wells, drilling fluid management
- Appraisal phase: drilling increases
- Development phase: drilling is now at its maximum with drilling fluids typically stored in ponds; drilling mud disposed
- Production phase: construction of pipeline network, production and processing of gas, disposal of waste water
- Rehabilitation (decommissioning (i.e. plugging wells with concrete, infrastructure removal, fluid storage infrastructure removal and rehabilitation) and abandonment) phase:

[3] Based on the 2008-2009 fiscal year reporting

2.3 Pathways related to soil and shallow groundwater

To develop conceptual models of potential chemical migration pathways for the assessment of contamination risks from surface handling of drilling and production fluids, an overview of potential scenarios of incidents involving fluid releases to soil and groundwater is provided. For each scenario a fluid or contamination source, migration pathway and receptor(s) needs to be defined. Fluid migration pathway conceptualization is considered only for semi-continuous and large volume sources (typically the volume of a truck or larger).

During the drilling phase potential sources of contamination include leaks of drilling fluid, loss of diesel during refuelling, etc. On-site disposal of drilling mud is another potential source of contamination.

During the gas production phase the potential sources of contamination associated with surface spills and leaks include infiltration (i) of water used for dust suppression, (ii) of water and fuel (e.g. diesel spills) from surface spills, (iii) of water from flooding of storage dams, and (iv) release of water from supply and discharge lines. Each of these contamination sources are briefly discussed.

Dust generation at the site and on access roads will need to be controlled which typically requires regular water spraying. When produced water is available, this water is generally treated, to varying degrees, prior to spraying. While deep infiltration of such produced water in the subsurface is not expected, and hence not considered in the modelling analysis for groundwater contamination risks in this study, care must be taken that when chemicals are present in the water used for spraying, no accumulation occurs.

The next contamination source involves incidental chemical spills on the surface from storage tanks, trucks, valves, refuelling, etc. Examples include failing pipes and hoses that connect different parts of infrastructure, including joints and fittings. Overflow of trucks and equipment used for mixing chemicals as part of drilling fluid preparation can also occur; however, the potentially contaminated surface area would be relatively small in comparison to overflow from a water holding pond. Spills are typically contained and managed through on-site spill containment processes (e.g. bunding). Depending on the volume of water released, antecedent soil moisture conditions, and the soil's capacity for natural attenuation, potential contamination is likely limited to the shallow soil zone (Mallants et al., 2017c, 2017d). This is one pathway of particular interest for groundwater contamination risk assessment and a relevant scenario is modelled in this study.

Infiltration into soil can also occur as a result from leaks in water/drilling fluid holding ponds, dam wall collapse, and hazardous events including flooding (Brantley et al., 2014; The Royal Society and The Royal Academy of Engineering, 2012). Produced water is stored in surface ponds before being either re-used (e.g. dust suppression) or treated onsite or offsite. Beach Energy, at their Katnook plant, are using above ground bunded storage tanks. Lined ponds are known to leak (the combination of advective and diffusive migration of fluids) over time – albeit at a very low rate – even when double lined (Chapuis, 2002; Council of Canadian Academies, 2014; Rowe, 2012). Leakage can be up to 5×10−9 m/s (157 mm/year) for a single geosynthetic membrane, 5.8×10−11 m/s (1.83 mm/year) for a composite geomembrane/compacted clay liner and up to 7×10−13 m/s (0.022 mm/year) for a composite geomembrane/geosynthetic clay liner (Bonaparte et al., 2002). Furthermore, the salinity of the stored produced water can increase the permeability of clay lined ponds (Folkes, 1982; Benson, 2001). In Australia, design requirements for storage basins include

the bottom of the basins being sealed with a clay liner or a material such as a geomembrane with an equivalent low maximum hydraulic conductivity of ~ 10−10 m/s (0.31 mm/year) (DITR, 2007). Current designs further include the use of leak detection systems. Overtopping or dam flooding as a result of extreme rainfall events is another potential pathway for chemical release. The leakage from a storage pond/drilling sump is also relevant for groundwater contamination risks and one plausible scenario is investigated using flow and transport modelling analysis.

The potential pathways and receptors for contaminant transport of fluids associated with surface-based spills and leaks at the gas production site include:

1. Runoff to wetlands and rivers. This includes the potential flow of spilt chemicals on the land surface to water courses and overtopping of water holding ponds during flood events. Such events are easily detected and managed immediately following standard regulatory protocols.

2. Subsurface flow from surface spills into the unsaturated soil/rock, potentially leaching into groundwater and further migration to water supply bores, recharge springs, wetlands, and rivers. These subsurface events are harder to detect and subsurface leakage may occur for longer duration (e.g. months) before they are detected and managed. One relevant scenario corresponding to this pathway is investigated using flow and transport modelling in this study. Additional receptors of potentially contaminated groundwater include groundwater dependent terrestrial vegetation, mainly along rivers with interconnected unconsolidated alluvial aquifers with a high porosity, and stygofauna (AE, 2012).

2.4 Pathways related to deep groundwater - drilling and well failure

2.4.1 Leaky bores

Wu et al. (2016) included in their review information on documented well failure rates for coal seam gas wells, water bores and coal exploration holes in Australia. The latter two categories are not directly related to oil or gas extraction but nevertheless could enhance inter-aquifer connectivity and as such provide pathways for migration of fluids and gases, given the right hydraulic conditions. If such pathways existed prior to any gas extraction taking place, the background groundwater hydrochemistry of productive aquifers may have been perturbed which, if undetected, may lead to concluding the wrong cause-effect relationships. Any baseline hydrochemical study should therefore also undertake a survey of potentially leaky water bores to identify whether or not the aquifer hydrochemistry is affected by pre-existing pathways.

Water bores, especially those with multiple screens across different geological formations including hydrocarbon reservoirs, can indeed provide pathways for enhanced inter-aquifer connectivity. Casing materials have a finite life span and this should be longer than the anticipated operational life of the bore. However, for many water bores in particular, from the outset consideration of the life span of casing materials has received little attention. As a consequence, a bore may remain in service well beyond the lifetime of the materials used in its construction. If a bore is not monitored and maintained during its life then loss of integrity of the casing is likely to result in loss of integrity of the bore and potentially result in interconnection of aquifers. To lose its integrity a bore casing must perforate and/or collapse. This may be as a result of physical and or chemical damage or weakening of the material before, during or after installation.

In addition to well casing material losing its integrity due to damage and/or degradation over time, the integrity of the sealing material emplaced in a well's annulus can also be compromised. The long term deterioration of bore seals, typically cement or bentonite, have been studied and the deterioration mechanisms are reasonable well understood (Carey et al., 2010; Goodwin and Crook, 1992; Kutchko et al., 2007). Even a good initial seal may lose its integrity during the lifetime of the bore due to cement shrinkage; shrinking occurs during curing of the cement which then generates cracks, but may also happen at later stages due to mechanical stress within the geological formation (Wu et al., 2016). Bores should be monitored for integrity at intervals throughout a bore's lifetime, even once it is decommissioned and abandoned.

2.4.2 Pathways related to geological faults

The role of faults as potential pathway for fluid movement from gas resources into productive aquifers was previously studied in relation to hydraulic fracturing. Kissinger et al. (2013) studied under which parametric conditions hydraulic fractures would connect into pre-existing natural pathways (faults, fractures) and deteriorated, pre-existing nearby wells was. They hypothesized flow paths for leakage of fracturing fluid, brine and methane from potential hydraulic fracturing sites into shallower layers. Fluid flow through natural fault zones was assessed for (i) long-term (tens of years) horizontal and vertical movement of hydraulic fracturing fluid and brine along vertical fault zones connecting deeper aquifers with shallower aquifers, and (ii) long-term (tens of years) methane gas migration from the gas reservoir into a fault zone owing to buoyancy and capillary forces.

Reagan et al. (2015) carried out numerical simulations of water and gas transport between a shallow tight-gas reservoir and a shallower freshwater aquifer following hydraulic fracturing. The general failure scenarios assumed connection between the reservoir and aquifer occurs via a fracture or fault.

While the above fault-related pathways were investigated in relation to hydraulic fracturing, analogous scenarios can be developed for drilling operations. Because drilling does not require the very high pressures used in fracturing, the consequences of intercepting a fault zone while drilling are likely much smaller.

Fault zone pathways may also be connected with poor integrity gas wells or water bores, where the natural flow of fluids and gases through a fault may be diverted via a poor integrity well annulus or degraded water bore casing. Especially where gas wells are drilling nearby important fault zones, as is the case with the fault dependent traps in the Pretty Hill Formation (current study area), such scenarios warrant an in-depth analysis (Figure 3).

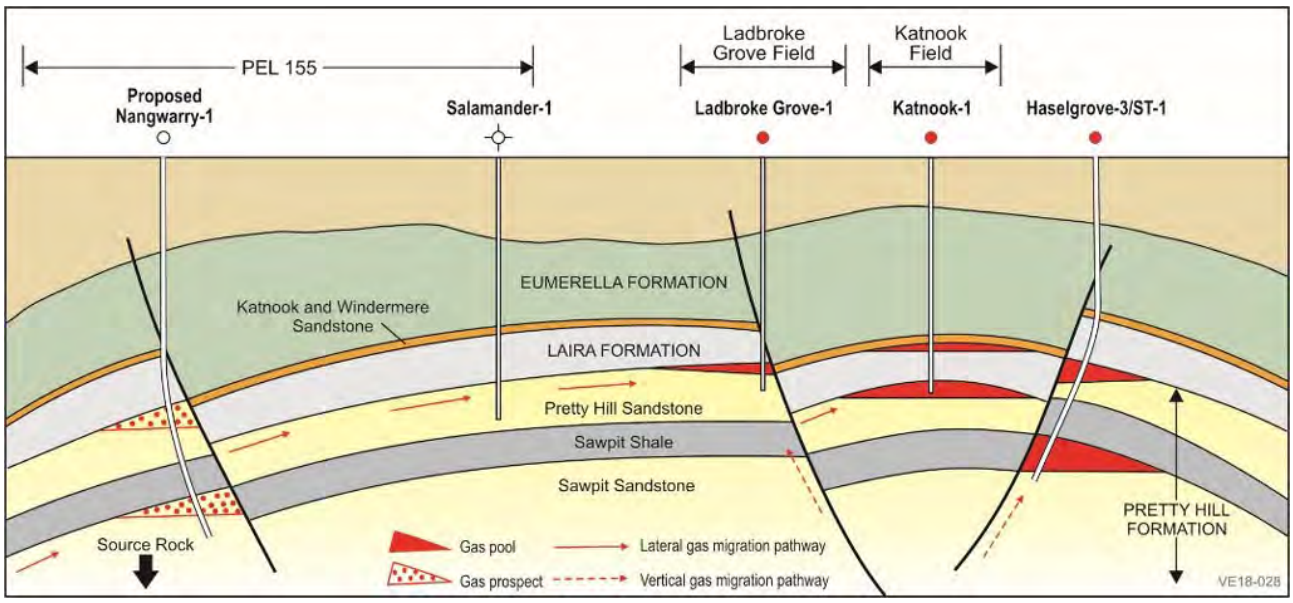

Figure 3 Geological cross-section with indication of gas traps in the Pretty Hill Formation.

In the context of conventional gas development from southeast SA, leakage through micro annulus developed in between the casing strings constitute a potential pathway for contamination. Unlike the case of coal seam gas development in Surat Basin in Queensland where multiple aquifer layers exists above and below the coal seam gas target formation, the aquifers that are currently used for groundwater development in the southeast exist in the top most layers and are separated from the gas target formations by many other formations. Hence, the likelihood of leaky bores enhancing inter-aquifer connectivity and resulting in pathways for contaminant migration from conventional gas development is low. Faults zone pathways are more likely when gas wells are drilled near fault zones. Site specific studies for characterising the hydraulic characteristics of fault zones and site specific modelling analysis are required for quantifying contamination risks.

A summary of the plausible hazards and pathways are identified in Table 1. The risks associated with these pathways and potential risk receptors are also identified. Based on historical evidence and likelihood of source activation in the South East South Australia context, appropriate scenarios will be developed for detailed quantification of risks for selected source-receptor combinations. A risk-based approach is adopted for undertaking this to ensure that the scenarios capture the likelihood of source activation, likelihood of contaminant migration to the receptors and the resulting consequence are evaluated in the risk quantification process. A detailed description of potential modelling methods that may be employed for the distinct pathway are described in Section 4.

Table 1: Summary of plausible pathways and risks

Source/Hazard	Pathway modelled	Receptors	Risk	Modelling approach
Slow leaking drilling sump, leakage in unsaturated zone under the influence of no recharge	Leakage from surface storage facility due to breach of lining and gravity flow to shallow groundwater	Groundwater bores, SW bodies (Wetlands, creeks and rivers), soil surface, GDEs and other vegetation,	Contamination of soil and shallow groundwater, SW bodies	Transport modelling for the vadose and saturated zones
Loss of well integrity, leaky bores, faults	Leakage through micro annulus	Deep/shallow aquifers, deep groundwater bores	Contamination of deep aquifers	Integrated modelling approach using particle tracks and fate analysis for residual concentrations
Pipeline pin hole leak	Pipeline from well to the facility leak underground resulting in solution reaching soil column	Shallow aquifer, groundwater bores, water courses near the facility	Contamination of shallow aquifer, bores	Integrated modelling approach using particle tracks and fate analysis for residual concentrations
Spill of fuel/chemical	Accidental spill of solution and migration through surface soil into shallow groundwater	Groundwater bores, SW bodies (Wetlands, creeks and rivers), soil surface, GDEs and other vegetation,	Contamination of soil and shallow groundwater	Transport modelling for the vadose and saturated zones

3 Physiographic characteristics, water-dependent asset density and groundwater vulnerability

3.1 Introduction

To assess the vulnerability of groundwater systems a geographic information system (GIS) based, multi-criteria decision analysis (MCDA) approach was applied (Malczewski, 1999). This type of method has a long history of use in similar assessments with perhaps the most well-known being the DRASTIC model developed by the US EPA (Aller et al., 1987). This generic method was developed to assess contamination potential of unconfined aquifers from land-based contaminants and focuses on the following parameters and rationale:

– Depth to water table – shallow water table is more vulnerable
– Recharge – higher recharge increases potential for transport to the aquifer
– Aquifer type – aquifer hydraulic characteristics affect the flow velocity and transport
– Soil type – lower clay content has greater permeability potential
– Topography – flatter areas generate less runoff therefore have more recharge potential
– Impact of vadose zone – vadose zone attenuation depends on matrix properties
– Hydraulic conductivity – higher conductivity is more vulnerable

In the context of this study, some of these parameters are more relevant than others and other considerations were required. The DRASTIC model is more applicable to diffuse pollution sources rather specific point sources. It was therefore important to apply a robust methodological framework to define the problem and determine appropriate criteria and constraints to conduct the assessment. A clear, systematic workflow was defined by Malczewski (1999). Briefly, this involves specific problem definition, defining objectives and attributes that relate to the problem (usually done in combination with data discovery and standardisation), constraint mapping or area elimination, determining criteria weights, applying a decision rule to generate one or more feasible alternatives, determining sensitivities (weights and attributes where appropriate), and finally providing recommendations on future action.

In addition to groundwater vulnerability, the relative magnitude of economic, environmental and sociocultural assets was considered. Areas with higher densities of assets that could potentially be affected by changes in the quality of groundwater resulting from gas development inherently carry more risk. The proximity of assets to the gas well locations was also evaluated.

3.2 Methods

3.2.1 Tertiary Limestone Aquifer groundwater vulnerability evaluation criteria and supporting data

The analysis defined two distinct problems to assess the vulnerability of the upper unconfined Tertiary Limestone Aquifer (known as the Gambier Limestone in the Otway Basin and the Murray Group limestone in the Murray Basin), and the presence of connected assets, to the hazards associated with gas development in the southeast region around Penola in South Australia. Firstly, to determine the vulnerability of the aquifer based on properties influencing exposure to contamination, and secondly asset spatial density and proximity to proposed gas wells in the child model extent.

The groundwater vulnerability assessment did not consider location-specific gas development; the child model extent was assessed for inherent vulnerability to contamination from gas exploration in any location. In many places the water table is very shallow and supports a range of groundwater-dependent ecosystems including swamps, wetlands and springs that rely on (Harrington and Lamontagne 2013). The Tertiary Limestone Aquifer (TLA) is extensively used for irrigated agriculture.

Potentially impacted assets formed three broad classes; economic, environmental and sociocultural. Economic assets included water bores used for domestic purposes, livestock watering, town water supply, irrigation, and commercial and industrial uses; and land used for productive agriculture e.g. fruit and nut production, wine and timber products. Environmental assets included parks, reserves, caves and other areas protected for conservation, groundwater dependent ecosystems (GDEs), watercourses, and known distributions or habitats of listed species of national environmental significance (SNES). Sociocultural assets included heritage listed areas e.g. buildings of historical significance and land with Native Title Determination or Indigenous Land Use Agreements.

Evaluation criteria for the vulnerability assessment were determined according to the defined problem and data discovery related to the required criteria. The metrics, or attributes, for each criterion were calculated at the extent and resolution (250 m) of the child groundwater model used in this project (Doble et al., 2020). Attributes for all criteria were normalised on a scale of 0-1 for subsequent aggregation so that all began with equal influence on the result.

Six criteria were determined to assess the vulnerability of the surficial Tertiary Limestone Aquifer to contamination pathways:

1. Depth to water table
2. Topographic slope
3. Internal drainage area height
4. Groundwater velocity

5. Recharge potential
6. Soil clay content

The first criterion was depth to water table; the shallower the water table, the more vulnerable it is to contamination due to faster transport of contaminants from the surface reaching the aquifer at higher peak concentrations. The depth to water table was calculated based on the difference between hydraulic heads from the regional scale groundwater model for the Tertiary Limestone Aquifer (Morgan et al., 2015) and surface elevation.

The second criterion was topographic slope; flatter areas generate less runoff therefore have greater potential for infiltration and transport of contaminants from the surface to the aquifer. This was calculated from surface elevation.

The third criterion was internal drainage area height which were theoretical pool heights within areas of internal sinks; greater internal pooling depth implying greater potential for runoff accumulation and higher gradient for transport of potentially contaminated runoff to the aquifer. This was calculated from surface elevation.

The fourth criterion related to groundwater velocity where higher velocity implies greater vulnerability through lower attenuation potential and longer and faster transport of contaminants. This criterion was calculated using aquifer properties in an existing regional scale groundwater model (South East Regional Water Balance, Morgan et al. 2015). Parameters related to initial conditions were used as inputs to the groundwater velocity calculation tool in ESRI ArcGIS that calculates the groundwater seepage velocity vector (direction and magnitude) for steady flow in an aquifer. The required fields for this grid-based calculation are groundwater head elevation, effective porosity, saturated thickness and transmissivity. The regional model used a resolution of 1 km, so data were resampled to this resolution. The elevation of the bottom of the TLA layer was subtracted from head elevation (where head elevation was less than or equal to ground level, otherwise subtracted from ground level) to give saturated thickness. Hydraulic conductivity ranging from 8-58 m/d in seven distinct zones across the child model extent was multiplied by saturated thickness to give transmissivity. Effective average porosity across the child model extent was assumed to be 15%. Results given at 1 km resolution were resampled back to the 250 m grid using nearest neighbour assignment to preserve values for input to the vulnerability assessment. Results using the GIS tool were similar to a calculation of velocity based on groundwater gradient (using the slope of heads) multiplied by hydraulic conductivity and divided by porosity.

The fifth criterion was recharge potential where greater recharge implies higher vulnerability as contaminants would be transported through the unsaturated zone more readily from the surface. Gridded annual rainfall averaged from 1961-1990 at a resolution of about 5 km (BOM, 2019) was used as an indicator for recharge potential to the unconfined TLA.

The sixth criterion related to the potential for the clay content in the upper soil layer to attenuate the permeation of contaminants spilled on the surface down through to the TLA;

lower clay content increasing potential vulnerability. This criterion used depth averaged estimates of clay content for the upper 2 m of soil from 6 depth intervals at ~90 m resolution (Viscarra Rossel et al., 2014).

3.2.2 Tertiary Confined Sands groundwater vulnerability

The Tertiary Confined Sand (TCS) aquifer is known as the Dilwyn Formation in the Otway Basin and the Renmark Group in the Murray Basin. The depth of the TCS aquifer and the presence of an overlying low permeability aquitard meant that surface contamination pathways were likely to be far reduced compared to the unconfined Tertiary Limestone Aquifer (TLA). To test this hypothesis, an analysis was conducted using existing data from the regional groundwater model (Morgan et al. 2015) and hydrogeological reporting of the region (Mustafa and Lawson, 2011).

Based on regional model parameters (Morgan et al. 2015) the estimated thickness (b) of the aquitard was 2.4 – 42 m across the child model extent, head differences (dh) between the TLA and the TCS aquifers ranged from 2 m to 36 m (indicating downward movement only), and the conductivity of the aquitard ranged from 4e-05 m/d to 5e-09 m/d.

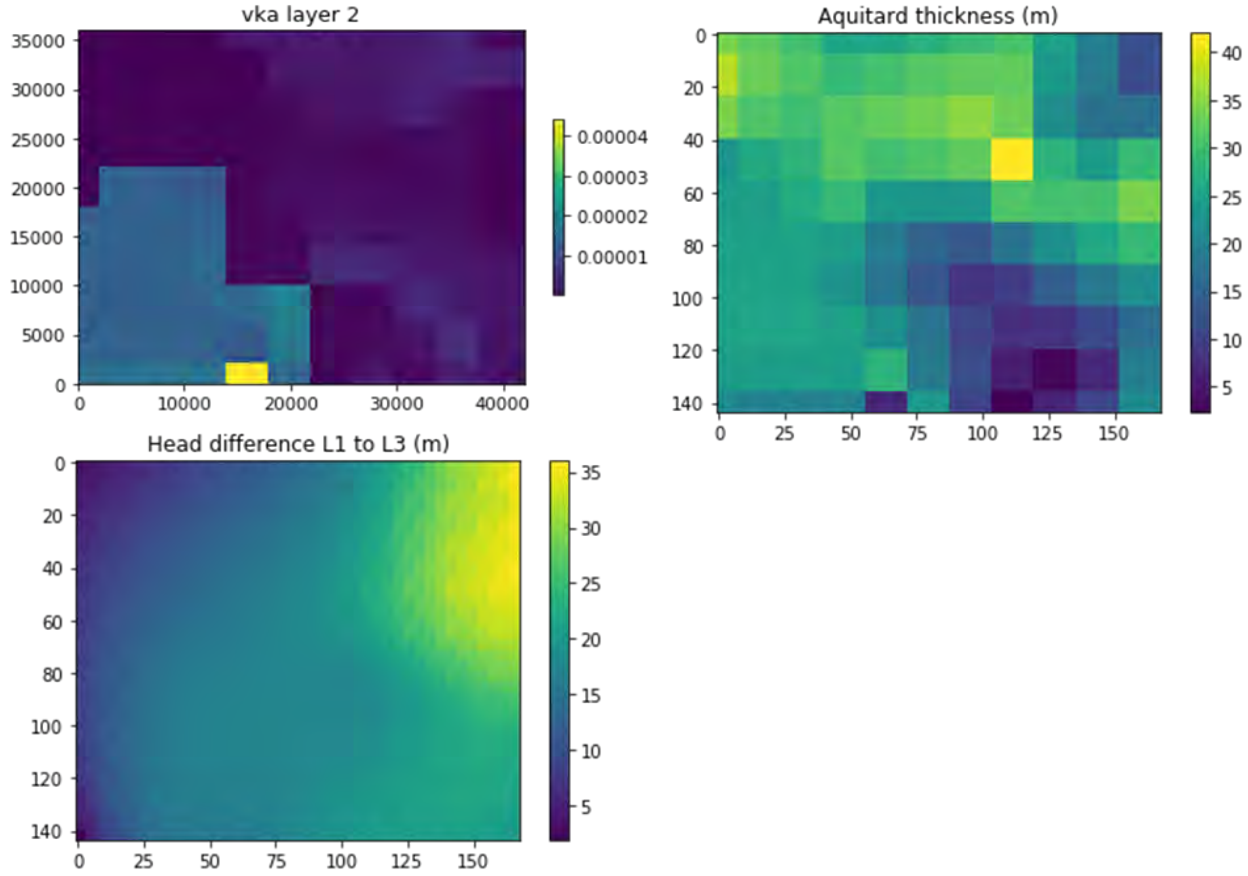

Figure 4: Aquitard properties based on initial conditions from the South East Regional Water Balance model (Morgan et al., 2015).

Aquitard porosity (n) around the Mepunga Formation was estimated at ~0.07 as cited in Harrington and Lamontagne (2013). Based on these data, aquitard groundwater velocities (V) of 9e-09 m/d to 2e-03 m/d (Eq. 1), and travel times (t) of 13 years to >1 million years (Eq. 2) were calculated.

$$V = \frac{\mathrm{K(dh/dl)/b}}{\mathrm{n}} \qquad \text{Eq. 1}$$

$$t = \frac{\mathrm{b/V}}{365.25} \qquad \text{Eq. 2}$$

Vertical conductivity of the aquitard determined from pump tests conducted on wells approximately 20-30 km south of the child model extent were between 3e-04 to 4e-02 m/d indicating that the TCS aquifer was leaky in places (Mustafa and Lawson, 2011). Substituting these K values uniformly across the area into Equations 1 and 2 resulted in aquitard travel times of less than 1 day to 1.7 years (median of 55 days) and 70 days to 230 years (median of 21 years) where K was 4e-02 m/d and 3e-04 m/d respectively.

Assuming a higher aquitard vertical conductivity value of 4e-02 m/d is plausible across the extent, the travel time from the surface through the TLA and aquitard was calculated to indicate whether it was reasonable to assume that surface contamination pathways existed for the TCS aquifer. Horizontal K for the TLA in the regional model ranged from 8 to 58 m/d (Morgan et al. 2015). A typical vertical to horizontal anisotropy ratio where clay is present is 0.01 (Todd, 1980), i.e. vertical K is about 1% of horizontal K. To estimate potential vertical travel times in the Gambier Limestone, equations 1 and 2 were applied using 1% of initial K values and the total thickness of the TLA, and the head difference between the aquifers. This was added to aquitard travel times. Total estimated vertical travel times through the TLA and aquitard ranged from 62 days to 334 years (Figure 5). Vertical aquitard travel times (assuming aquitard K = 4e-02 m/d) did not notably add to travel times from the surface to the confined aquifer. There was an area in the southern part of the model extent where vertical travel times of less than one year were estimated, gas well locations were in areas where vertical travel times were likely to exceed 1 year (Figure 5).

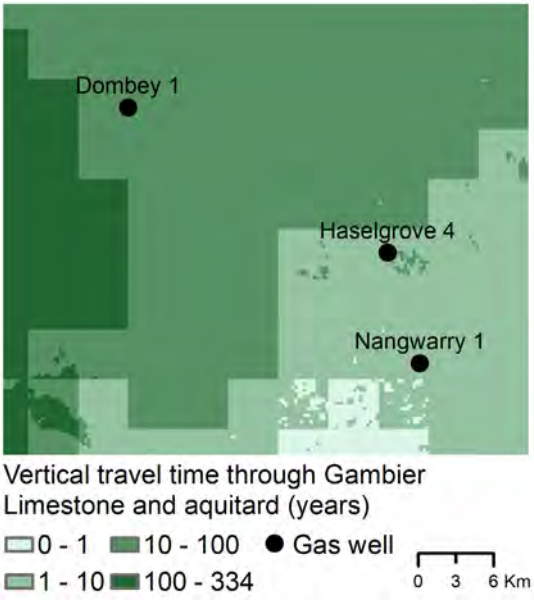

Figure 5: Estimated vertical travel times through the Tertiary Limestone Aquifer and aquitard (assuming aquitard K = 4e-02 m/d) to reach the Tertiary Confined Sands aquifer.

In terms of the vulnerability of the TCS aquifer, surface contamination pathways or pathways involving contaminant migration from the TLA through the aquitard to the TCS aquifer were considered unlikely enough to warrant exclusion for the majority of the area. For input to the vulnerability assessment, travel times of less than one year were reclassified as 0.99 (high vulnerability), 1-2 years 0.5 (moderate vulnerability), and over 2 years 0.01 (low vulnerability).

The vulnerability of the TCS aquifer is driven by the hydraulic properties of the aquifer that influence groundwater velocity. Groundwater velocity was calculated based on initial model conditions for porosity (specific yield), conductivity, initial heads, and saturated thickness, using the groundwater velocity calculation tool in ESRI ArcGIS, results ranged from <0.0001 to 1.8 m/d. Velocities are likely to be higher at the Haselgrove 4 and Nangwarry 1 well locations, and considerably slower at Dombey. The groundwater vulnerability index for the TCS aquifer was then a sum of the reclassified vertical travel time to reach the TCS aquifer, and normalised groundwater velocity.

3.2.3 Asset evaluation criteria and supporting data

The presence or relative density of assets in the area assumed that more assets present higher risk (more likely to be impacted with greater consequence) associated with contamination hazards. The metrics or attributes were related to the geometries of the assets. Polygon features were analysed as area per unit area, line features as length per unit area, and point features as number per unit area. The unit area in this study was the child model grid with a resolution of 250 m. A summary of the assets occurring in the child model

extent is given in Table 2. Several databases were queried. Table 2 also includes assets that were queried but not found to occur in the child model extent e.g. Indigenous Land Use Agreement and Native Title Determination areas.

Table 2: Assets located within the child model extent.

Asset class	Geometry	Description	Count	Area (ha)	Source
Economic	Polygon	Environmental forest plantation		36.6	ABARES (ALUM)
Economic	Polygon	Hardwood plantation forestry		19,653.9	ABARES (ALUM)
Economic	Polygon	Irrigated grapes		4,413.6	ABARES (ALUM)
Economic	Polygon	Irrigated olives		15.2	ABARES (ALUM)
Economic	Polygon	Irrigated tree fruits		200.0	ABARES (ALUM)
Economic	Polygon	Irrigated tree nuts		6.1	ABARES (ALUM)
Economic	Polygon	Plantation forests		1,290.5	ABARES (ALUM)
Economic	Polygon	Softwood plantation forestry		26,019.2	ABARES (ALUM)
Economic	Point	Well - Domestic	967		DEW Drillholes database
Economic	Point	Well - Fire Fighting	9		DEW Drillholes database
Economic	Point	Well - General Usage	17		DEW Drillholes database
Economic	Point	Well - Industrial	49		DEW Drillholes database
Economic	Point	Well - Irrigation	1529		DEW Drillholes database
Economic	Point	Well - Monitoring	84		DEW Drillholes database
Economic	Point	Well - Observation	248		DEW Drillholes database
Economic	Point	Well - Recreational	2		DEW Drillholes database
Economic	Point	Well - Stock	1150		DEW Drillholes database
Economic	Point	Well - Town Water Supply (Public/Municipal)	12		DEW Drillholes database
Environmental	Line	Watercourses - other		361 km	DEW Waterconnect watercourses database
Environmental	Line	Watercourses - drains		224 km	DEW Waterconnect watercourses database
Environmental	Polygon	Conservation Park	2	240.1	Collaborative Australian Protected Areas Database (CAPAD) 2016
Environmental	Polygon	Forest Reserve	11	3,290.0	Collaborative Australian Protected Areas Database (CAPAD) 2016

Environmental	Polygon	GDE - River		0.4	GDE Atlas
Environmental	Polygon	GDE - Saline wetland		3.2	GDE Atlas
Environmental	Polygon	GDE - Vegetation		11,514.7	GDE Atlas
Environmental	Polygon	GDE - Waterhole		0.1	GDE Atlas
Environmental	Polygon	GDE - Wetland		12,373.0	GDE Atlas
Environmental	Polygon	Important Bird Areas		-	Birds Australia
Environmental	Polygon	Important wetlands		-	Directory of Important Wetlands
Environmental	Polygon	Critically Endangered birds		569,380.9	Species of National Environmental Significance Database (Public Grids)
Environmental	Polygon	Endangered birds		453,600.0	Species of National Environmental Significance Database (Public Grids)
Environmental	Polygon	Vulnerable birds		175,517.8	Species of National Environmental Significance Database (Public Grids)
Environmental	Polygon	Vulnerable fishes		151,200.0	Species of National Environmental Significance Database (Public Grids)
Environmental	Polygon	Endangered flora		234,486.5	Species of National Environmental Significance Database (Public Grids)
Environmental	Polygon	Vulnerable flora		829,747.2	Species of National Environmental Significance Database (Public Grids)
Environmental	Polygon	Vulnerable frogs		151,200.0	Species of National Environmental Significance Database (Public Grids)
Environmental	Polygon	Critically Endangered mammals		151,200.0	Species of National Environmental Significance Database (Public Grids)
Environmental	Polygon	Endangered mammals		144,948.2	Species of National Environmental Significance Database (Public Grids)
Environmental	Polygon	Vulnerable mammals		316,704.9	Species of National Environmental Significance Database (Public Grids)
Environmental	Polygon	Vulnerable reptiles		132,014.9	Species of National Environmental Significance Database (Public Grids)
Environmental	Polygon	Natural places	7	2951.1	Register of the National Estate (RNE) Australian Government

					Department of the Environment and Energy
Sociocultural	Polygon	Indigenous land use agreement (registered or notified)		-	National Native Title Tribunal
Sociocultural	Polygon	National Heritage List places		-	National Heritage List Spatial Database (NHL) - public
Sociocultural	Polygon	Native Title Determination areas		-	National Native Title Tribunal
Sociocultural	Polygon	Register of the National Estate Historic places	15	2.0	Australian Government Department of the Environment and Energy
Sociocultural	Point	SA Heritage places	103		Department of Planning, Transport and Infrastructure
Sociocultural	Polygon	World Heritage areas		-	Australia World Heritage Areas
Sociocultural	Polygon	Heritage Agreement	9	603.5	Collaborative Australian Protected Areas Database (CAPAD) 2016

Many of the species and habitat distributions held in the Species of National Environmental Significance (SNES) database overlapped. In order to represent the relative importance of certain areas, a species richness metric was applied that enumerated the number of species habitats or distributions occurring within each grid cell.

Due to duplication of some assets with similar geometries in multiple databases, polygons were merged into mutually exclusive groups within each asset class for generating proportional area grids to avoid double-accounting. The datasets using their original geometry formats (i.e. points, lines or polygons) were used for proximity analysis. The proximity analysis measured the distances to all assets within a search radius of 5km from proposed gas well locations (considered a conservative upper limit for particle travel distances). The nearest point, polygon boundary or line section was recorded for each unique feature. For calculation of asset density, all input data were converted to a common grid format by calculating proportional areas, counts or lengths per cell.

Table 3: Asset density assessment input data representation.

Asset class	Input data	Grid representation
Environmental	Merged CAPAD ('type' = conservation park, forest reserve); RNE ('class' = natural); GDE Atlas	Proportional area per cell
Environmental	SNES species and habitat distributions	Number per cell
Environmental	DEW watercourses (incl. drains)	Length per cell
Economic	ALUM agricultural land	Proportional area per cell
Economic	DEW drillholes water bores	Bores per cell
Sociocultural	Merged RNE ('class' = historic); CAPAD ('type' = heritage agreement); SA Heritage places	Proportional area per cell

3.2.4 Criteria weights and aggregation

For groundwater vulnerability and asset density assessments, all input data layers were represented as gridded values using a common grid (at the extent and resolution of the child model grid) and normalised on a linear scale of 0-1 where higher values imply greater vulnerability or greater asset density. The standardisation of values means that whatever weights are applied are done on data that initially have equal influence on the result. The base case was evenly weighted so that sensitivities of each criterion could be determined. Weighting is applied to reflect the relative importance of some factors over others and inherently involves a degree of subjectivity. There are methods of deriving weights that try to reduce subjectivity by using for example, a multi-influencing factor system to determine the level of influence of one factor over one or more others, or hierarchical pair-wise comparison to iteratively determine the relative importance of one factor over another. Simple rating and ranking systems for assigning weights are also commonly applied but lack statistical basis and are often opaque in the rationale behind weighting decisions (Malczewski, 1999). Criteria were aggregated using an additive function for groundwater vulnerability and asset density layers separately.

Evenly weighted groundwater vulnerability index values were approximately normally distributed. Values were categorised into low, medium and high vulnerability classes based on quantile breaks (at 33rd and 66th percentiles) in pixel counts for the evenly weighted result giving 3 classes of equal area. While these classes are arbitrary, they served for relative assessment of vulnerability within the study area and for comparison against results of perturbed weights for sensitivity analysis.

The asset density assessment differed in that different asset classes were not considered to vary in their significance so did not require weighting sensitivities to be analysed. The normalisation of asset data was performed in order to integrate data with different geometries and units of measure into a common format so that the total asset 'density' could be determined on a relative scale for the child model extent.

3.2.5 Groundwater vulnerability sensitivity analysis

Sensitivity analysis is a critical step in GIS MCDA problems and gives valuable information as to the relative influence of criteria used in the assessment and the underlying assumptions regarding the certainty in weight assignments and attribute values. It is of particular importance regarding weights due to the subjectivity of prioritising criteria and where a decision maker's choices can greatly influence the results hence this is often the largest source of uncertainty in MCDA problems. The other often more difficult to quantify source of uncertainty relates to the data accuracy both in terms of positional error and values. Stochastic approaches to quantify this uncertainty is a direction of active study in this field. Sensitivity analysis comparing slight perturbations from the evenly weighted scenario guides decisions on, and informs implications of, applying weights if deemed necessary.

In this study the sensitivity of each criterion related to the groundwater vulnerability index was assessed in terms of deviations of total area in each vulnerability class compared to the evenly weighted, base case scenario. Each criterion was normalised on a linear scale of 0-1 so began with equal influence on the result. Weight sensitivities were assessed by increasing the relative weight of one criterion at a time by 10%. Class break values consistent with the evenly weighted base case were used to classify results of the sensitivity tests in order to compare the change in class areas.

3.3 Results

3.3.1 Tertiary Limestone Aquifer groundwater vulnerability

Depth to water table across much of the child model extent was <1m and generally <5m in the vicinity of proposed gas wells (Figure 6**Error! Reference source not found.**A). A zone corresponding with higher topography and slope extending from the south west and up through the centre of the child model extent coincided with deeper water tables and lower clay content. The flat topography of the region results in a large amount of internal drainage areas and these are largest and deepest on the western side of the child model extent (Figure 6C). Soil clay content follows the pattern of slope where lower slope areas contain higher clay content (Figure 6D). Groundwater velocities are expected to be higher in some central areas and areas to the north-west and south-west of the child model extent (E). Based on the initial heads from the South East Regional Water Balance model (Morgan, et al., 2015), groundwater gradients in the area ranged from 2% in the south-central and south-western area through to 27% in the north-east and south-western corner. Saturated thickness varied from 11 m in the south-east up to 245 m in the north-west. Hydraulic

conductivities ranged from 8 m/d along the western edge of the model area (except for a section in the north-west of 58 m/d), around 20-45 m/d in the centre of the child model extent, and 12-20 m/d for most of the eastern part of the area. Historically, higher average annual rainfall, and consequently rainfall driven recharge, occurs in the south west of the child model extent and is lower toward the north (Figure 6F).

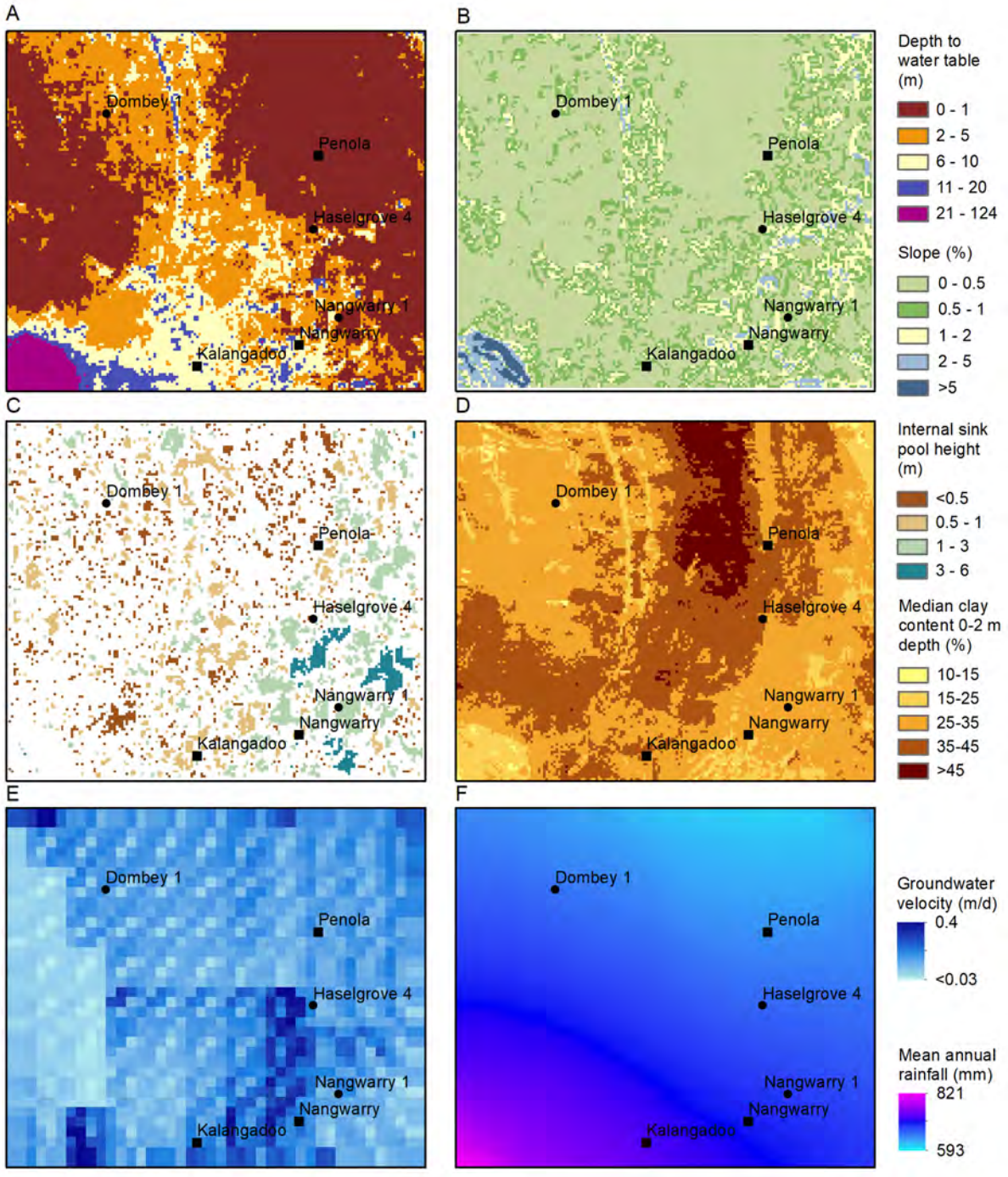

Figure 6: Groundwater vulnerability indicators per 250 m model cell within the 36 x 42 km child model extent; A) depth to Tertiary Limestone Aquifer water table); B) slope; C) internal sink pool height; D) median clay

content integrated over the upper 2m of soil; E) groundwater velocity based steady flow using regional scale model initial parameters; F) mean annual rainfall resampled to 250 m resolution.

An evenly weighted additive combination of normalised input layers is visualised in Figure 7 as a groundwater vulnerability index. It is apparent when comparing Figure 7A with the input layers shown in Figure 6 that lower vulnerability across the north-east of the child model extent corresponds with lower internal drainage, higher clay content, lower groundwater velocities, and lower rainfall and appear to offset the effects of shallow water tables and lower slopes in this area. Similarly, in the south west corner of the area, higher vulnerability associated with greater recharge potential and lower clay content, are offset by the higher slope, less internal drainage area, and deeper water tables.

All gas well locations have relatively high vulnerability areas near them (Figure 7A). The average vulnerability index value (on a scale of 0-1) for a 5 km radius around the Nangwarry 1 well was higher (0.54) compared to Dombey 1 and Haselgrove 4 (both 0.45). The Nangwarry 1 was within an area of high vulnerability (Figure 7D) that extended throughout much of the southern part of the child model extent (Figure 7A) that was mainly related to slope and water table depth, and higher estimated groundwater velocities particularly in the central and south-western parts of the child model extent (Figure 7D). The area of high vulnerability around the Dombey 1 (Figure 7B) is due to a combination of low slope, shallow water table and low clay content. High vulnerability areas around Haselgrove 4 (Figure 7C) were also related to slope, water table and clay, and to a lesser extent higher groundwater velocity. The adjacent area of low vulnerability to the west of this location is a result a step change in (higher) estimated groundwater velocities (Figure 7E).

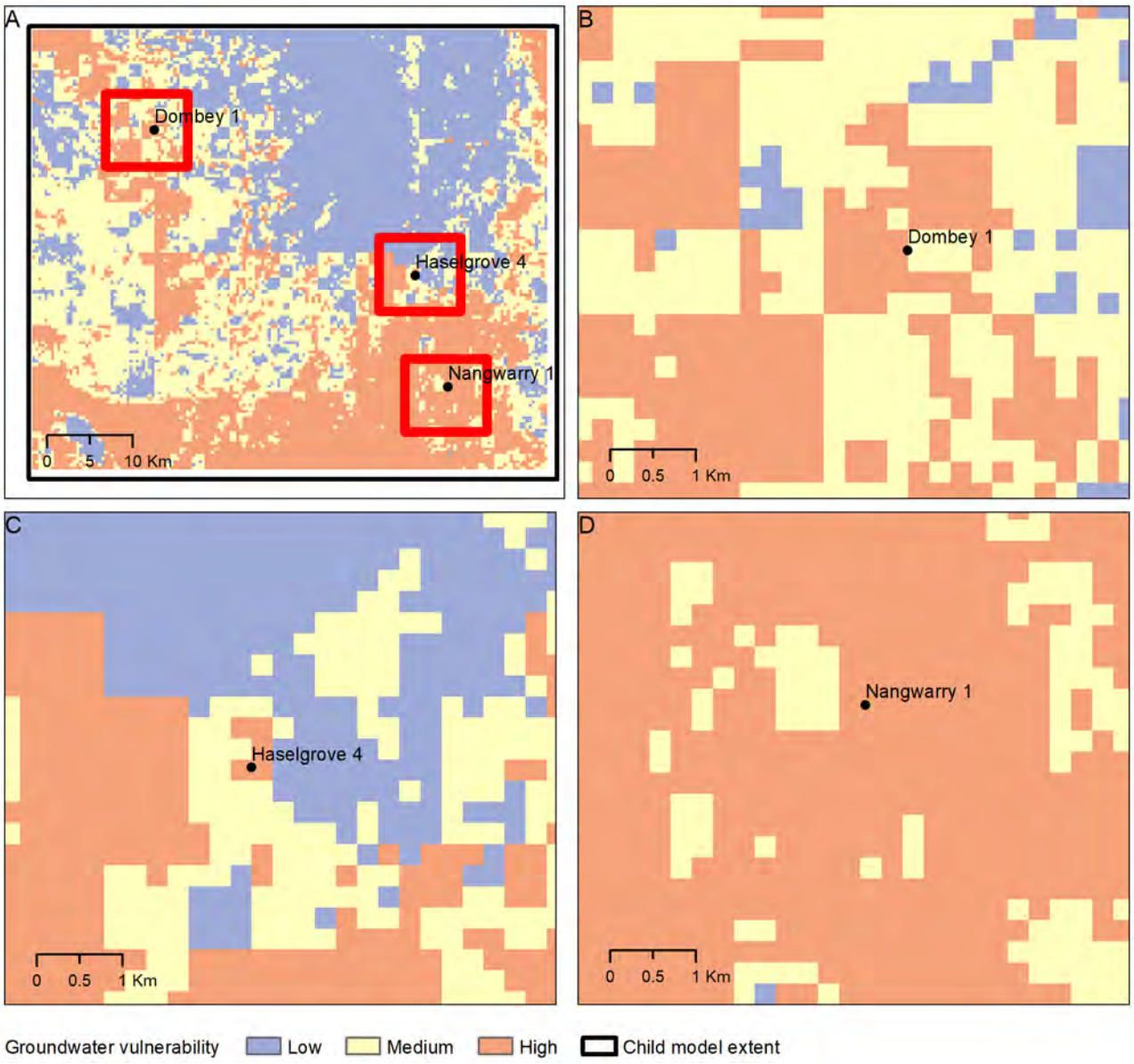

Figure 7: Groundwater vulnerability using evenly weighted criteria in the child model extent (A), and around gas well locations Dombey 1 (B); Haselgrove 4 (C); and Nangwarry 1 (D).

3.3.2 Tertiary Limestone Aquifer sensitivity analysis

The groundwater vulnerability sensitivity analysis revealed the most sensitive parameters were internal sink pool height, slope and depth to water table Table 4. Increasing the weight of internal sink pool height resulted in a 31% increase in low vulnerability area and this can be attributed to the heavily left skewed distribution of the data that were dominated by zero and very shallow pool heights with limited areas of deep internal sinks (Figure 6C). Increasing the weight of the depth to water table parameter resulted in increasing the area of high vulnerability by 28% The heavily right skewed distribution (in terms of the normalised input where shallow water table areas received values closer to 1 representing higher vulnerability) explains this result as there were large areas of very shallow water tables throughout the child model extent. A similar pattern was evident for slope where most of the extent is very flat and hence more vulnerable so increasing the weight of this parameter resulted in larger areas falling in the high vulnerability class.

The least sensitive parameter was clay content; a 10% increase in relative weight resulted in a 1% increase of area in low and high classes. This result is due to the clay content data across the child model extent being normally distributed and applying the tercile class breaks from the evenly weighted realisation.

Table 4: Change in groundwater vulnerability class areas as a result of 10% increases in each criterion weight compared to even weights.

	Change in area (km²)			Percent change in area		
Criteria	Low	Medium	High	Low	Medium	High
Internal sink pool height	152.8	-40.6	-112.3	31.4	-8.3	-24.3
Groundwater velocity	90.8	-34.5	-56.3	18.7	-7.1	-12.2
Rainfall recharge	48.9	-21.3	-27.6	10.1	-4.4	-6.0
Clay content	5.2	-10.4	5.2	1.1	-2.1	1.1
Slope	-118.8	-7.9	126.8	-24.4	-1.6	27.5
Depth to water table	-123.3	-4.7	128.0	-25.4	-1.0	27.8

3.3.3 Tertiary Confined Sands groundwater vulnerability

The groundwater vulnerability index (normalised on a scale of 0-1) for the TCS aquifer was a sum of normalised vertical travel time to reach the TCS aquifer, and groundwater velocity estimates which were based on initial conditions from a regional model v(Morgan et al. 2015) and reported values for aquitard conductivity (Mustafa and Lawson 2011). The result is shown in Figure 8 and indicates the highest vulnerability in the southern area corresponding mainly to vertical travel times to the TCS aquifer of <1 year (Figure 5). The 5 km radius around the Nangwarry 1 well location had the highest average vulnerability index value (0.28) compared to the areas around Dombey (0.02) and Haselgrove (0.05).

A sensitivity analysis on two parameters was not required. The classification of the vertical travel time to the TCS aquifer effectively applied a weighting to the areas with <1 year and <2 year travel times, and areas with higher travel times (from 2 to 334 years) had much lower overall influence on the result. If vertical travel times to the TCS aquifer were to be ignored, and vulnerability was related to groundwater velocity, the Dombey well location would have the lowest vulnerability, and the other wells would be about the same.

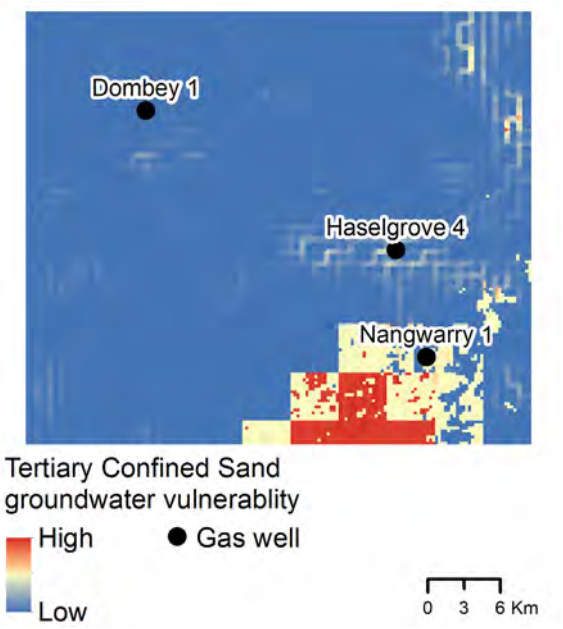

Figure 8: Groundwater vulnerability of the Tertiary Confined Sand (TCS) aquifer based on evenly weighted addition of vertical travel time to reach the TCS aquifer and TCS groundwater velocity.

3.3.4 Asset density and proximity

Input data for the vulnerability assessment prior to normalisation are shown in Figure 9. Economic assets included productive land uses with hydrological connection to the TLA such that a reduction in the quality of the groundwater as a result of contamination could adversely affect the economic value of the land. These were predominantly agricultural land uses growing deeper rooted plants, e.g. softwood and hardwood forests, fruit trees and nuts and grape vines, and excluded other land uses for example industrial and commercial land, and those growing shallower rooted plants like cereals and pastures that would be less likely to be affected by contamination of the aquifer. Together, these land uses occupy a considerable proportion of the child model extent (Figure 9A). Most of this land consisted of soft and hard wood forestry together occupying around 46,000 ha within the child model extent. In addition, 4,400 ha of vineyards occur within the study extent that are part of the Coonawarra wine region. The second group of economic assets were water bores for private, commercial and industrial water production. Bore density was highest near the town of Penola and north around the town of Coonawarra (Figure 9B). There was a total of 57 bores within 2 km of the 3 proposed gas wells (Dombey 1, Haselgrove 4 and Nangwarry 1).

Proportional areas per model cell of GDEs, protected conservation parks and forest reserves, the largest of which is the Nangwarry Forest Reserve north of the Nangwarry 1 proposed gas well location, are shown in Figure 9C. GDEs are widespread throughout the child model extent and consisted mainly of vegetation (typically Eucalypt forests) and wetland areas (Figure 9C). Species richness per model cell based on overlapping distributions from the SNES database (DOEE, 2018) indicated areas of higher richness in the east and north-east of the child model extent (Figure 3E). Watercourse and drain density were generally higher toward the western part of the child model extent (Figure 9F).

Sociocultural assets included a variety of heritage and historic buildings listed in National and South Australian State databases and are shown in Figure 9D. The rationale for inclusion of buildings of sociocultural significance follows that taken for the Bioregional Assessments Program where such assets were included due mainly to exposure to risks associated with inundation due to the potential for induced changes in hydrology (Mount et al., 2015). It could be argued that the applicability of this rationale to the specific problem as defined in this study is unfounded as changes to surface hydrology as a result of gas development are not expected. The combined area of these features was <0.5% (6 km^2) of the child model extent and not near any proposed gas well location; inclusion in this assessment was therefore inconsequential. Indigenous Land Use Agreement and Native Title Determination areas were not present in the child model area.

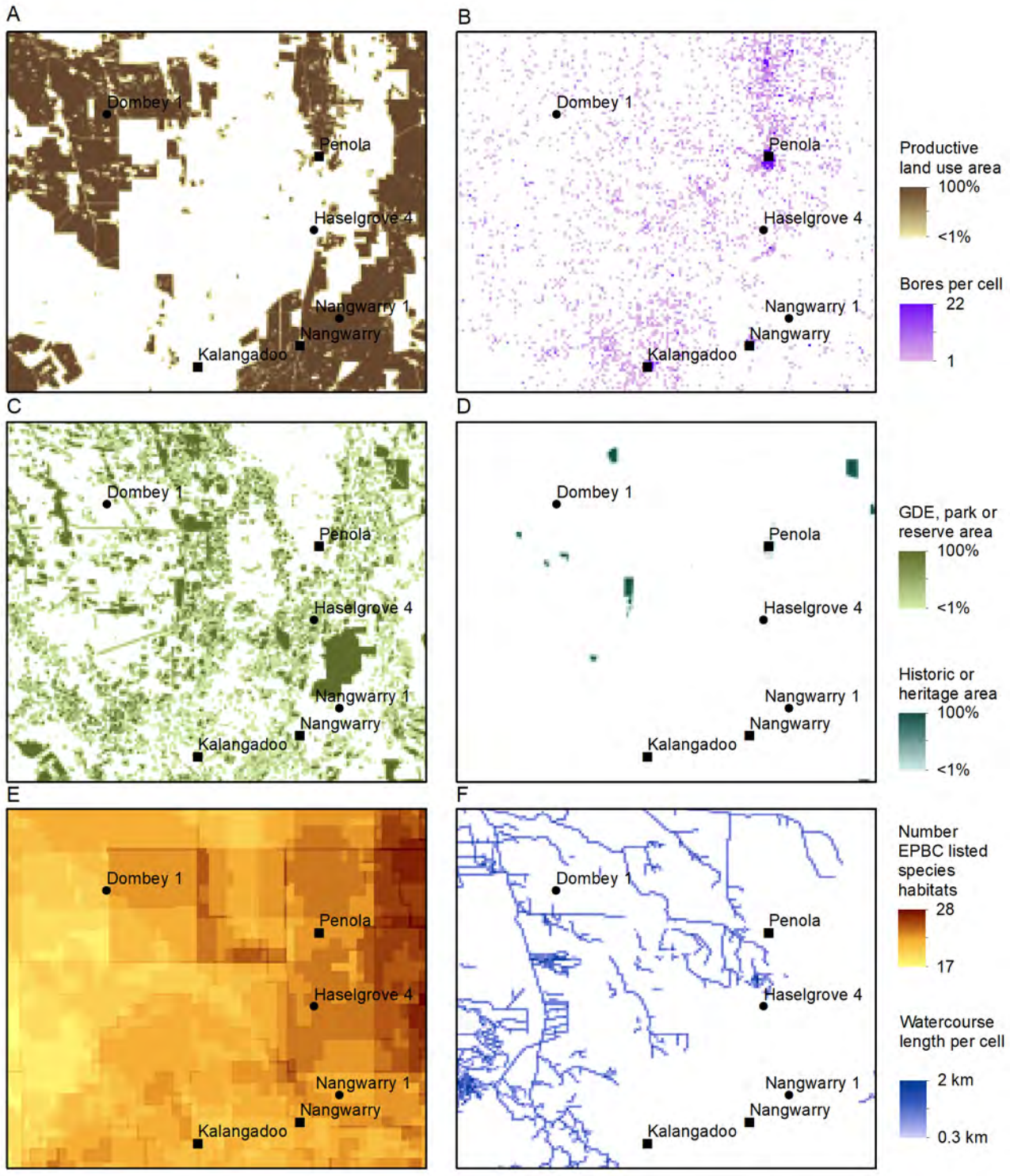

Figure 9: Asset densities per 250 m model cell within the 36 x 42 km child model extent; A) agricultural and forestry land use with dependence on surficial aquifers; B) water extraction wells; C) GDEs and protected reserves and conservation areas; D) Historic or heritage listed areas; E) listed species distributions and habitats; F) watercourses.

The evenly weighted additive combination of normalised asset density input layers is visualised in Figure 10. The area of high density along the eastern side of the child model extent (Figure 10A) results mainly from the overlap between economic land uses (Figure 10A) and habitat distributions of listed species (9E).

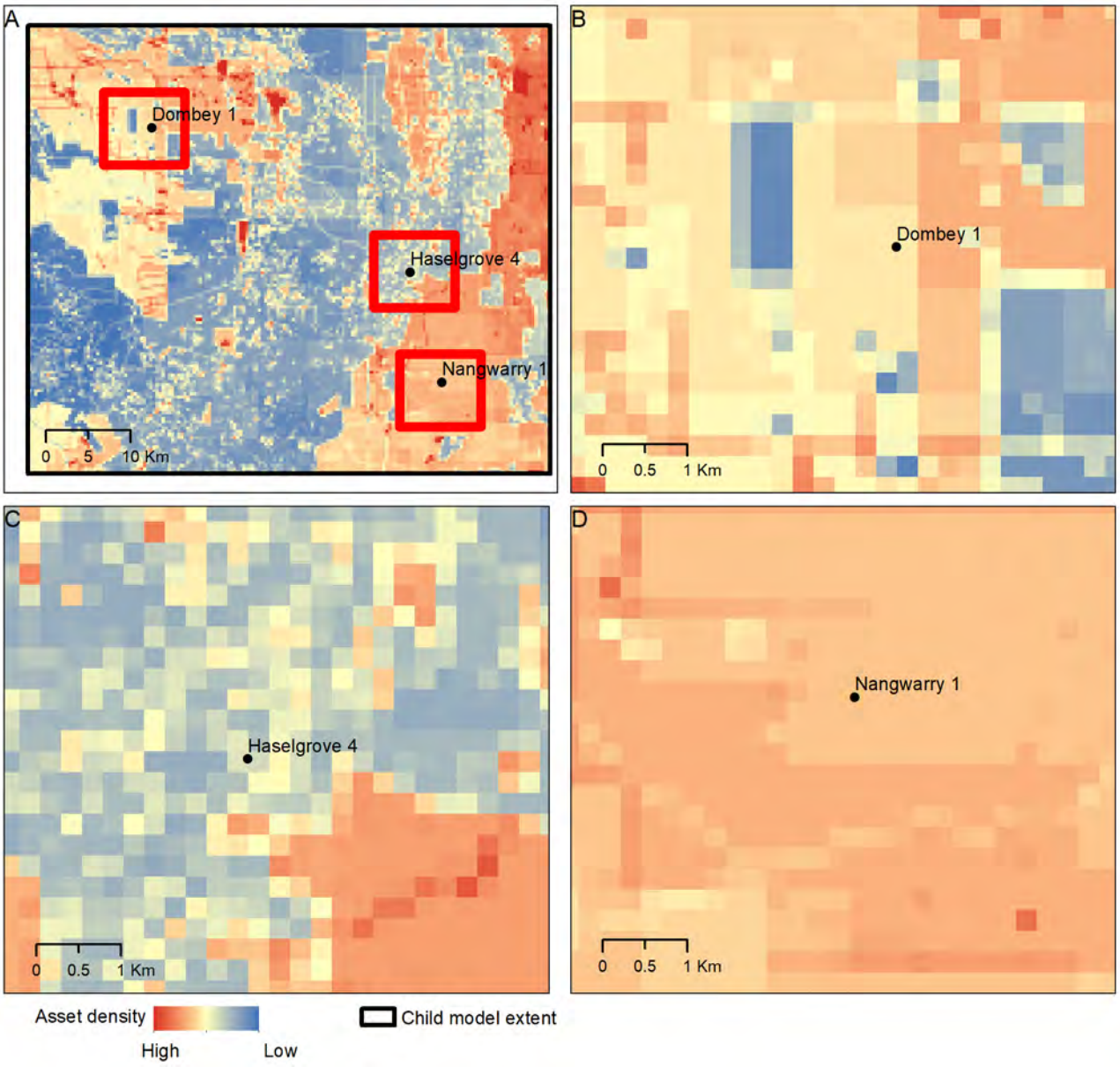

Figure 10: Asset density using evenly weighted criteria at child model extent (A), and around gas well locations Dombey 1 (B); Haselgrove 4 (C); and Nangwarry 1 (D).

Dombey 1 is located in an area of medium asset density (Figure 10B), Haselgrove 4 in an area of relatively low asset density (Figure 10C), and Nangwarry 1 in an area of relatively high asset density (Figure 10D).

3.4 Key findings from the vulnerability and asset density analysis

The vulnerability and asset density analysis using the physiographic characteristics informed that there are areas with relatively high vulnerability and high asset density in the vicinity of the three gas wells. While the vulnerability index is derived as a weighted sum of the different physiographic factors and is subjective, it still demonstrated that some of the physiographic characteristics are conducive for contaminant migration from the land surface towards groundwater. For example, characteristics like shallow depth to water table and high recharge rates resulting from flat terrain informed that there is some likelihood that contamination pathways arising from events such as spill or leakage on the land surface do have a potential to migrate towards groundwater faster than other areas that are having deeper water table and steeper slope. Flow and transport modelling analysis to simulate the transport of such contaminants in the soil and aquifer is warranted to investigate the concentration changes in the soil and aquifer and assess the risk of contamination at potential receptor locations. The modelling analysis should quantitatively incorporate the physiographic characteristics and properties of the soil and aquifer media to simulate the dilution characteristics of contaminant transport. The details of the modelling analysis and the key results are described in the following sections.

4 Modelling methods

4.1 Flow pathways

The conceptual models underpinning the assessment of deep groundwater pathways related to drilling consider previously discussed plausible pathways for exposure and allow assessment of contamination risk on the basis of comparing particle transport time to a receptor against time to attenuate the chemical to a certain percentage of the initial concentration. This is consistent with the methodology applied for deep groundwater pathways associated with migration of hydraulic fracturing chemicals used in coal seam gas developments (Mallants et al., 2017b). Chemicals may be considered to present elevated exposure potential if they have more than a predefined % of their initial source concentration remaining at the target receptor (see e.g. recent work by Rogers et al., 2015). How much attenuation will occur for a given chemical depends on the chemical's transport time, the geologic formations that provide sorption potential, and the geochemical conditions of the groundwater between source and receptor. Transport time depends on transport distance, groundwater velocity and geological attenuation (retardation) for a defined pathway.

Because of the complexity of calculating transport pathways from the surface or deep formations to adjacent aquifers, the total transport pathway is segmented into two individual segments consistent with previous assessments (Mallants et al., 2017b) (Figure 11). The first segment of the pathway takes the contaminant from the source to the groundwater and the second segment considers the transport within the saturated zone. In the case of surface-based pathway, the first segment comprises the transport of contaminants from the surface holdings or spills through the vadose or unsaturated zone into surficial groundwater. In case of a deeper pathway such as leakage through the micro annulus of a gas well, the first segment comprises the movement of the contaminant through the annulus into the aquifer. Because of the complexity of calculating fluid movement through such micro annulus, this segment is not explicitly simulated but it is assumed that a certain fraction of the used fluid (here drilling fluid) leaks into the overlying aquifer. From then onwards, a solute plume will develop in the aquifer as the chemicals are transported by the groundwater. This comprises the second segment.

The second segment for both pathways is conceptually similar and involves the use of particle tracking to calculate travel times between source (e.g. location of the leaky well) and receptor. From the transport times, chemical attenuation is calculated and a predicted environmental concentration at the source is derived. Using this flow segmentation approach different transport models or approaches may be used to derive the travel time in each segment separately. If indeed the transport time can be assessed in each of the individual segments, then total transport time is obtained from aggregation of the individual travel times for each segment. In this study, a loosely coupled modelling framework is

developed to provide an integrated assessment of transport and attenuation in the unsaturated and saturated zones. In this approach, the breakthrough curve (time series of concentration) obtained from the unsaturated zone modelling is used as an input into the saturated zone models for cumulative quantification of concentration changes and attenuation.

For the current study, to provide a broad range of plausible transport pathways across gas production areas in the southeast of South Australia, the transport pathways and the corresponding travel time from a contaminant source to a receptor will be calculated in the target study area. The groundwater model developed for the study area in the companion GISERA project (Doble et al, 2020) is used for this purpose.

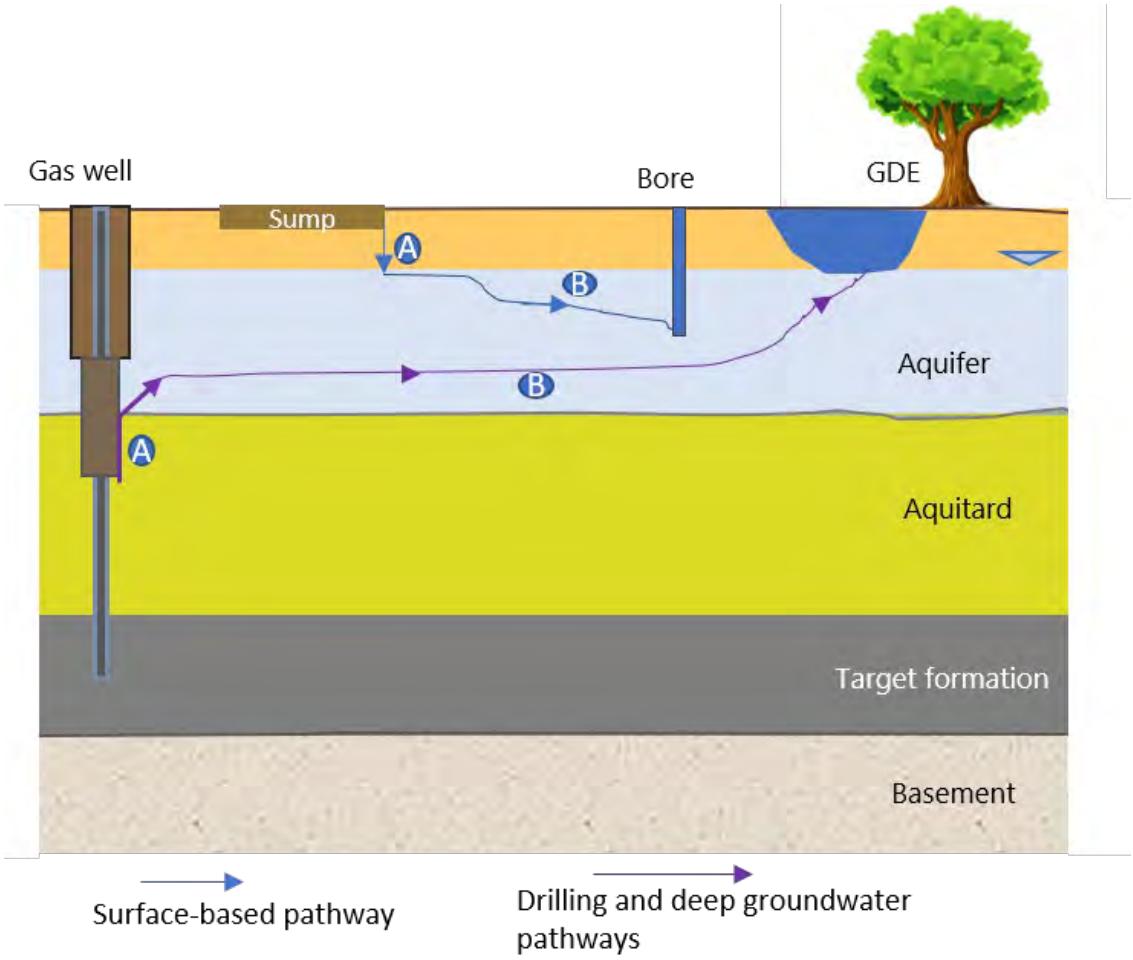

Figure 11 Conceptual diagram illustrating the segmentation of the flow path for the two broad pathways; the surficial groundwater-based pathway and the deep groundwater pathway (modified after Mallants et al. 2017b)

4.2 Solute transformations

As solutes travel in porous media, they undergo natural attenuation processes that include (1) physical attenuation (dilution and dispersion), (2) geological attenuation (adsorption), and (3) chemical/biological attenuation (degradation). These naturally occurring processes in soil and groundwater environments reduce the mass, toxicity, mobility, volume, or concentration of contaminants in these media without human intervention (US EPA, 1998a).

Physical attenuation involves dilution and dispersion whereby solutes spread and mix within the porous media. Dispersion is mainly attributed to the tortuous nature of the porous media that lead to variations in the local pore water velocities. The dispersive solute mass flux is given by:

$$J_d = \theta D \frac{\partial C}{\partial x} \quad \text{(Eq. 3)}$$

where C is solute concentration (M/L^3, where M and L are mass and length units, respectively), D is the mechanical dispersion coefficient (L^2/T, where T is a time unit) with molecular diffusion neglected, θ is the volumetric water content (L^3/L^3), and x represents the spatial scale in the flow direction (L). The coefficient of mechanical dispersion is dependent on the pore structure of the porous media, and is often approximated as being linearly related to the pore water velocity:

$$D = \lambda v \quad \text{(Eq. 4)}$$

where v is the flow velocity (L/T), and λ (L) is the dispersivity, which is a scale-dependent characteristic property of the porous medium. The parameter λ can be approximated by assuming it is roughly equal to 10% of the transport distance (Gelhar et al. 1992; Skaggs and Leij, 2002).

Geological attenuation causes a temporary removal of solutes from the water phase as they interact with the solid phase (the soil or rock matrix) by chemical, physical or electrostatic forces. This process is referred to as adsorption with solutes having the potential to return to the liquid phase via the desorption process. When solutes are adsorbed to the surface of the soil particles, this causes a delay in solute breakthrough. Linear equilibrium sorption has been widely used to describe solute retention by soils and aquifer sediments (Helfferich, 1962; Sposito, 1984; among others). K_d is an empirical distribution factor of the linear adsorption isotherm that relates S (adsorbed concentration) to C (liquid concentration). The K_d parameter quantifies instantaneous, linear and reversible sorption, and describes the capacity of a solid to remove a dissolved chemical from the liquid phase to the solid phase. When sorption is fast compared to the groundwater flow velocity, it is almost

instantaneous, and thus time-independent, and is referred to as equilibrium sorption. More details about adsorption isotherms are mentioned in Appendix II.

Chemical/biological attenuation is often described as a first-order degradation or decay of the source concentration, C_0 (M/L):

$$C = C_0 e^{-\mu t} \quad \text{(Eq. 5)}$$

where μ is a first-order decay constant (1/L), and t is time (T). The decay constant may be defined as:

$$\mu = \frac{ln(2)}{T_{1/2}} \quad \text{(Eq. 6)}$$

where $t_{1/2}$ is chemical half-life (T) with a shorter half-life leading to a faster decrease in concentration.

The geological and chemical/biological attenuation parameter for the drilling chemicals, which are listed in detail in Appendix III, were used to inform the parameters ranges adopted in the stochastic modelling of solutes in this work.

4.3 Mechanisms and pathways of solute delivery

A critical component when assessing the risks associated with gas operations is identifying various gas production activities that may potentially cause contamination, and hence define the mechanisms and plausible pathways of contaminant (solute) delivery to groundwater and/or surface water. Figure 13 shows the three potential solute transport mechanisms (hereby termed 'Scenarios'), that were considered in this study, each having a different mode for solute delivery, here represented by the concentration history $C(t)$. The contamination scenarios considered in this work are described herein. Modelling of each scenario was considered for the three gas wells considered in this study.

4.3.1 Scenario 1: Leakage from a drilling sump

Drilling sumps range in size and configuration, however a typical size as used in the Otway Basin would be 25 m × 30 m × 2 m sumps built to hold drill cuttings and waste drilling muds (as per discussions with SA DEM team at the workshop/meetings). These sumps are lined with a low-density polyethylene liner (LDPE) and a geosynthetic liner underneath. The latter liner does not contribute directly to containment of fluids but adds to the robustness of the LDPE line. The position of the sump is generally within 10-20 m of the well head. In this scenario we consider slow leakage from a drilling sump caused by a tear on the LDPE lining. Such a leakage may not be immediately detected and hence leakage for a hypothetical period of 1 month was considered for simulation.

Lining systems used in water holding ponds can vary considerably in complexity. The simplest lining systems consist of a compacted clay liner (CCL), a geosynthetic clay liner

(GCL), or a geomembrane (GM) liner overlain by a granular drainage collection layer. A more sophisticated and effective lining system incorporates a composite liner comprised of a GM placed directly on top of a clay liner (or other type of soil liner). The most effective design considers a double composite liner with a leak detector and / or leachate collection system. The advantage of GCLs over traditional clay liners is that they are easy to install, have a low hydraulic conductivity and they can self-repair holes upon contact with leachate water, caused by the swelling and self-healing bentonite. Current engineering practices for lining landfills and storage ponds consider double liner systems which incorporate leakage collection systems. While generally low, leakage (the combination of advective and diffusive migration of chemicals) from a composite liner (GM combined with either a CCL or a GCL) cannot be avoided and is mainly due to the fact that a GM installed as part of liner system will generally have some holes (Rowe, 2012; Rowe et al, 2004, Rowe and Hosney, 2010).

Leakage rates compiled from waste containment systems range from 5×10^{-13} m/s (0.016 mm/year) to 5×10^{-9} m/s (158 mm/year) depending on the type of liner [Bonaparte et al, 2002]. Any selection of a leak rate for solute transport calculations should represent normal operations of the water holding pond, i.e. a performance that is at least as good as the design specifications and possibly better. The selected leak rate also has to account for additional factors, including the variation in liner designs across the Australian landscape, the uncertainty about the leak rate for a specific liner design, and the advances in installation quality and construction quality assurance practices yielding better performing liners. Therefore, any risk assessment should consider a range of leak rates rather than a single “best estimate” leak rate.

As discussed above, there are several alternatives for lining systems. Drilling sumps are temporary and either rehabilitated intermediately following drilling or in general within 12 months post drilling. The drilling sumps considered here are lined with a low-density polyethylene (LDPE) GM liner with geo-synthetic liner (GCL) below to provide protection. Such a composite liner provides an effective barrier to leakage but may still be prone to being punctured. In this modelling scenario, a tear is assumed to occur for a period of 30 days, this exposes the soil surface underneath the liner to a pressure head of 2 m (equal to the depth of the sump, assuming it is completely filled with fluid). Subsequently the liner is assumed to be sealed (i.e., repaired), which results in a freely draining soil profile underneath the liner (for as long as the liner is present and prohibits rainwater from entering the soil).

4.3.2 Scenario 2: Gas well of compromised integrity

This scenario corresponds to release of solute directly into the aquifer due to incidents leading to well integrity loss. High pressure release of fluids into aquifers is extremely unlikely due to the presence of multiple cemented casing strings. Figure 12 demonstrates an example of well design showing the multiple cemented casing strings that protect the aquifer. Full failure of three cemented casing strings resulting in the full well pressure entering the aquifer is extremely unlikely. A more realistic and plausible scenario for well

integrity loss is leakage into the aquifer due to the formation of a micro-annulus between the cement and casing/formation. This would result in a low flow rate of drilling fluids and gas entering the aquifer over a longer period of time. Two sub-scenarios are considered here: (a) leakage into the unconfined Tertiary Limestone Aquifer (TLA), and (b) leakage into confined Tertiary Sands Aquifer.

Leakage into the unconfined aquifer considered the release of drilling fluid into the bottom half of the TLA and its movement within the aquifer due to advection dispersion and dilution processes. The second sub-scenario is similar but considers leakage and transport processes within the confined Tertiary Sands Aquifer.

A comprehensive analysis of effective conductivity ranges for water flow through compromised well integrity was undertaken by Wu et al (2018). Based on this report and in consultation with the SA DEM engineers, it was revealed that the flow rates through micro annulus are extremely small. Calculations provided by SA SEM team using simplifying assumptions and data from the Haselgrove 3 well, resulted in a maximum flow rate of 0.0005 L/day (as per the discussions with SA DEM).

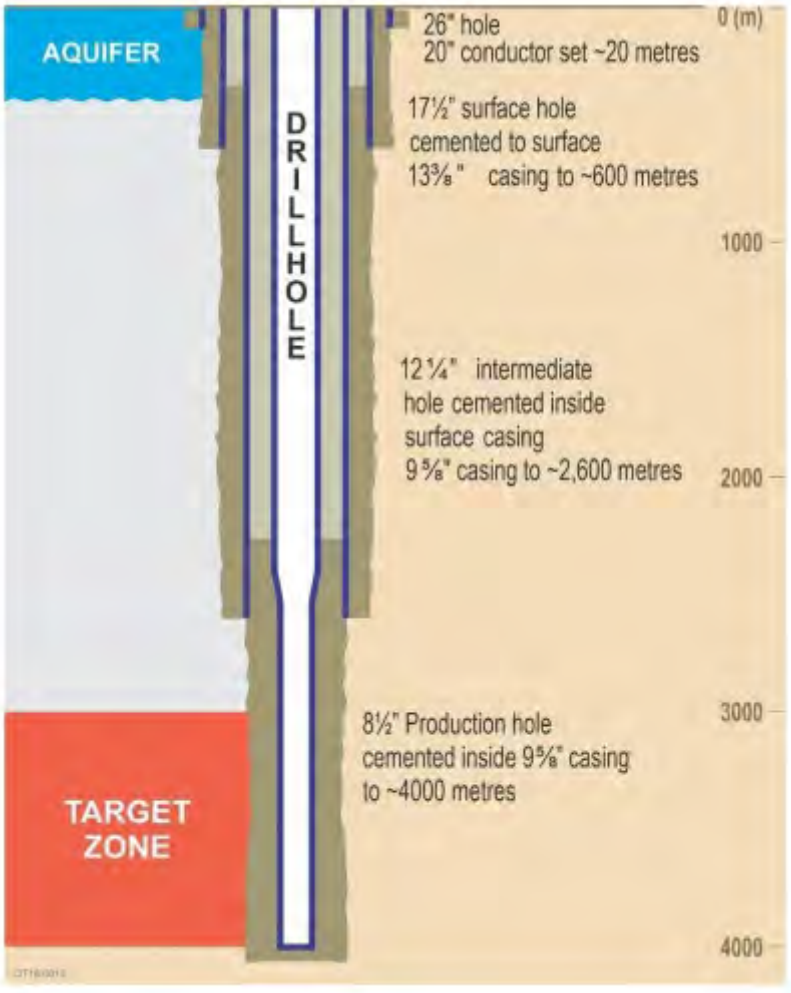

Figure 12: Well design with three cemented casing strings (Beach Energy Limited, 2019)

4.3.3 Scenario 3: Accidental surface spills and subsurface leakage

This scenario corresponds to leaking of fluids at or in the shallow sub-surface due to spills or leaks from pipelines. Two sub-scenarios are considered for this scenario: a) a spill at the surface and b) a pinhole leak from a pipeline in the subsurface.

Spill at the surface

Besides the drilling fluid and condensate, fuels are the most likely contaminant that could be spilled. Liquid storage, bund and spill management in South Australia is regulated by the relevant standards and acts stipulated by the SA EPA (2020). Spills of fuels and other substances is a risk that is associated with not only gas development operations, but with many other industrial operations. In most circumstances, there are standard bunding, management and clean-up protocols established to ensure that the residual risks for groundwater contamination is minimal. Detailed and site-specific modelling of solute and immiscible fluids is not warranted in this study. Separate modelling for Non-Aqueous Phase Liquids (NAPLs), nor for individual chemicals is beyond the scope of this study and will require site specific models. However, we considered one sub-scenario of spill, where solute spill occurs at the surface.

The major difference of the spill sub-scenario from the pipeline leak is that the spill occurs at the land surface and is instantaneously detected, immediately contained and cleaned up with spill kits available on-site. Hence the duration of the spill is very short and is assumed to be remediated within 1 day. The total volume of drilling fluid spill is assumed to be 1000 L and the surface area affected is 10 m^2. Solutes that have infiltrated the profile would either slowly drain freely or be pushed down and diluted by rainfall, in case the site is not remediated.

Pinhole leak from the pipeline

Flowline is the pipeline from the gas well to the facility and is usually located approximately 700 mm below the land surface. This sub-scenario considers a very small rate of leakage through a very small pin hole caused by corrosion from subsurface pipeline. Since the pipeline is buried under the ground and the rate of leakage is very low, such leaks may take some time before being detected and repaired, hence a 3-month duration of leak is considered. Total volume of spill considered in this scenario is 5000 L and is assumed to be uniformly distributed across the duration. The surface area that is affected by the leak is considered as 30 m^2. Solutes that have infiltrated the profile would either slowly drain freely or be pushed down and diluted by rainfall.

4.4 Stages for modelling solute transport

After defining the plausible pathways that can potentially cause contamination, groundwater-dependent assets that may potentially be contaminated should be identified. This involves the identification of all groundwater dependent assets within the flow domain then singling out those that intercept the calculated groundwater flow paths. Finally, one must select the appropriate tools to model solute transport from source to target for each scenario.

Given the complexity of the problem, the modelling work was carried out in stages with different modelling tools employed during each stage and different combinations of modelling tools employed for each contamination scenario. Figure 13 shows that Scenarios (1) and (3) involve transport in the unsaturated and saturated zones, whereas Scenario (2) involves transport only in the saturated zones. Flow in the vadose (unsaturated) zone involves the vertical leaching of solutes from the surface or shallow sub-surface through soil media to the groundwater table (the saturated zone, unconfined aquifer). Transport through the saturated zone involves the lateral movement of solutes until they intercept groundwater dependent assets. Hence, the solute modelling described herein involves two parts, which are relevant to the unsaturated and saturated zones.

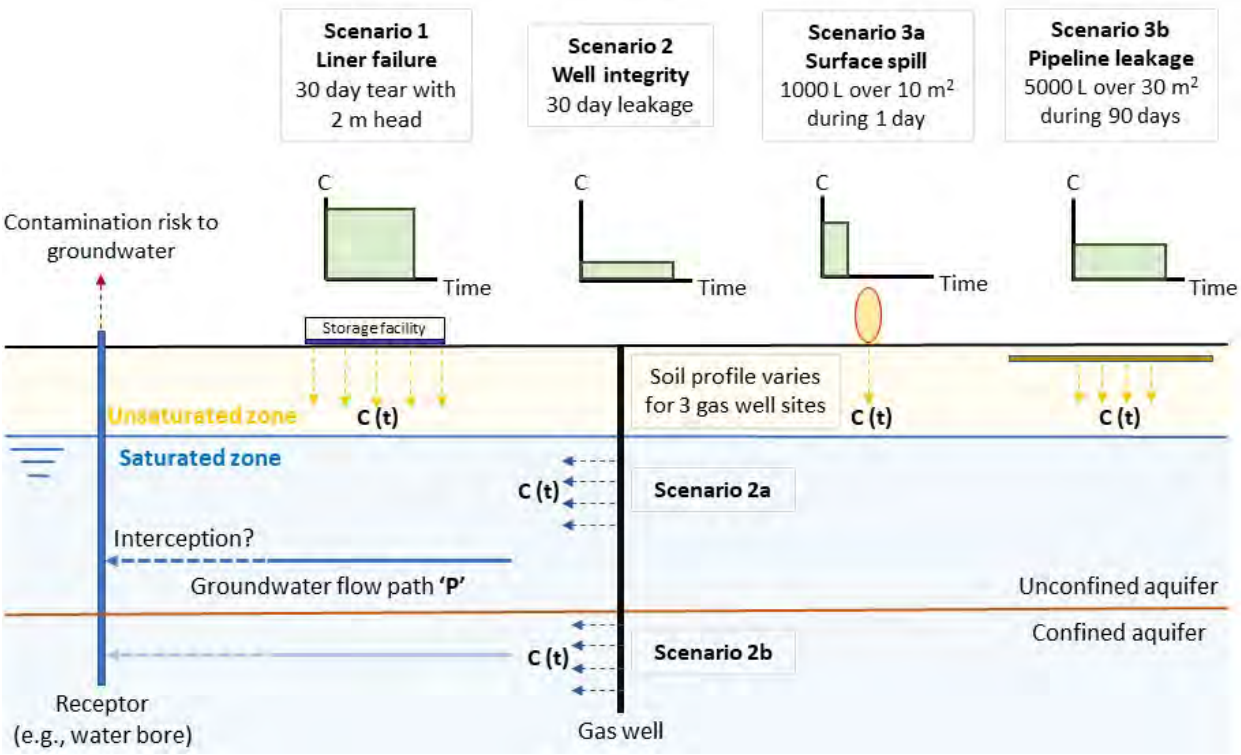

Figure 13: Conceptual diagram showing mechanisms of solute delivery from various gas production activities

4.4.1 Modelling solute transport in the unsaturated (vadose) zone.

Modelling solute transport in the unsaturated zone was carried out using HYDRUS-1D (Simunek et al., 2016). It is a one-dimensional numerical model that couples transient water flow with solute transport, where the governing differential equation for solute transport is given by:

$$\frac{\partial}{\partial t}(\theta C + \rho S) = \frac{\partial}{\partial x}\left(\theta D \frac{\partial C}{\partial x} - JC\right) - \mu_l \theta C - \mu_s \rho S \quad \text{(Eq. 7)}$$

where C is solute concentration in the liquid phase (M/L^3, where M and L are mass and length units, respectively), S is solute concentration in the adsorbed phase (M/L^3), D is the dispersion coefficient (L^2/T, where T is a time unit), θ is the volumetric water content (L^3/L^3), J is the volumetric water flux density (L/T), ρ is the soil bulk density (M/L^3), μ_l and μ_s are first-order decay coefficients for degradation of the solute in the liquid and adsorbed phases, respectively (1/T). Solute transformations that are modelled by Eq. 7 have been discussed in detail in Section 4.2.

The numerical solution for Eq. 7 involves a temporal discretisation of simulation time and a spatial discretisation of the flow domain. The former is done automatically by the software following stringent numerical stability requirements for both flow and transport. The flow domain is discretised into one hundred elements representing three different soil horizons for each of the three gas well sites considered in this work (Table 5). The hydraulic parameters for the three soil horizons for each of the three gas well sites are listed in Table 5, and include the saturated hydraulic conductivity, K_S, and the van Genuchten parameters θ_s, θ_r, α and n (van Genuchten, 1980); they were derived from the HYDRUS soil catalogue (Carsel and Parrish, 1988). The solute transport parameters listed in Table 5 are based on the information relating to drilling chemicals listed in Appendix III. With the exception of α, and n, all parameters in Table 5 are listed as ranges, from which values were sampled for the stochastic simulations.

The flow rate in the unsaturated zone depends on the hydraulic properties of the various layers comprising it. Depth of the groundwater table represents the length of the path through the unsaturated zone, considering one-dimensional flow. This is generally true, unless the soil has a significant slope with soil layers that promote lateral flow and transport. The flow rate and length of the pathway would dictate the travel (residence) time through the unsaturated zone, during which solute concentration would change due to various processes described in Section 4.2.

Table 5: Profile layers, hydraulic and solute transport parameters for three well sites

	Profile discretisation for gas well locations			Hydraulic parameters				
	Dombey	**Haselgrove 4**	**Nangwarry 1**	θ_s	θ_r	α (cm^{-1})	n	K_S (cm/day)
Horizon 1 sand	0 – 0.85 m	0 – 0.7 m	0 – 4.0 m	0.43	0.045	0.145	2.68	300 - 500
Horizon 2 sandy clay	0.85 – 2.5 m	0.7 – 3.0 m	4.0 – 7.0 m	0.38	0.1	0.027	1.23	4 - 14
Horizon 3 fine sand	2.5 – 5.0 m	3.0 – 5.0 m	7.0 – 9.0 m	0.43	0.045	0.145	2.68	80 – 150
Solute transport parameters								
Dispersivity			Triangular distribution (0.01L, 0.1 L, L); L is the length of flow path (m)					
Degradation half life			Triangular distribution (10, 80, 150) days					
Adsorption K_d			Log uniform distribution K_{OC} (0.002, 10); multiply by fraction of organic carbon, f_{OC} (1-2%), to obtain K_d ($K_d = K_{OC} \times f_{OC}$, where f_{OC} = 0.01 – 0.02).					

To be able to solve Eq. 7, simulation models require known initial conditions (initial pressure head and solute concentration distribution along the flow domain), and boundary conditions (in this case, pressure and solute concentration during the entire simulation period at the upper and lower end of the flow model as flow is 1-dimensional). The initial pressure head for the entire flow domain was set to a slight negative pressure of -10 cm (close to saturation), and initial concentration equal to zero (solute free). The lower boundary condition was assumed to be a freely draining boundary whereas the upper boundary conditions vary with the scenario under consideration. Scenario 1 assumes a constant head boundary at the soil surface of 2 m for 30 days, which represents the condition during liner failure, after which the simulation is stopped because the contaminated soil is removed. The other scenarios (3a and 3b) adopt a flux boundary condition. As Scenario 3 occurs in an open area, an atmospheric boundary is implemented, which includes rainfall and evaporation that drive recharge into the aquifer. The solute input for each scenario is represented by a function of concentration versus time $C(t)$ as shown in Figure 13, a unit concentration (C = 1) is assumed.

The outcome of the HYDRUS model simulation is a solute breakthrough curve (BTC-1, concentration versus time) at the interphase with the water table (see Figure 14: Stages for modelling solute transport). This becomes an input to the subsequent modelling stage in the saturated zone.

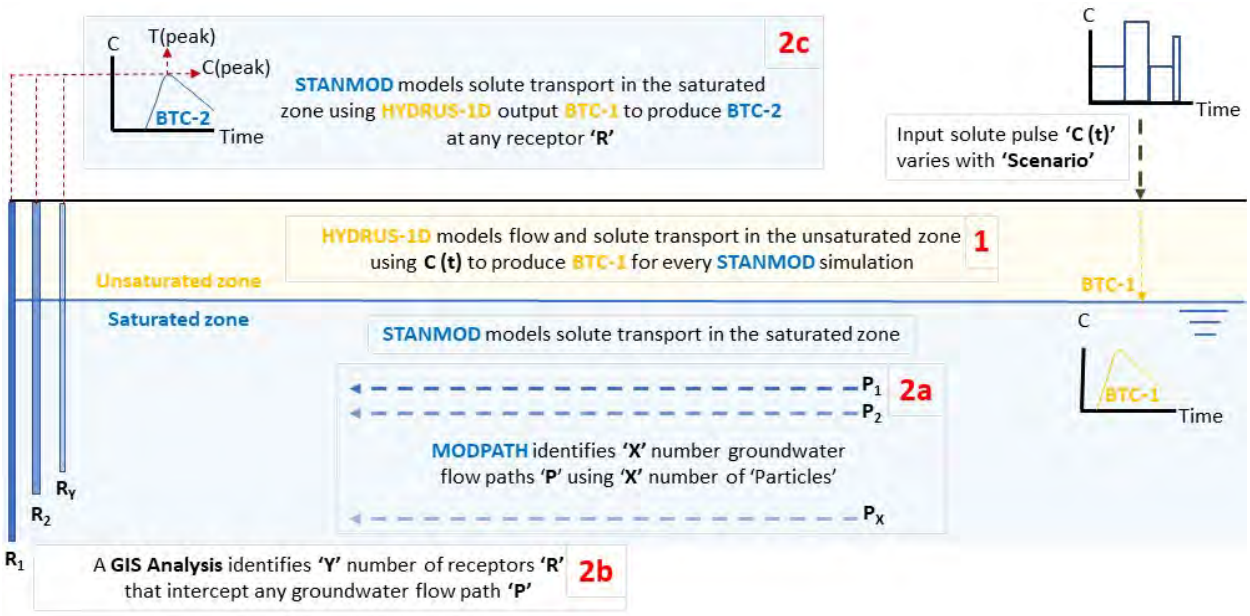

Figure 14: Stages for modelling solute transport

4.4.2 Modelling solute transport in the saturated zone

Modelling solute transport in the saturated zone is carried out using an explicit analytical solution for 1-dimensional transport under steady-state flow conditions, which means that the flow rate and the length of the flow path must both be known a priori. Hence, the modelling exercise involves three separate parts: (1) particle tracking analysis to identify potential flow paths and the associated flow rate for each (marked '2a' in red, Figure 14: Stages for modelling solute transport); (2) a GIS analysis to determine which of the potential flow paths do intercept a groundwater dependent asset, and hence identify the actual length of the path from source to asset (marked '2b' in red, Figure 14: Stages for modelling solute transport); and (3) solve the differential equation for solute transport to identify the BTC-2 at relevant receptors R (marked '2c' in red, Figure 14: Stages for modelling solute transport).

Particle tracking analysis

The child groundwater model developed in the companion GISERA project (Doble et al, 2020) was used for the particle tracking analysis. This child model formed the basis for running the particle tracking with MODPATH model (Pollock, 2012) to determine travel time of water particles (as proxies for chemical substances) in groundwater (i.e. the second segment of a chemical's pathway) and subsequently adjusts the chemical's travel time for any relevant attenuation process. Particle-tracking analyses are commonly used for mapping the recharge-contributing area to pumping wells (US EPA, 1994) and for obtaining transit times of groundwater at the discharge point (McGuire and McDonnell, 2006; Gusyev et al., 2014). The MODPATH-generated transit times represent the time taken by groundwater

molecules to travel in groundwater from the starting cell, e.g. the groundwater recharge area at the aquifer top, to an outlet cell such as a pumping well or a spring (Boronina et al., 2005; McGuire and McDonnell, 2006; Sanford, 2010).

MODPATH is a particle-tracking post-processing model that computes three-dimensional flow paths using output from groundwater flow simulations based on MODFLOW (Harbaugh, 2005). The program uses a semi-analytical particle-tracking scheme that allows an analytical expression of a particle's flow path to be obtained within each finite-difference grid cell. A particle's path is computed by tracking the particle from one cell to the next until it reaches a boundary, an internal sink/source, or satisfies another termination criterion. Output from steady-state or transient MODFLOW groundwater flow simulations is used in MODPATH to compute paths for imaginary "particles" of water moving through the simulated groundwater system. In addition to computing particle paths from the point of release until its final location, MODPATH computes the time of travel for particles moving through the system. The particle travel or residence time represents the velocity of a non-reactive chemical (no interaction with the solids) due to flowing groundwater; the effect of hydrodynamic dispersion and molecular diffusion on solute migration is neglected. A simplified way to account for the effect of dispersion and diffusion on dilution is by implementing an analytical solution of the three-dimensional advection-dispersion model for given particle pathways (see e.g. Mallants et al., 2017b).

The accuracy of numerically generated path lines, and a proper interpretation of what they represent, depends on the extent to which the groundwater system can be realistically represented by a discrete network of finite-difference or finite-element cells. The degree of spatial discretization in a finite-difference model influences:

– the level of detail at which hydrogeologic and system boundaries can be represented,
– the accuracy of velocity calculations,
– the ability to accurately and unambiguously represent internal sources and sinks.

In this study the numerical grid of the pre-existing groundwater model was locally refined to improve the accuracy of the tracks in the child model developed in the companion poject (Doble et al, 2020).

Particles are stopped whenever they reach points of termination or whenever the cumulative tracking time equals the maximum allowed value of 100 years. A particle terminates when:

– it reaches an external boundary face or an internal sink/source cell that captures the particle,
– it enters a cell with a zone code that designates the cell as a termination location,
– the cumulative tracking time has reached the maximum allowed value, or
– it encounters an abnormal condition that will not allow tracking to continue.

Particle tracking may evolve in two ways: either so-called “backtracking” is done starting from a selection of receptors working backwards to identify which part of the aquifer is connected to the receptor and what the travel time is, should there be a connection, or the tracking starts at the contaminant source and moves forward to identify pathways that may intersect a receptor. The latter is called “forward tracking”. Forward tracking is used in this study to determine how far particles will theoretically travel when released within the gas well area. Particle tracking is undertaken in a probabilistic model considering a wide range of plausible hydraulic characteristics of the Tertiary Unconfined Aquifer and Tertiary Confined Sand Aquifer to account for uncertainties in groundwater flow. Then the water bore and water course receptors that are located within a 10 m buffer of the particle tracks were selected to generate a subset of receptors in the region at which concentrations are calculated corresponding to relevant contamination scenarios.

Interception with groundwater-dependent assets

Locations of receptors (water bores, water bodies, drains and water courses) in relation to particle tracks and gas well locations were recorded to provide distances at which concentrations would be calculated corresponding to relevant contamination scenarios. For water bores, the distance along a track line from the start point to an intercepting bore (within 10 m of the line) was recorded, and from which the travel time was calculated based on average particle velocity. For water courses and water bodies, the Euclidian distance from a gas well location to the nearest vertex of a receptor intercepting a particle track line was recorded. Agricultural land and listed species habitats that while potentially vulnerable to contamination in the unconfined aquifer, were not analysed in relation to particle tracking. Start point locations were often within one or more overlapping boundaries of these features so were unsuitable for assembling contaminant transport scenarios.

Analytical solution of solute transport

The governing differential equation for 1-dimensional, advective-dispersive solute transport with first order degradation under steady-state flow conditions in a homogenous aquifer is giver by:

$$R_e \frac{\partial C}{\partial t} = D \frac{\partial^2 C}{\partial x^2} - v \frac{\partial C}{\partial x} - \mu C \qquad \text{(Eq. 8)}$$

where v (=J/η) is the average pore-water Darcian velocity (L/T), with η the effective porosity (-), and R_e is the retardation factor given by:

$$R_e = 1 + \frac{\rho K_d}{\eta} \qquad \text{(Eq. 9)}$$

The CXTFIT code, which is part of the software package STANMOD (Šimůnek et al., 2009) was used to solve Eq. 9. Solute transport parameters were sampled from the parameter ranges listed in Table 5. The output of solute modelling is BTC-2 (marked 2c in red, Figure 14: Stages for modelling solute transport) at each receptor location R (Figure 14: Stages for

modelling solute transport). The maximal concentration and the time at which it occurs are then derived from each BTC.

4.4.3 Stochastic coupled modelling approach

As hydraulic and solute transport parameters are highly uncertain, a probabilistic modelling approach was adopted where the uncertainty associated with input parameters was accounted for and results presented as probability distributions that reflect the risk of aquifer contamination. As three-dimensional flow and solute transport models are associated with long simulation times, they are not readily conducive to stochastic modelling methods. Hence, a one-dimensional approach was preferred. Note that varying model parameters stochastically can reflect heterogeneity effects that not accounted for in a 1-dimensional analysis. It is worth noting that lateral dispersion effects are not accounted in the current models, thus leading to an overestimation of solute concentrations. A one-dimensional analytical solution with one-dimensional dispersion in the saturated zone was selected, such that it is consistent with the unsaturated zone model HYDRUS-1D.

As flow and transport processes in the unsaturated and saturated zones were modelled using two different approaches, the relevant models were loosely coupled to achieve the modelling goal, which is identifying a range of maximal concentrations (for a range of plausible parameters sets) at receptors that intercept the flow path. The staged stochastic modelling process was carried out in this sequence:

The following steps were carried out once:

- Particle tracking analysis was carried out using MODPATH with a number of particles released within the vicinity of the three gas well sites to identify plausible flow paths within the MODFLOW model flow domain. The particle tracking was undertaken in a Monte Carlo simulation framework whereby many different plausible realizations of the model parameters constrained by available observations were used for simulating the particle tracks.
- A GIS analysis identified groundwater dependent assets that may potentially intercept these flow paths, and hence define their lengths and the flow rate for each path.

The following steps were repeated ‘n’ number of times. The number of simulations for each site and scenario was different as the number of interceptions with assets did vary. However, at least one thousand stochastic simulations were carried out at every site and for each scenario.

- A random parameter set for the unsaturated flow and transport model HYDRUS-1D was selected, which included the saturated hydraulic conductivity, adsorption coefficient, dispersivity, and degradation coefficient. For each contamination scenario (e.g., surface spill), one unique solute input function $C(t)$ was used for all stochastic simulations.

– HYDRUS-1D was executed once resulting in one BTC (marked BTC-1_1 …. BTC-1_n in Figure 15) for a unique flow path intercepting a receptor. For Scenario-1, a simulation period of 100 days was deemed to be enough to capture solute breakthrough approaching concentrations very close to zero. For Scenario-3 that involves recharge from rainfall, 4000-day simulations were conducted.

– The output from the HYDRUS-1D simulations was used as the solute input function to the saturated flow and transport model STANMOD; the function was approximated as the number of points in STANMOD is limited to ten. A random parameter set for STANMOD was selected, which included the retardation factor, dispersion coefficient, and degradation coefficient; the flow rate identified by MODPATH was explicitly used for each track.

– STANMOD was executed once resulting in one BTC (marked BTC-2_1 …. BTC-2_n in Figure 15). The time series of the BTC was analysed with the maximal concentration and time of its occurrence recorded (marked C(peak) and T(peak) in Figure 15). Depending on the length of the flow path, the time period of the simulations ranged from 500 to 7,000 days.

– The process was repeated n-times.

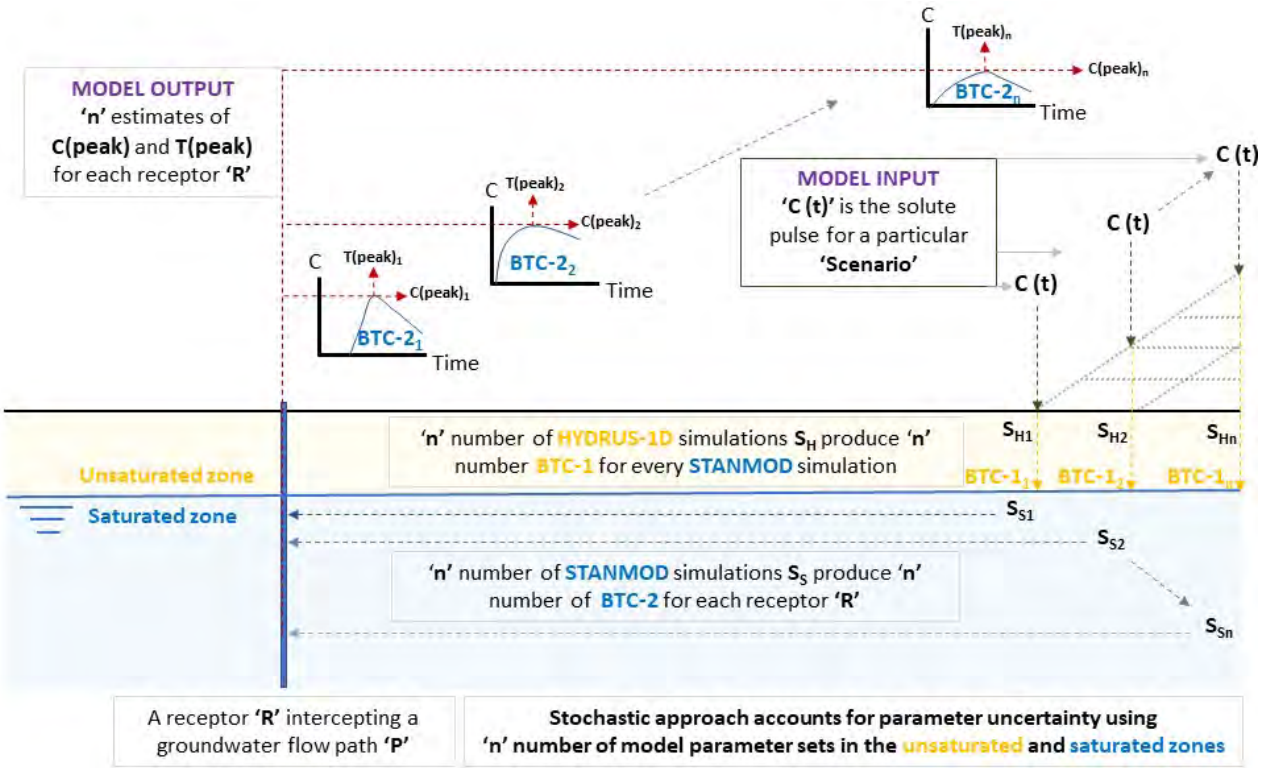

Figure 15: Implementation of stochastic modelling approach

5 Results

The methods described in Chapter 4 are generic and could be applied to contamination risk assessment of gas development in areas where pathways are likely to occur as described in Chapter 2. In this study, three existing gas well locations in southeast SA were chosen to illustrate this methodology for selected scenarios. However, the method could be used for other existing or new gas well locations as well. Three scenarios were constituted from the broader pathways of contamination identified in Chapter 2 for modelling-based risk assessment. These scenarios were developed in consultation with the Department of Energy and Mining of South Australia ensuring that the scenarios, whilst unlikely, are plausible to occur accounting for the regulatory and management mechanisms including realistic timeframes of detection and clean up set in place for minimising contamination risks at gas well sites. Particle tracking was undertaken to simulate the travel paths, distances and times from the three gas well site for all scenarios.

Particle tracking

The numerical groundwater flow model developed for the gas development region in the companion project (Doble et al, 2020) was used for simulating the particle tracks. This numerical model was built as a child model of the southeast regional water balance model (Morgan et al, 2015). The regional model has grid cells of 1 km × 1 km and the child model has a finer grid resolution of 250 m × 250 m. The regional extent of the regional and child models are shown in Figure 16.

The three-layer flow model was calibrated to observed groundwater heads from the Upper Tertiary Limestone and Lower Tertiary Confined aquifer. The most important processes that influence groundwater flow that are considered in the model comprises diffuse recharge from rainfall, groundwater contribution for evapotranspiration, groundwater flow into the drain network and groundwater use for irrigation, stock and domestic use in the region. The flow modelling considered two alternative approaches for simulating the recharge. First one used the MODLFOW recharge package and the second approach used the netR package for simulating the net recharge (Recharge minus evapotranspiration contributions) that was developed in CSIRO (Doble et al, 2017). The former version of the model using the recharge package was used for the particle tracking analysis. The details of the MODFLOW model development, calibration and uncertainty analysis are reported in the final report of the companion project (Doble et al, 2020).

Figure 16: Extent of the child model area used for particle tracking

Doble et al. (2020) carried out an uncertainty analysis with the parent groundwater model as summarised next. The uncertain parameters in the model comprised horizontal and vertical hydraulic conductivity, specific yield and specific storage of the two aquifers and intervening aquitard and conductance of the drains. These properties were represented in calibration and uncertainty analysis by using pilot points. Model calibration and uncertainty analysis for the model was done using the newly developed PEST-IES utility (White, 2018). The method employed by PEST-IES enables starting from a prior ensemble of parameter realization to evaluate the calibration objective function and progressively derive the posterior parameter set as the calibration procedure progresses. The calibration and uncertainty analysis of the model using the PEST-IES software resulted in the generation of 500 equally likely realizations of the model parameters that can calibrate the model to the observations. The parameter distributions corresponding to these model runs and other details of the MODFLOW model are described in detail in the companion project report (Doble et al, 2020). The spatial hydraulic properties comprising horizontal and vertical

hydraulic conductivity, specific yield and specific storage were represented in the model using the parameterisation devise called pilot points. This enabled to vary the spatially distributed pilot points during model calibration and uncertainty analysis while the heterogeneous spatial fields were generated by interpolating from the pilot points. The posterior distribution of the hydraulic properties in model layers 1 and 3 obtained from a calibrated run is shown in Figure 17. The uncertainty analysis resulted in the generation of 500 sets of model parameters constrained by available observations. A subset of 200 stochastic realizations from the posterior parameter sets was used in the particle tracking analysis. The number of realizations used in the stochastic particle tracking was largely guided by the available computing resources. However, given use of heterogeneous spatial fields in these realizations are constrained by only groundwater head observations, the Monte Carlo simulation resulted in a wide range of groundwater flow rates (Figure 21,Figure 23) encompassing the ranges calculated for the region for similar purposes in the recent study (Jacob, 2016).

One of the most important parameter-sets that influences the particle tracking is the effective porosity of the aquifer media. A wide range for the specific yield (effective porosity) was chosen for the prior distribution given the Karstic nature of the aquifer in the region. The calibrated specific yield value at the pilot points varied in the range 0.05 to 0.4. Realizations of the model parameters were used with the particle tracking software, MODPATH-7 to generate an ensemble of particle tracks that start from their initial locations around the gas wells. The vertical distribution of starting points of the particles differed depending on the scenarios. For the scenarios corresponding to the surface-based pathway (e.g. slow leakage from drilling sump), the particles are all starting near the top of the water table, assuming that the leaked fluid reaches the water table. The HYDRUS-1D model simulates the transport in the unsaturated zone and provides the breakthrough curve at the water table. The particle tracks starting from the water table are then able to compute the travel times and distances in the saturated zone. For the deep groundwater pathways, the particles were also distributed along a vertical column around the gas well. This is intended to simulate the travel path for different possibilities of the contaminant release occurring at any vertical distance within the aquifer due to micro-annulus leak or other factors in the vicinity of the gas wells. For all scenarios it was assumed that the starting point of the particle tracks could be horizontally located anywhere within the model cell containing the gas well or any cell adjacent to it. Forty-five particles were started from near each of the three gas wells, uniformly distributed across 9 grid cells each 250 x 250 m^2. The configuration of the particle starting locations around the Dombey well is illustrated in Figure 18.

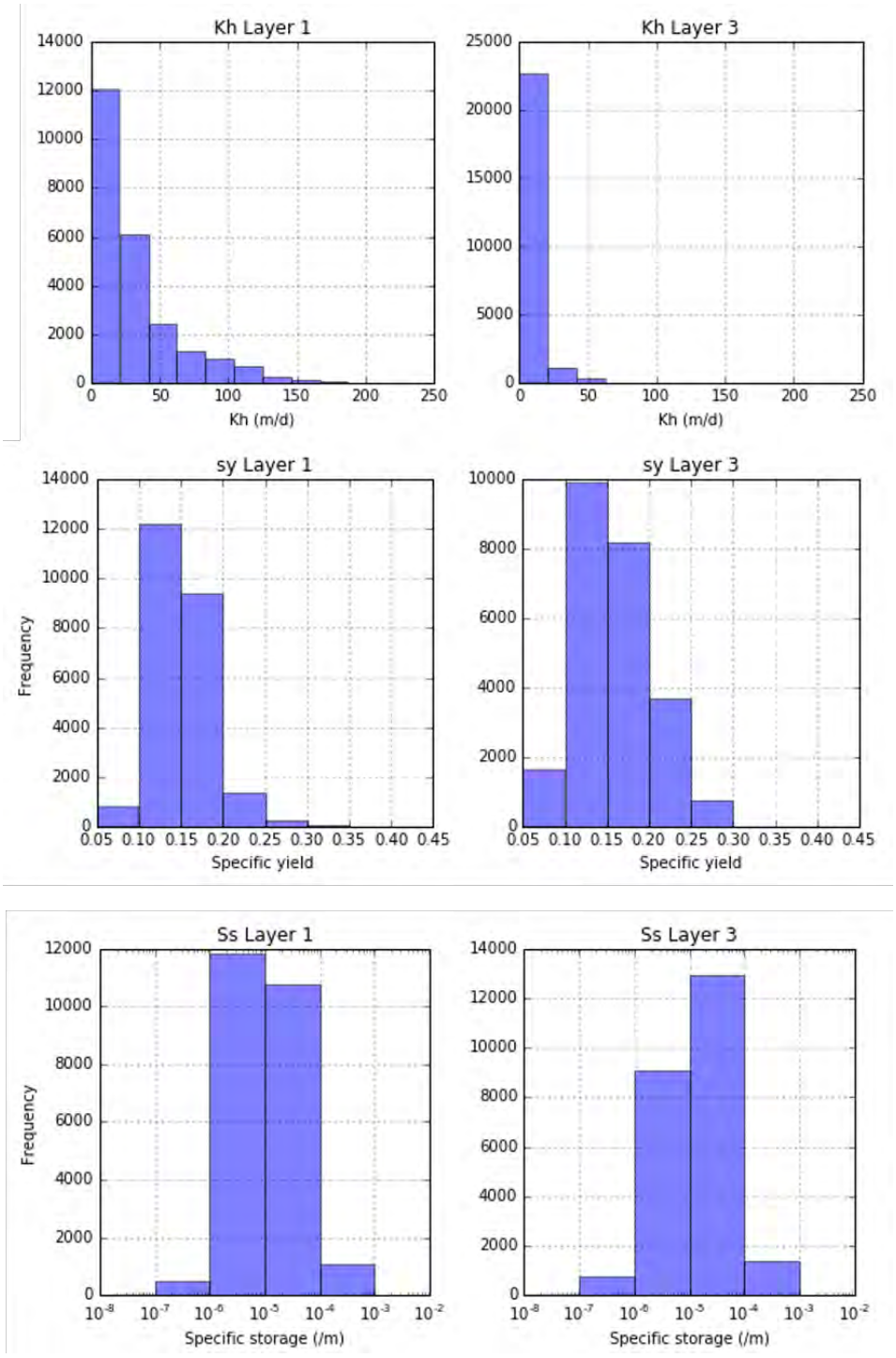

Figure 17: Posterior distribution of hydraulic properties in layer 1 and layer 3 obtained from a calibrated model run (Doble et al, 2020).

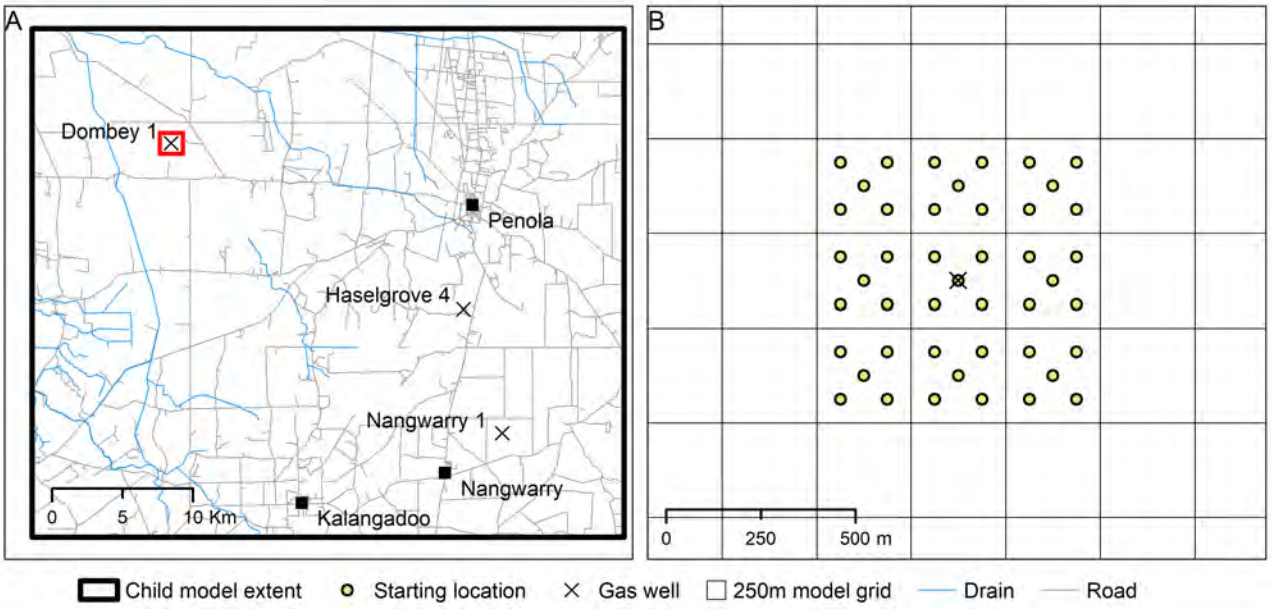

Figure 18: Configuration of particle starting location for the Dombey 1 well for scenario 1

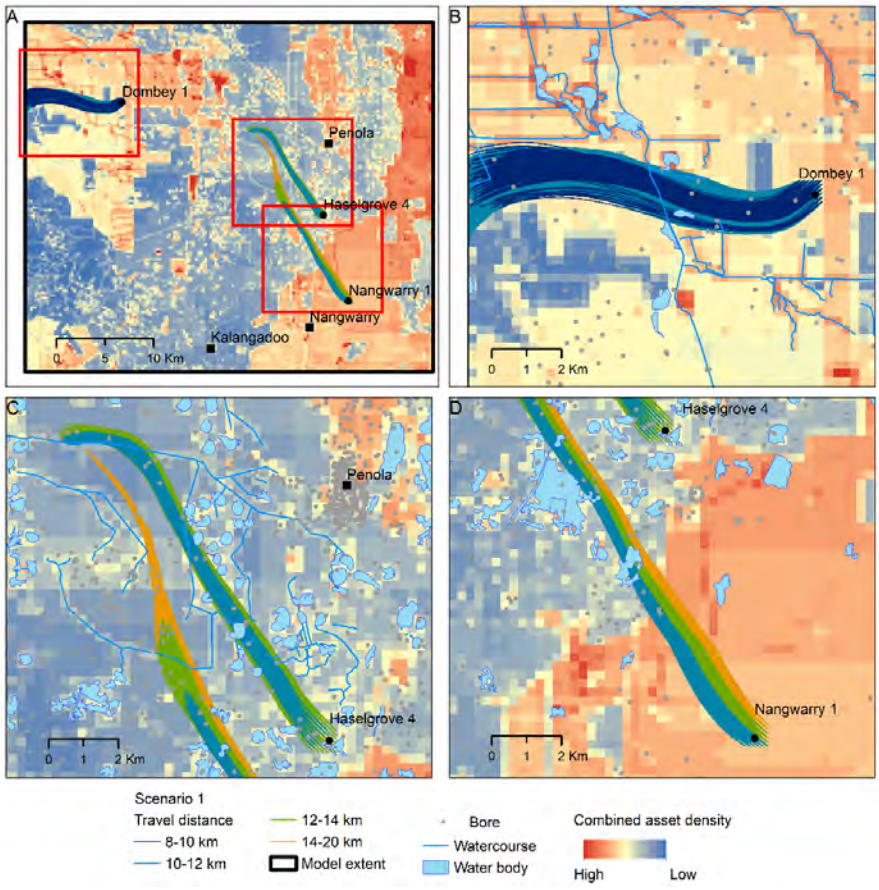

Figure 19: Ensemble of 100-year particle tracks simulated for the three selected well locations. Particle are started from 45 different starting points within the MODFLOW model cell containing each of the gas wells and its adjacent cells. The different colours of the tracks indicate distances travelled by the particles corresponding to different plausible realisations of the hydrogeological characteristics

5.1 Scenario 1 – Slow leakage from drilling sump

5.1.1 Particle tracking analysis

The particle tracking Monte Carlo simulation provided 179 completed model runs resulting in a total of 8055 particle tracks (45 × 179) from each of the three gas well sites (Figure 19). Spatial analysis was undertaken to identify the primary risk receptors – groundwater bores and water courses that are intercepted by the particle tracks within a 10 m vicinity. For all the three gas wells, the nearest receptors within a 2-km distance class were all groundwater bores, so the solute transport analyses were focussed on groundwater bores as the risk receptors.

Dombey well site

Figure 20 shows the distribution of distances from source to interceptions with groundwater-dependent receptors. There were 16 groundwater bores and 6 water bodies that were intersected by the particle tracks from the Dombey 1 gas well. Out of the 8055 tracks, 1476 tracks have intercepted the 16 bores; this is an interception probability of 18.34% with 6.77% of the wells within a 2 km radius from a water bore. The number of groundwater bores intersected by the particle tracks for various distance classes and percentage of tracks intercepting them are listed in Table 6. The distribution of flow rates along the flow paths (tracks) obtained from the particle tracking analysis for the Dombey site is shown in Figure 21.

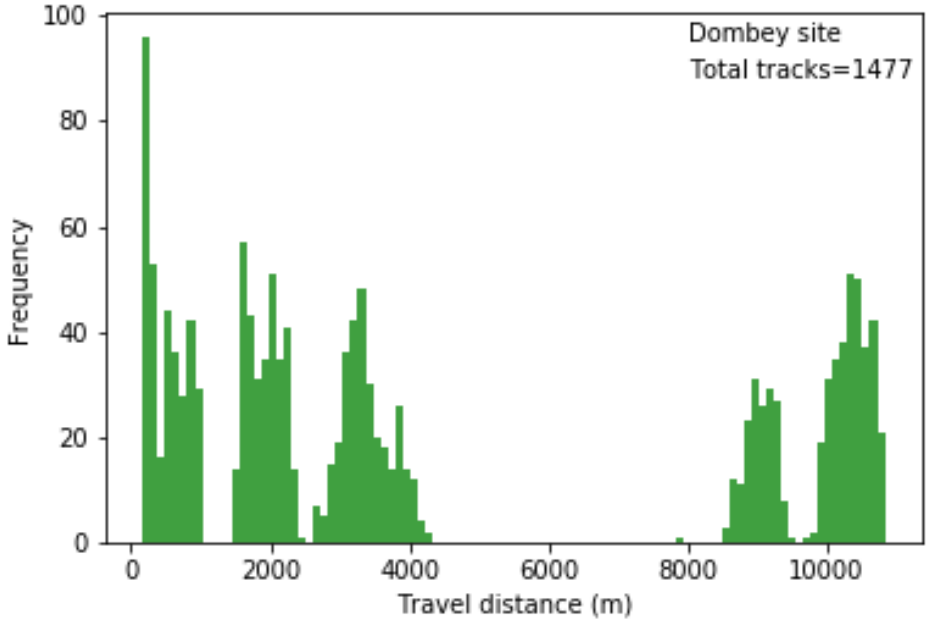

Figure 20: Distribution of particle tracks intercepting groundwater-dependent assets for Dombey Site

Table 6: Groundwater bore risk receptors intersecting with the particle tracks and probability of interception for Dombey 1 Site

Distance to receptors (m)	No. of interceptions with receptors (from the MC simulation)	Number of groundwater bores	Probability of interception %
0 - 2000	545	3	6.77
2000 - 4000	413	6	5.13
4000 - 6000	20	2	0.25
6000 - 8000	1	1	0.01
8000 - 10000	196	3	2.43
10000 - 12000	301	1	3.75
Total	**1476**	**16**	**18.34**

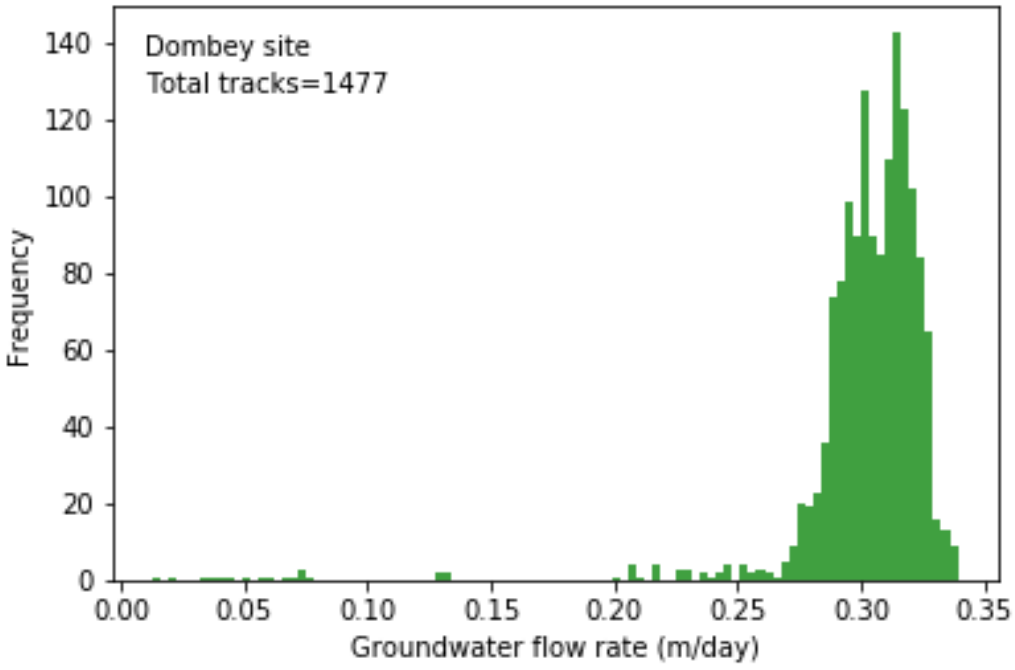

Figure 21: Distribution of groundwater flow rates along particle tracks for Dombey 1 well

Haselgrove 4 well site

Figure 22 shows the distribution of distances from source to interceptions with groundwater-dependent receptors. There were 22 groundwater bores and 15 water bodies that were intersected by the particle tracks from the Haselgrove 4 gas well. Out of the 8055 tracks, 5412 tracks have intercepted these 22 bores; this is an interception probability of

67.19% with 12.09% within a 2 km radius. The number of groundwater bores intersected by the particle tracks for various distance classes and percentage of tracks intercepting them are listed in Table 7. The distribution of flow rates along the flow paths (tracks) obtained from the particle tracking analysis for the Haselgrove 4 site is shown in Figure 23.

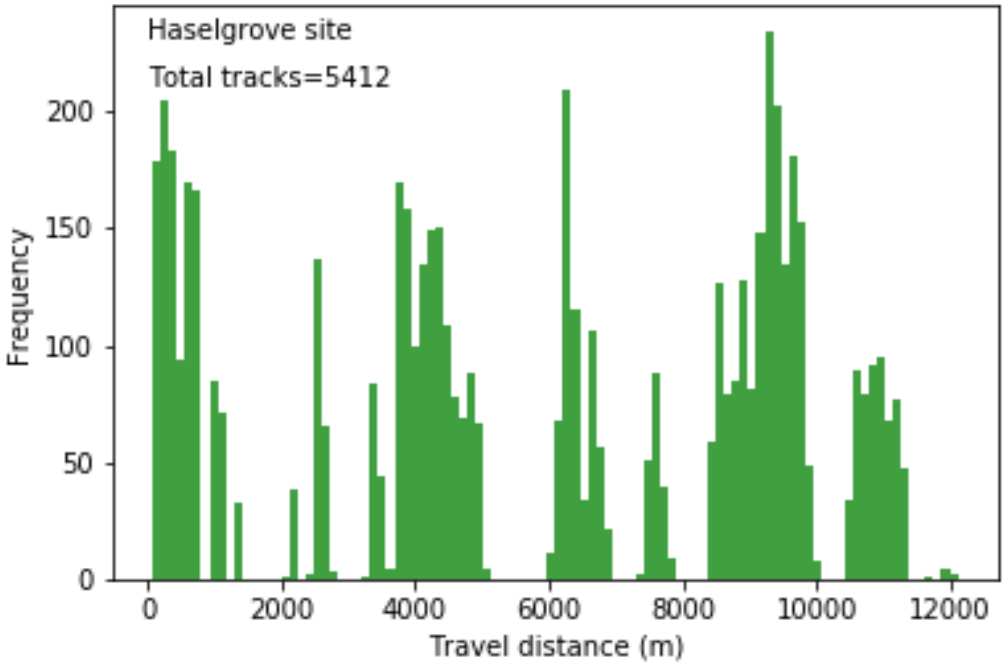

Figure 22: Distribution of particle tracks intercepting groundwater-dependent assets for Haselgrove 4 Site

Table 7: Groundwater bore risk receptors intersecting with the particle tracks and probability of interception for Haselgrove 4 Site

Distance to receptor (m)	No. of interceptions with receptors	Number of groundwater bores	Probability of interception %
0 - 2000	974	4	12.09
2000 - 4000	769	5	9.55
4000 - 6000	887	3	11.01
6000 - 8000	810	3	10.06
8000 - 10000	1668	4	20.71
10000 - 12000	302	2	3.75
12000 - 14000	2	1	0.02
Total	**5412**	**22**	**67.19**

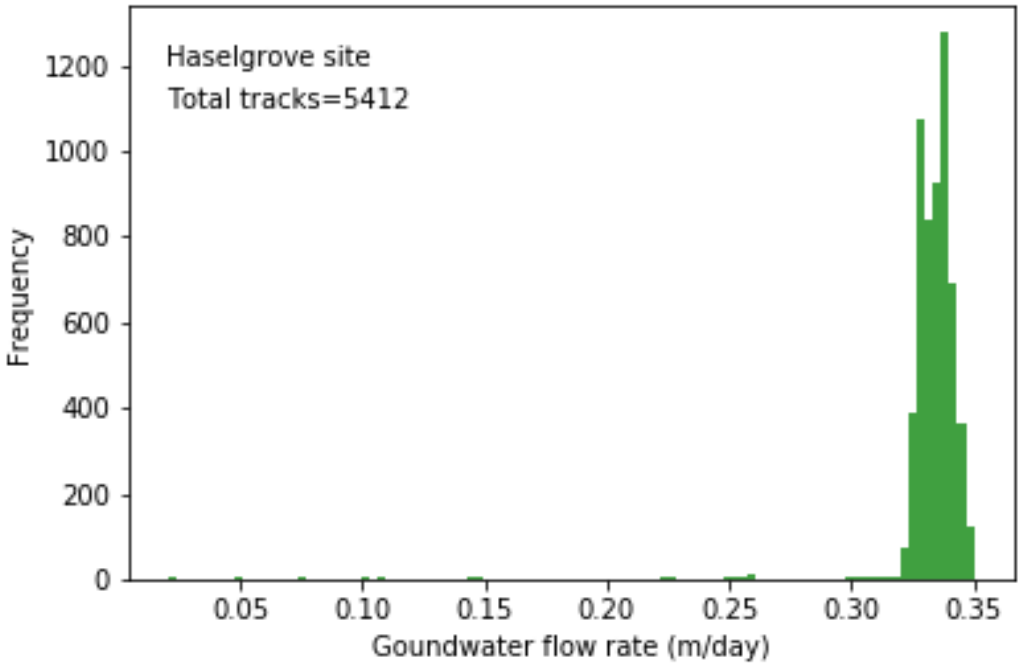

Figure 23: Distribution of groundwater flow rates along particle tracks for Haselgrove 4 Site

Nangwarry 1 well site

Figure 24 shows the distribution of distances from source to interceptions with groundwater-dependent receptors for the gas well Nangwarry 1. There were 31 groundwater bores and 15 water bodies that were intersected by the particle tracks from the Nangwarry 1 gas well. Out of the 8055 tracks, 5719 tracks have intercepted these 31 bores; this is an interception probability of 71% all of which are outside a 4 km radius. The number of groundwater bores intersected by the particle tracks for various distance classes and percentage of tracks intercepting them are listed in Table 8. The analyses of solute transport for the other two sites, described in the next section, show very low concentrations for travel distances greater than 4 km, hence, no further analysis was warranted for this site.

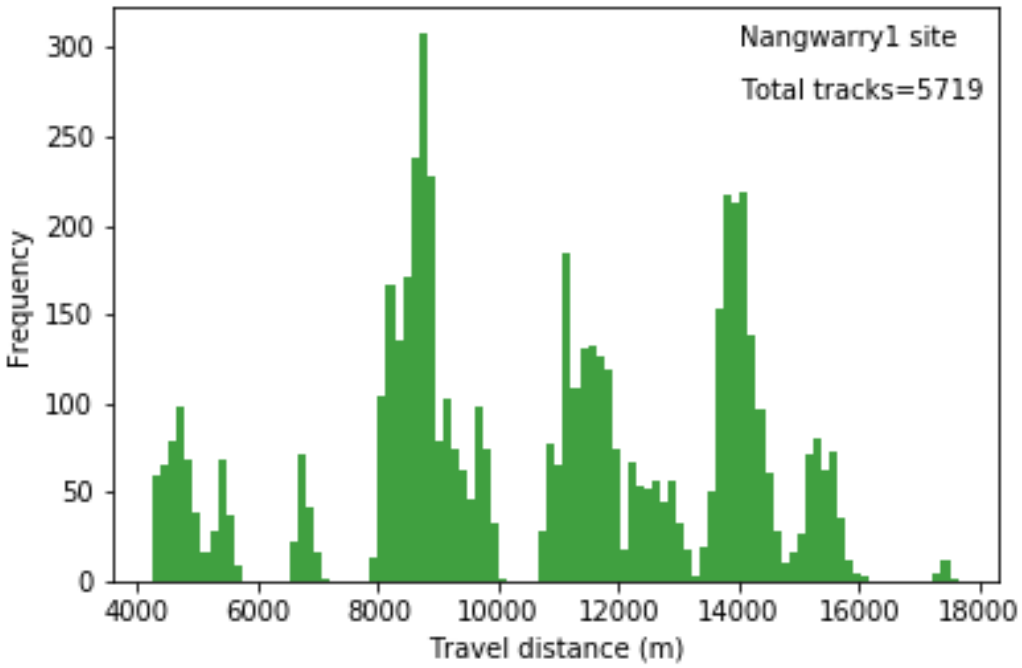

Figure 24: Distribution of particle tracks intercepting groundwater-dependent assets for Nangwarry 1 Site

Table 8: Groundwater bore risk receptors intersecting with the particle tracks and probability of interception for Nangwarry 1 Site

Distance to receptor (m)	No. of interceptions with receptors	Number of groundwater bores	Probability of interception %
0 - 2000	0	0	0.00
2000 - 4000	0	0	0.00
4000 - 6000	571	2	7.09
6000 - 8000	158	1	1.96
8000 - 10000	1929	3	23.95
10000 - 12000	1047	1	13.00
12000 - 14000	1029	12	12.77
> 14000	985	12	12.23
Total	**5719**	**31**	**71**

5.1.2 Flow and solute transport in the unsaturated zone

The Dombey 1 and Haselgrove 4 well sites have similar depths to groundwater table with subtle differences in soil horizons (Table 5), therefore, results for the Dombey 1 site will only be shown herein. Two cases of solute transport results are presented for all wells. One set of results consider degradation of chemicals in the soil and aquifer media and another set assumes no degradation of the chemicals. A companion GISERA project (Tran Dinh et al, 2019) that evaluated the biodegradation characteristics of chemicals used for drilling in the onshore Otway Basin, South Australia, informed that all of nine chemical compounds examined by commercially available accredited tests were undetectable in the soil after 34 days of incubation (Tran Dinh et al, 2019). At least for those chemicals analyses, the results that consider chemical degradation are more realistic and more representative of what would happen in the soil compared to the conservative calculations (i.e. no degradation). However, the no-degradation results are presented as a conservative simulation representing a worst-case scenario, especially because degradation parameters are not available for many other chemical compounds and the reported test conditions are often different from the in-situ biogeochemical conditions.

Dombey 1 well site

In scenario 1, the liner failure of the drilling fluid/mud sump, fluid from a containment was allowed to flow freely into the soil surface for a period of 30 days. Simulations were continued for another 70 days to continue tracking of the plume as it develops across the vadose zone. Figure 25 shows the solute flux (water flux multiplied by solute concentration) at the groundwater table. The flux reaches a steady-state indicating that solute concentration across the entire 5-m deep soil profile has equalised to the input unit concentration. Note that the governing equations of solute transport are linear in concentration, and hence results presented in this work can be scaled up or down by any other concentration. After flow through the failed liner into the soil surface ceases, the soil profile continues to freely drain, which results in a diminishing solute flux into the saturated zone. Introducing solute degradation obviously reduces the solute flux, resulting in a 35% drop in peak flux for a half-life of 10 days.

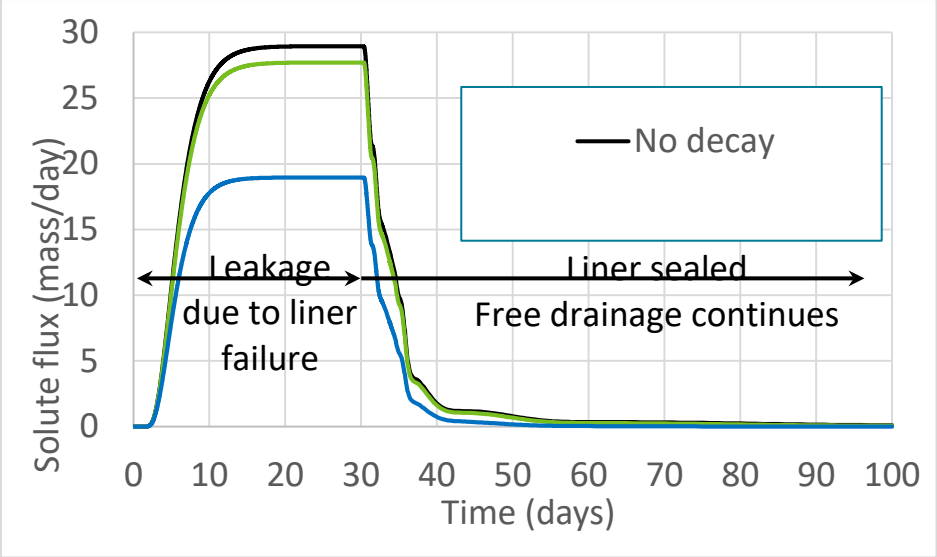

Figure 25: Breakthrough curves at 5-m depth due to 30-day leakage at unit-concentration with and without solute degradation at Dombey site

Figure 26 shows the typical effect of solute dispersion, whereby higher dispersion causes solute breakthrough to be a flatter S-shaped curve compared to a sudden breakthrough resembling piston-flow when dispersion is low. Dispersion significantly influences the shape (slope) of the BTC and hence the solute flux into the aquifer. On the other hand, adsorption causes a shift in the BTC. The chemicals listed in Appendix III undergo adsorption to organic material, and hence their influence on solute fluxes is marginal (Figure 26).

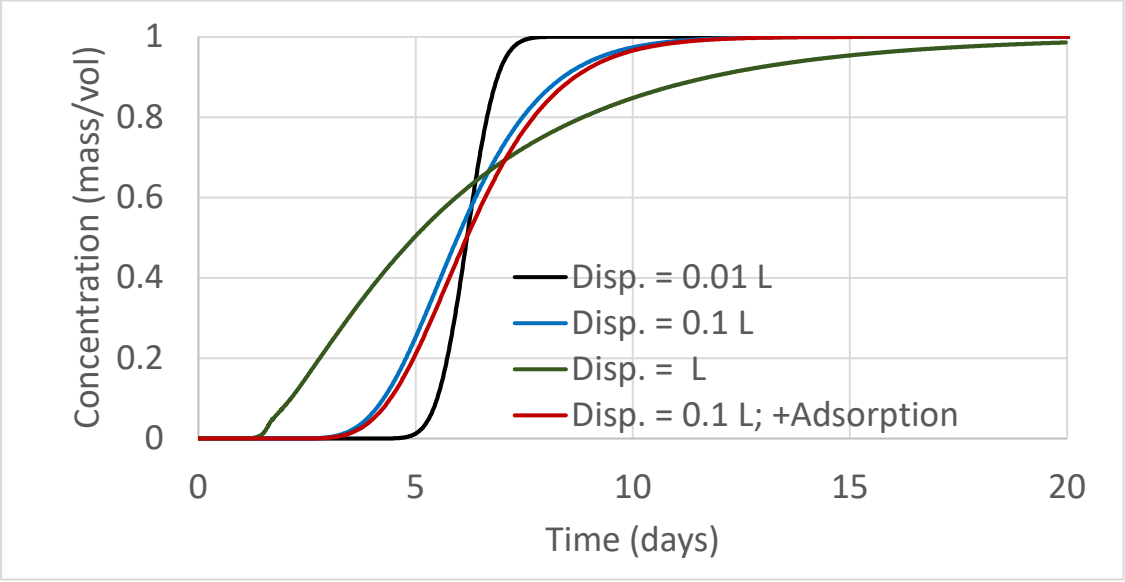

Figure 26: BTCs showing dispersion and adsorption effects at Dombey 1 site

Nangwarry 1 well site

The Nangwarry 1 site has a 9-m depth to groundwater table compared to the other two sites with a 5-m depth (Table 5). In the absence of solute degradation, a larger depth to groundwater table has a subtle effect on solute flux with a later arrival of the solute front. However, in the presence of solute degradation, the longer travel path results in a greater residence time, and hence higher solute degradation occurs resulting in a significantly lower solute concentration and flux. Figure 27 shows a larger drop in peak solute flux of 55% compared to a 35% drop for the Dombey 1 site (having a 5-m depth to groundwater table).

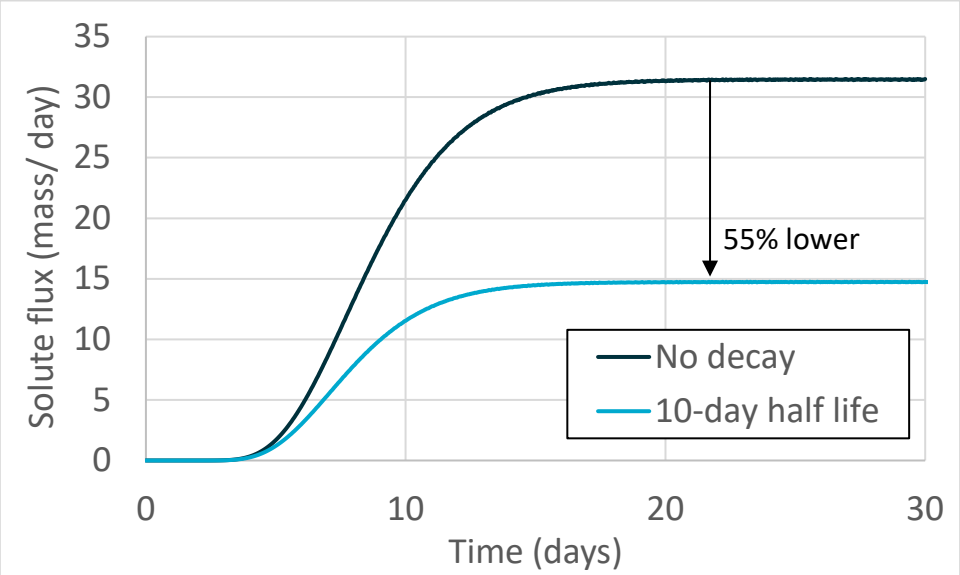

Figure 27: BTC's due to 30-day leakage at unit-concentration with and without solute degradation at Nangwarry 1 site

5.1.3 Flow and solute transport in the saturated zone:

Results presented herein were derived from the 1-dimensional solution of the advective-dispersive equation under steady-state flow conditions. Explicit values for pore water velocities and track length were derived from the stochastic particle tracking analyses. Dispersion coefficients and degradation parameters were stochastically sampled from triangular distributions (details in Table 5 and Appendix III).

Dombey well site; without solute degradation

The results for Dombey 1 site without solute degradation are shown in Figure 28 with solute concentrations decreasing exponentially as distances to receptors increase thus leading to lower concentrations along the longer path. The maximum peak concentration across the entire stochastic analysis amounted to only 7.1% of the input unit concentration at the source, with 79.8% of the simulations having a peak concentration of less than 1% of the input unit concentration at the source.

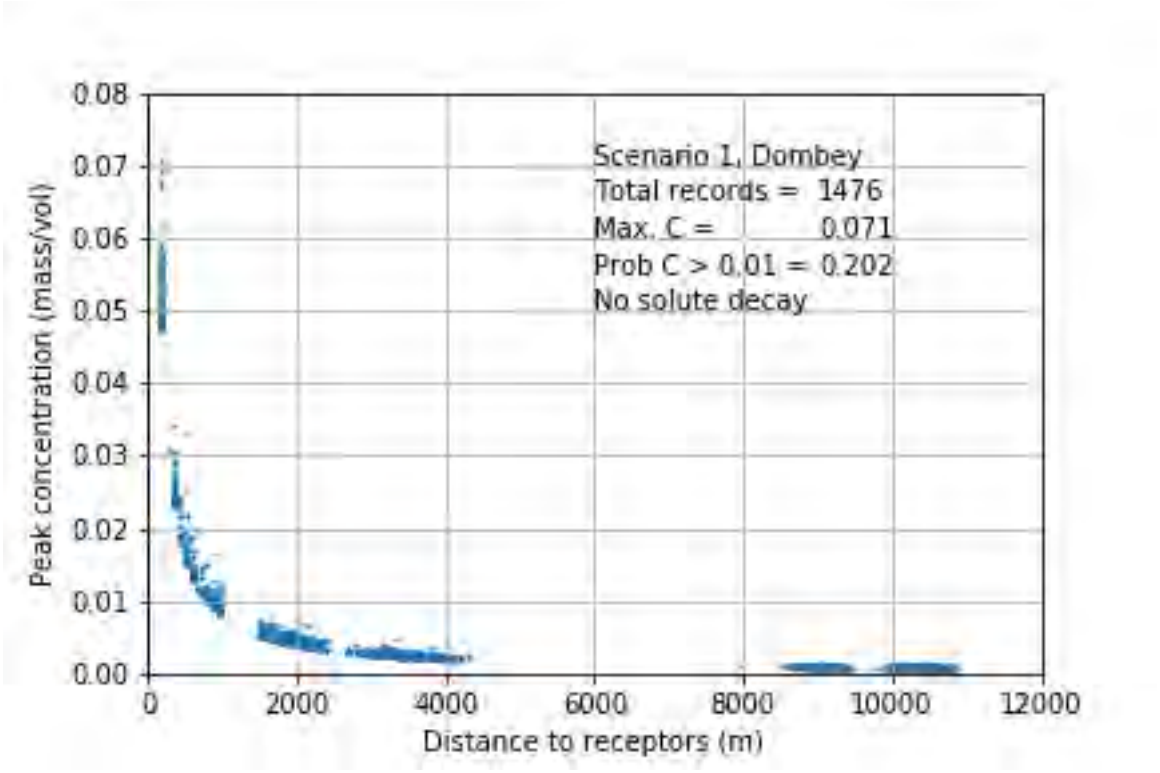

Figure 28: Peak concentrations (without solute degration) versus distances to receptors for Scenario 1 at Dombey site

The time required to arrive at peak concentration obviously increases with travel distance; Figure 29 shows that peak concentrations decrease exponentially with increased travel times (associated with larger travel distances).

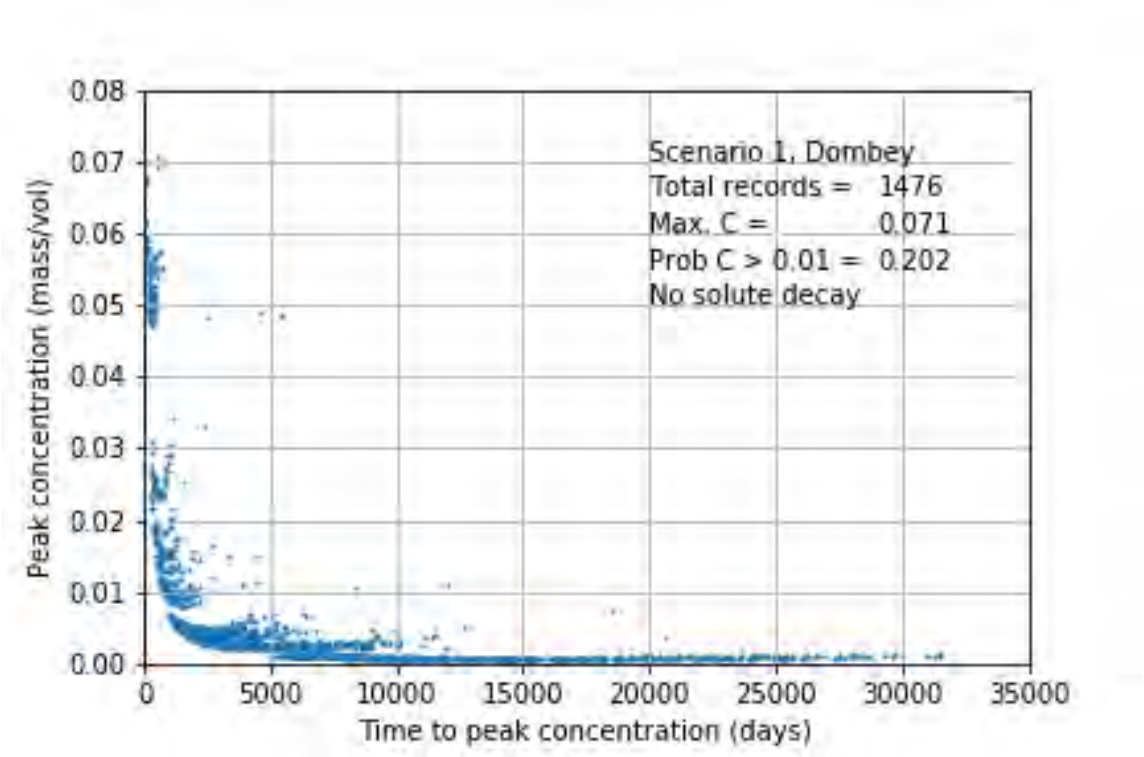

Figure 29: Peak concentrations (without solute degradation) versus time T-peak for Scenario 1 at Dombey site

The distributions of peak concentrations and times at which they were reached are shown in Figure 30 and Figure 31, respectively. The earliest time when peak concentration was reached across the entire stochastic simulations was 120 days for the nearest receptor located at 167 m from the well location.

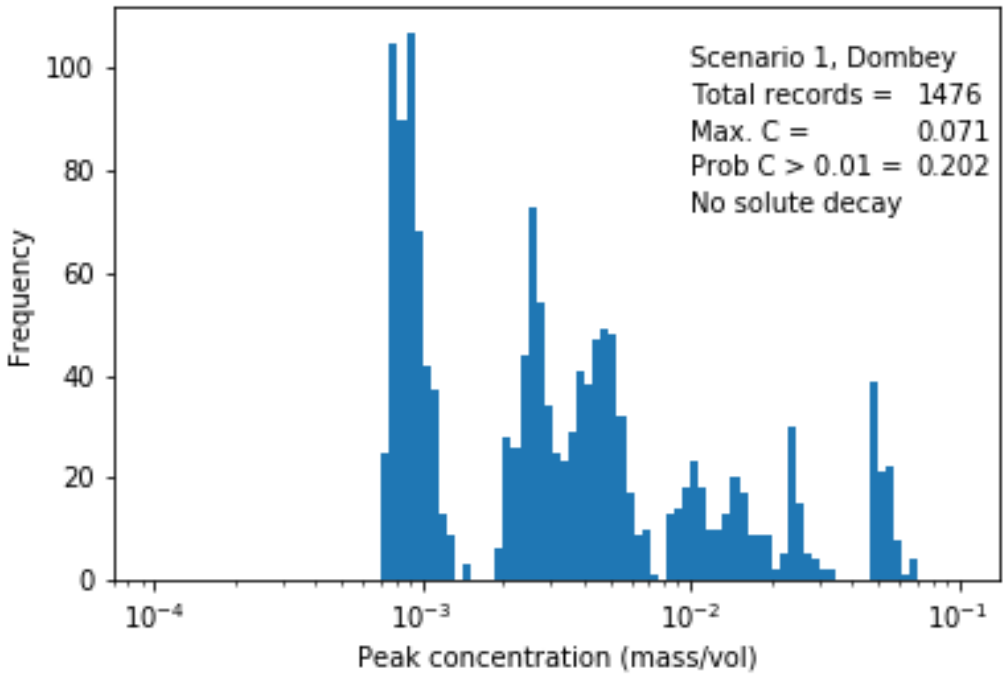

Figure 30: Distribution of peak concentrations (without solute degradation) for Scenario 1 at Dombey site

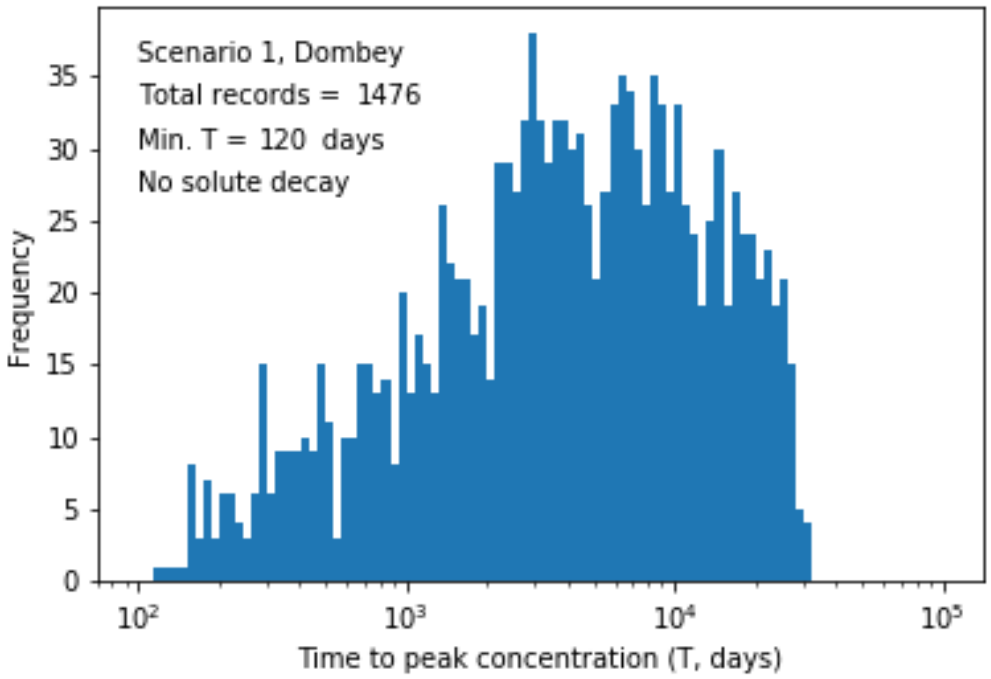

Figure 31: Distribution of times to reach peak concentrations (without solute degradation) for Scenario 1 at Dombey site

Dombey well site; with solute degradation

Given the significant drop in solute concentrations within a 1 km distance (see Figure 28), and due to the fact that solute degradation would lead to further significant drops in concentration, only receptors within a 1 km distance were included in this analysis. However, the number of stochastic simulations was maintained over 1000 while keeping the observed distribution of distances to receptors identified by the spatial analysis. Note that the distinct vertical groups of concentrations correspond to specific receptor locations (nearest located at 167 m).

Figure 32 shows a very significant drop in solute concentrations of up to 24 orders of magnitude relative to the unit input concentration, which is much higher than that observed for the case without solute degradation. The spread of the stochastic solute concentrations increases with distance as larger residence times significantly increases the mass of degraded solutes. Figure 33 shows a steep drop in peak concentration as distance to receptor increases.

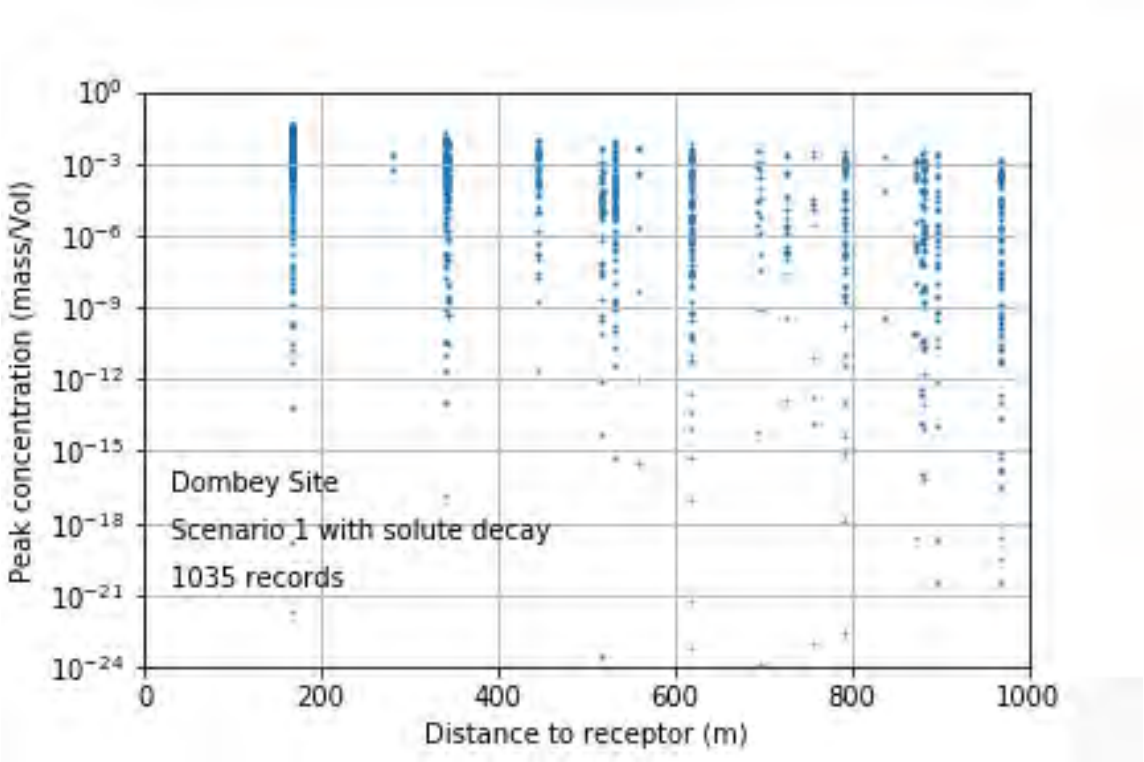

Figure 32: Peak concentrations (with solute degradation) versus distances to receptors (up to 1000 m) for Scenario 1 at Dombey site

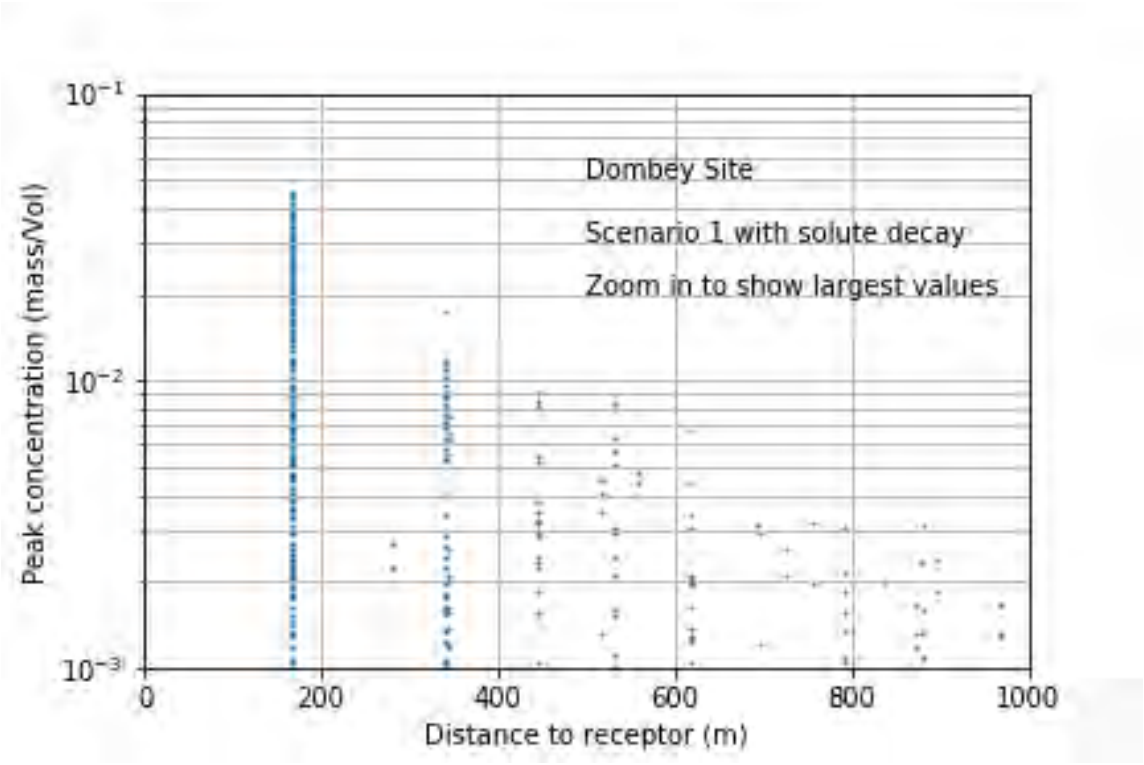

Figure 33: Peak concentrations (with solute degradation) versus distances to receptors (up to 1000 m) for Scenario 1 at Dombey site showing the higher concentration range

Figure 34 shows the distribution of concentrations across the stochastic simulations. The maximal peak concentration was 4.5% of the input unit concentration, which is lower than that observed without solute degradation; note that the maximal peak concentration (one unique value) corresponds the minimal degradation coefficient used in the stochastic simulation. In 91.2% of the stochastic simulations, the peak concentration was less than 1% of the input unit concentration at the source.

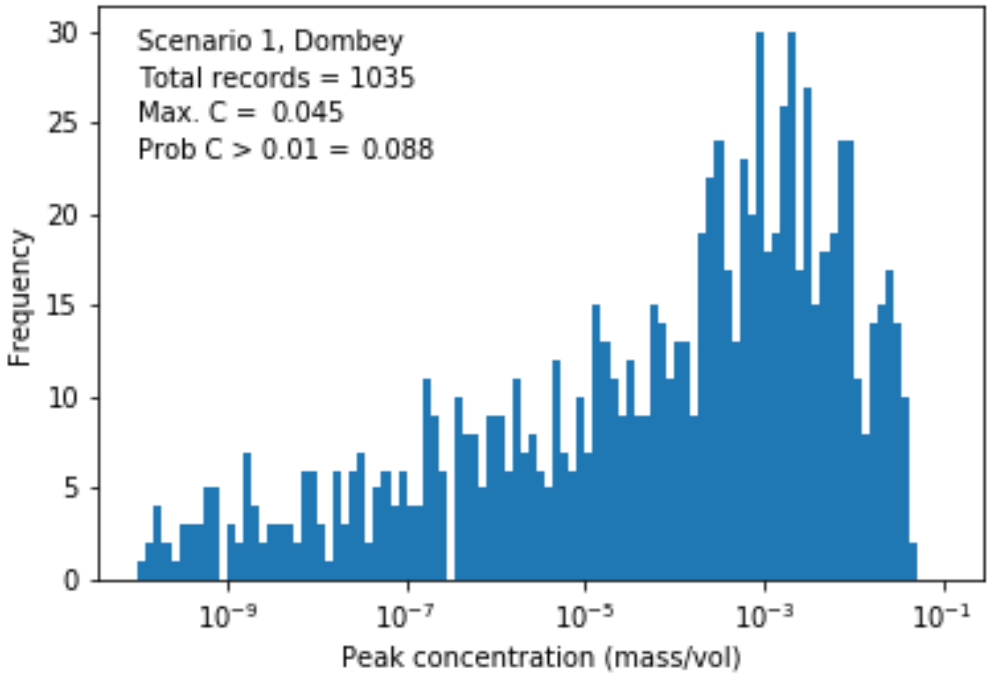

Figure 34: Distribution of peak concentrations (with solute degradation) for Scenario 1 at Dombey site

Figure 35 shows the effect of solute degradation on concentrations where a shorter half-life (higher degradation coefficient) leads to much lower concentrations. Note that the spread of concentrations significantly increases with higher degradation. As the degradation process is exponential, it is very sensitive to residence times, varying the dispersion coefficient and flow rate greatly influences residence times; higher solute dispersion reflects a wider distribution of residence times.

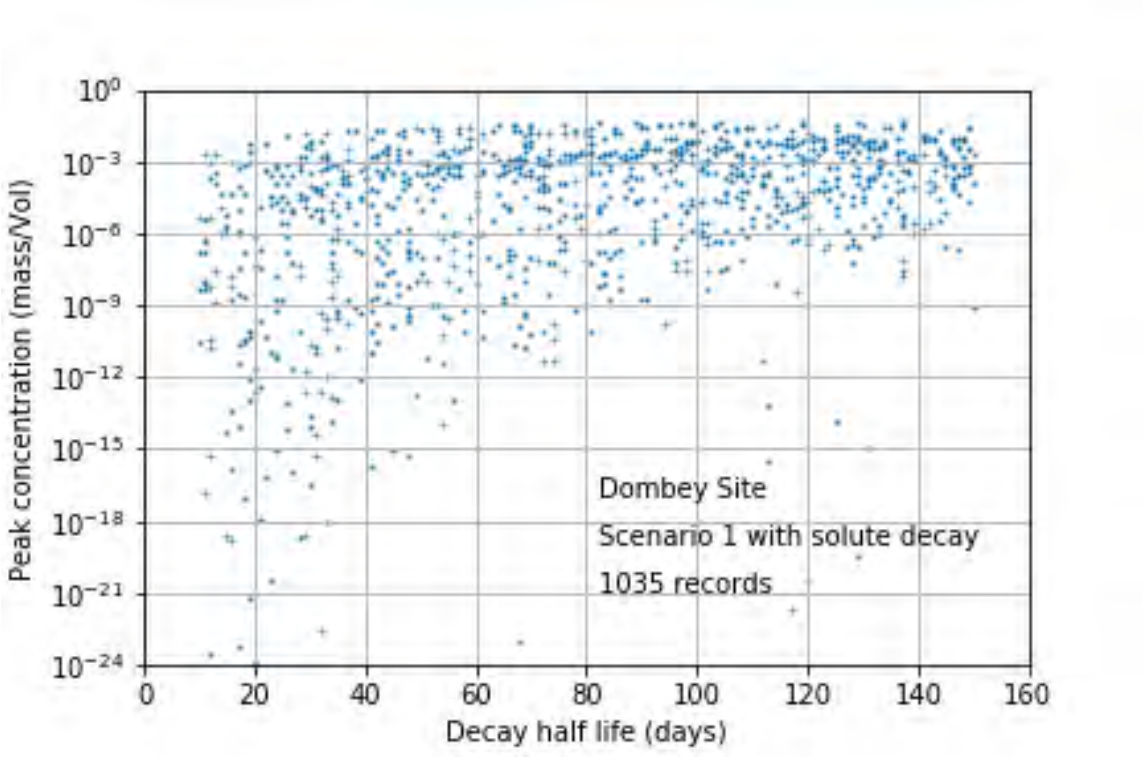

Figure 35: Peak concentrations versus degradation half-life for Scenario 1 at Dombey site

Haselgrove 4 well site; without solute degradation

The results for Haselgrove 4 site without solute degradation are shown in Figure 36 with solute concentrations decreasing exponentially as distances to receptors increase thus leading to lower solute transformations along the longer path. The maximal peak concentration across the entire stochastic analysis amounted to 14.3% of the input unit concentration at the source, with 84.5% of the simulations having a peak concentration of less than 1% of the input unit concentration at the source. The maximum peak concentration for Haselgrove 4 is higher than that for Dombey 1 as the closest asset to Haselgrove 4 site is 88 m whereas it is 167 m for Dombey 1.

The time required to arrive at peak concentration obviously increases with travel distance; Figure 37 shows that peak concentrations decrease exponentially with increased travel times (associated with larger travel distances).

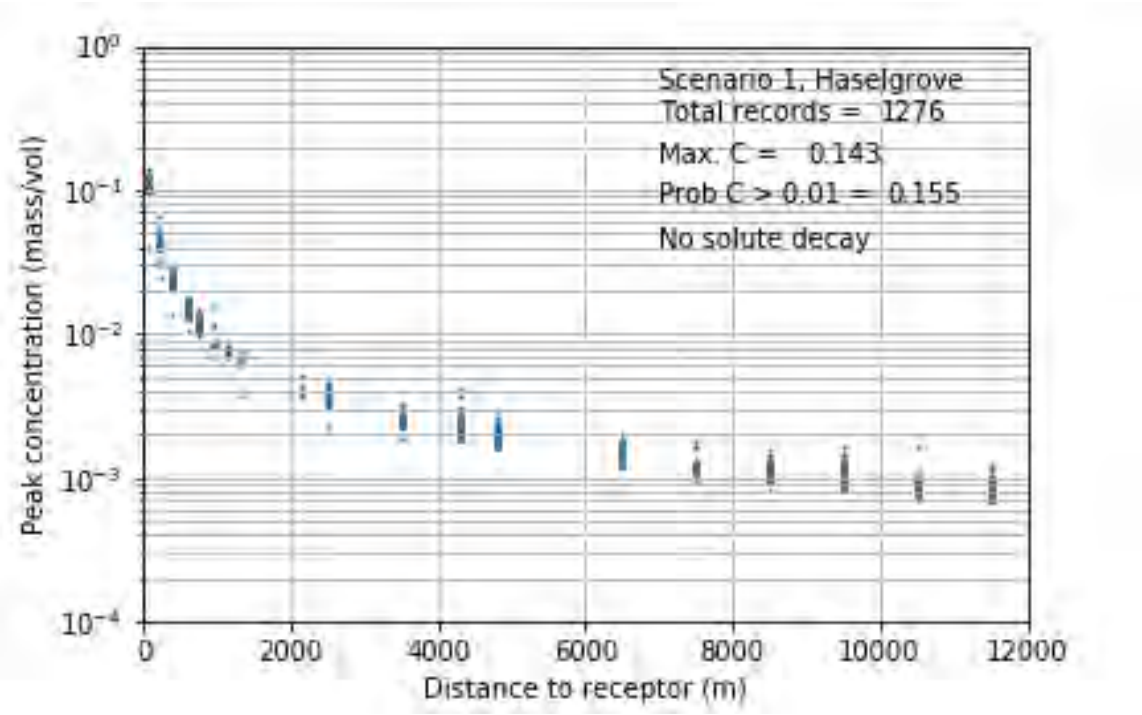

Figure 36: Peak concentrations (without solute degradation) versus distances to receptors for Scenario 1 at Haselgrove 4 site

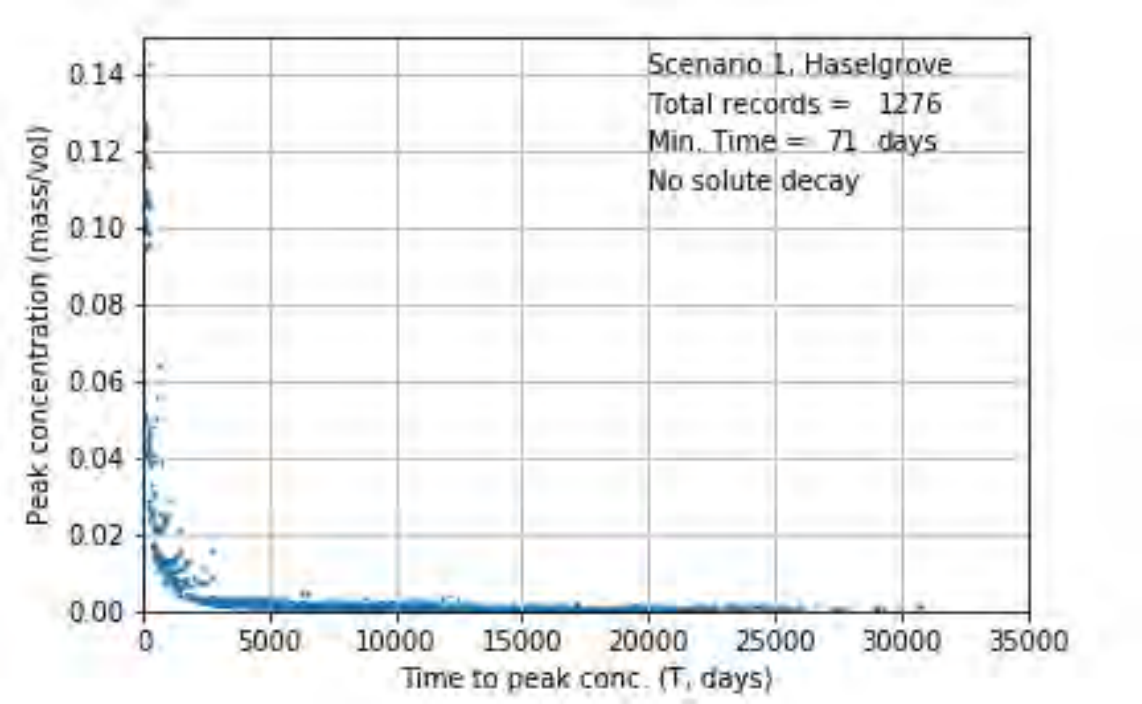

Figure 37: Peak concentrations (without solute degradation) versus time T-peak for Scenario 1 at Haselgrove 4 site

The distributions of peak concentrations and times at which they were reached are shown in Figure 38 and Figure 39, respectively. The earliest time when peak concentration was reached across the entire stochastic simulations was 71 days for the nearest receptor located at 88 m from the well location.

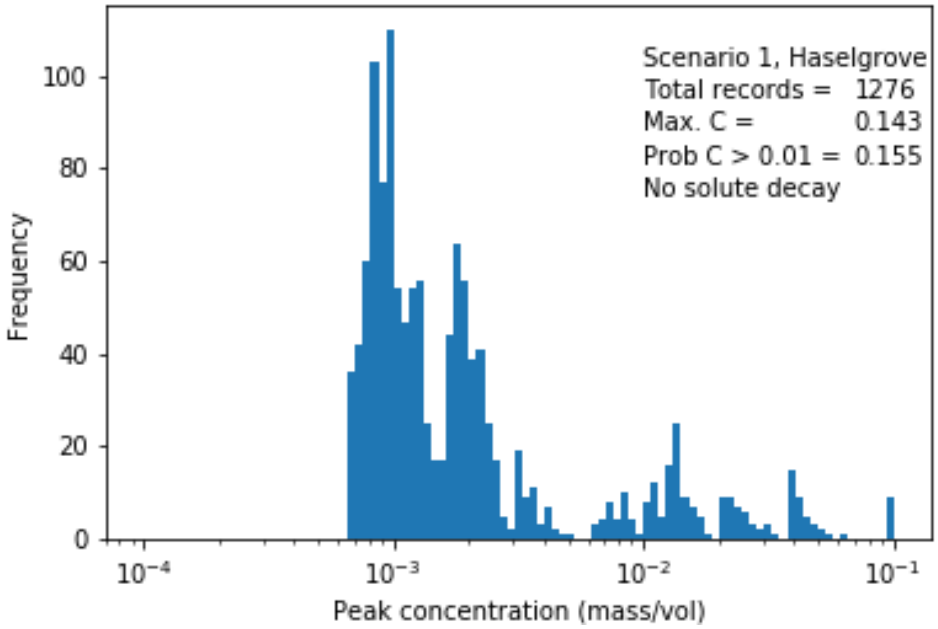

Figure 38: Distribution of peak concentrations (without solute degradation) for Scenario 1 at Haselgrove 4 site

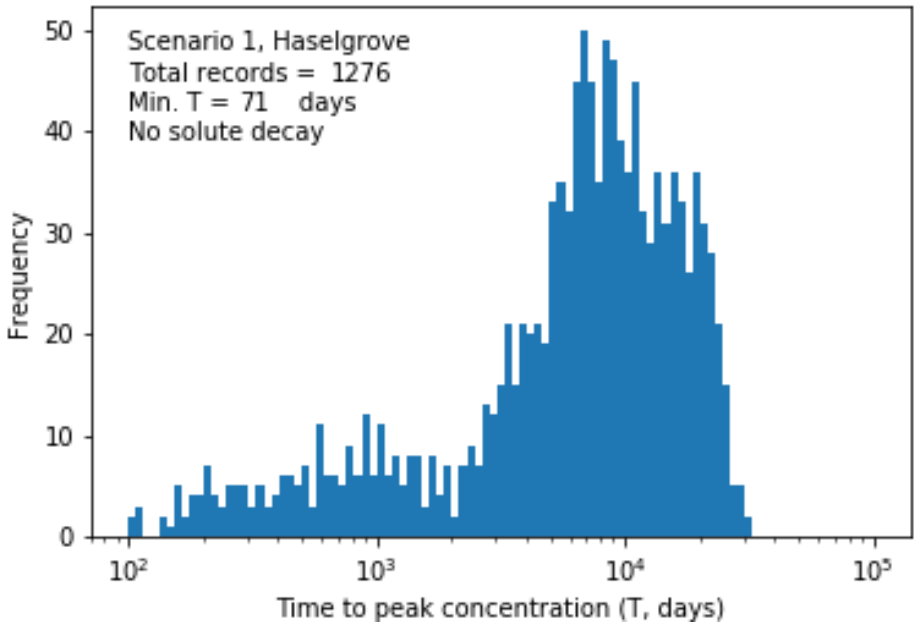

Figure 39: Distribution of times to reach peak concentrations (without solute degradation) for Scenario 1 at Haselgrove 4 site

Haselgrove 4 well site; with solute degradation

As described earlier for the Dombey site, only receptors within a 1 km distance were included in this analysis. However, the number of stochastic simulations was maintained over 1000 while keeping the observed distribution of distances to receptors identified by the spatial analysis. Note that the distinct vertical groups of concentrations correspond to specific receptor locations (nearest located at 167 m).

Figure 40 shows a very significant drop in solute concentrations of up to 28 orders of magnitude relative to the unit input concentration, which is much higher than that simulated for the case without solute degradation. The spread of the stochastic solute concentrations increases with distance as larger residence times significantly increases the mass of degraded solutes. Figure 41 shows a steep drop in peak concentration as distance to receptor increases.

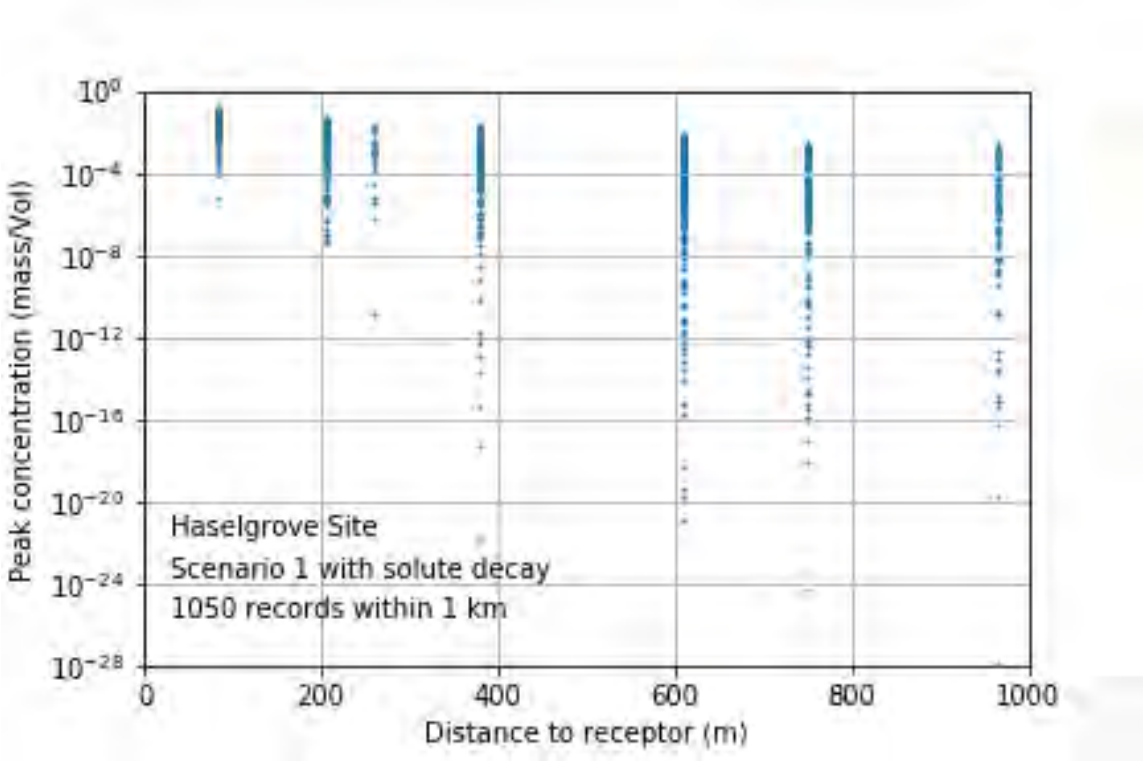

Figure 40: Peak concentrations (with solute degradation) versus distances to receptors (up to 1000 m) for Scenario 1 at Haselgrove 4 site

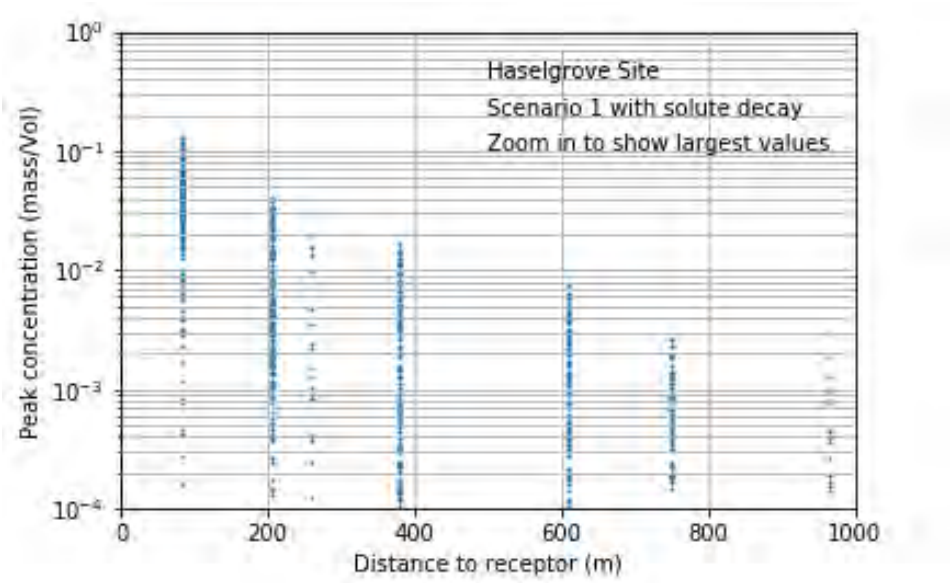

Figure 41: Peak concentrations (with solute degradation) versus distances to receptors (up to 1000 m) for Scenario 1 at Haselgrove 4 site showing the higher concentration range

Figure 42 shows the distribution of concentrations across the stochastic simulations. The maximal peak concentration was 12.9% of the input unit concentration, which is higher than that observed for Dombey site (the closet asset is 88 m away compared to 167 m away for Dombey). The peak concentration was less than 1% of the input unit concentration at the source in 91.6% of the simulations.

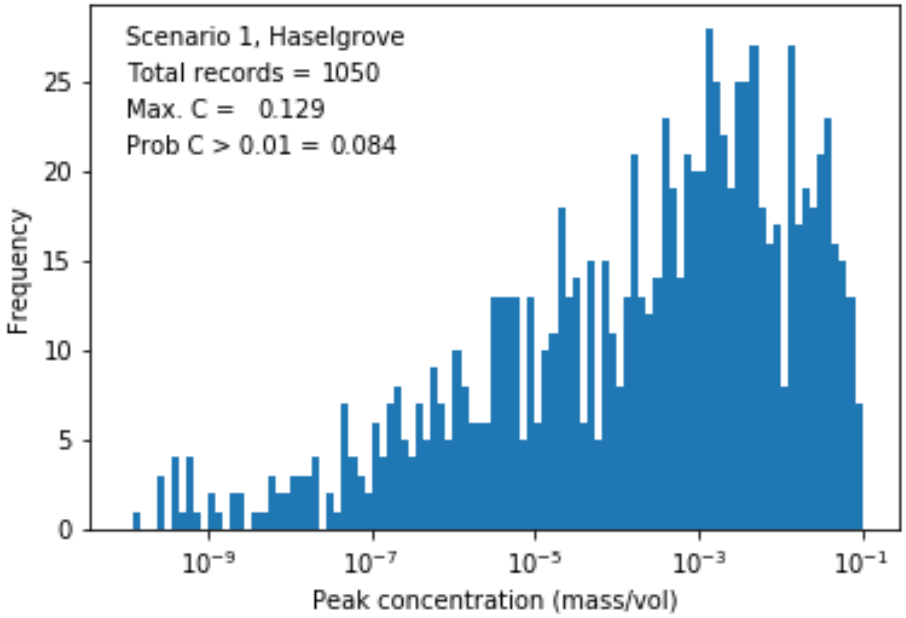

Figure 42: Distribution of peak concentrations (with solute degradation) for Scenario 1 at Haselgrove 4 site

Figure 43 shows the effect of solute degradation on concentrations where a shorter half-life (higher degradation coefficient) leads to much lower concentrations. Note that the spread of concentrations significantly increases with higher degradation. As the degradation process is exponential, it is very sensitive to residence times, varying the dispersion coefficient and flow rate greatly influences residence times; higher solute dispersion reflects a wider distribution of residence times.

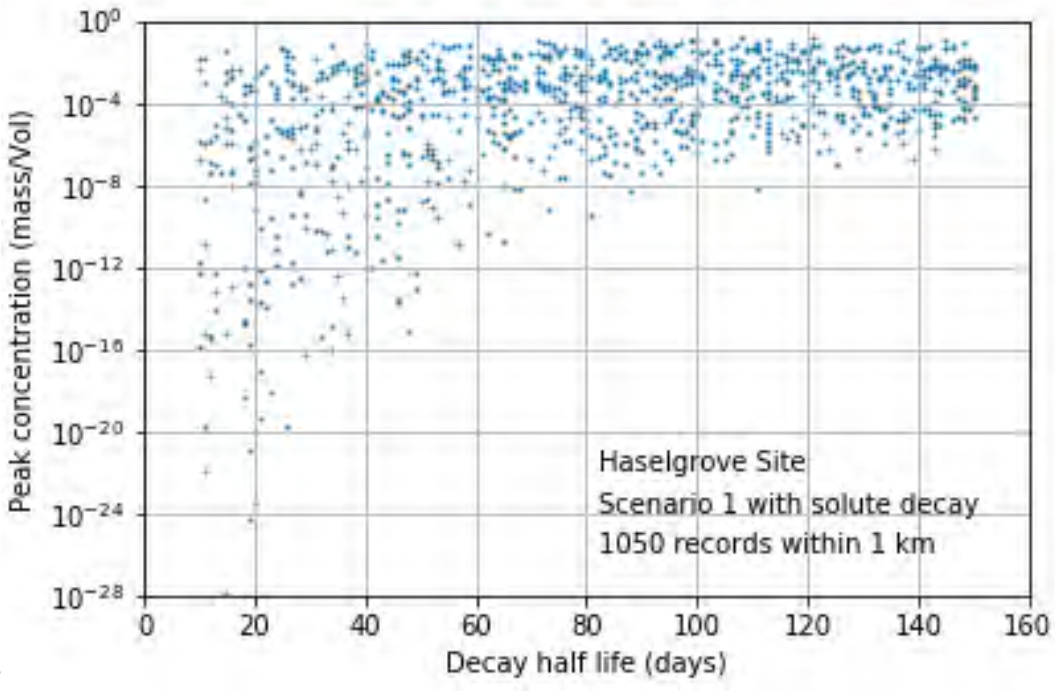

7

Figure 43: Peak concentrations versus degradation half-life for Scenario 1 at Haselgrove 4 site

5.2 Scenario 2: Well integrity loss

5.2.1 Scenario 2a: Leakage into the Upper Tertiary Limestone Aquifer

Scenario 2a assumes a well of compromised integrity whereby drilling fluid leaks within the bottom half of the unconfined aquifer for 30 days. The analysis described herein assumes a unit input concentration being released from the well into the unconfined aquifer and the reported concentrations reflect solute attenuations due to dispersion, adsorption, and degradation.

It was reported in Section 4.3.2 that the estimated leakage rate from a compromised well casing is about 0.0005 L/day (0.5×10^{-6} m^3/day). The average flow rate within the confined aquifer is 0.33 m/day. This would result in a dilution factor of six orders of magnitude upon release of a leaking fluid ($0.5 \times 10^{-6}/0.33 = 1.5 \times 10^{-6}$). Concentrations at receptors that are reported in this section must hence be multiplied by this dilution factor to obtain the actual estimate.

Dombey 1 well site; without solute degradation

The results for Dombey site without solute degradation are shown in Figure 44 where solute concentrations decrease exponentially as distances to receptors increase as longer travel paths lead to higher solute dispersion. The distribution of peak concentrations is shown in Figure 45. The maximum peak concentration across the entire stochastic analysis amounted to only 26.5% of the input unit concentration at the source, with 20% of the simulations having a peak concentration of 5% of the input unit concentration at the source. These values are higher than those reported for Scenario 1, due to absence of solute attenuation in the unsaturated zone. It is reemphasized here that these concentrations are yet to be diluted as a result of mixing with the groundwater, which has a flow rate that significantly higher than the leakage rate.

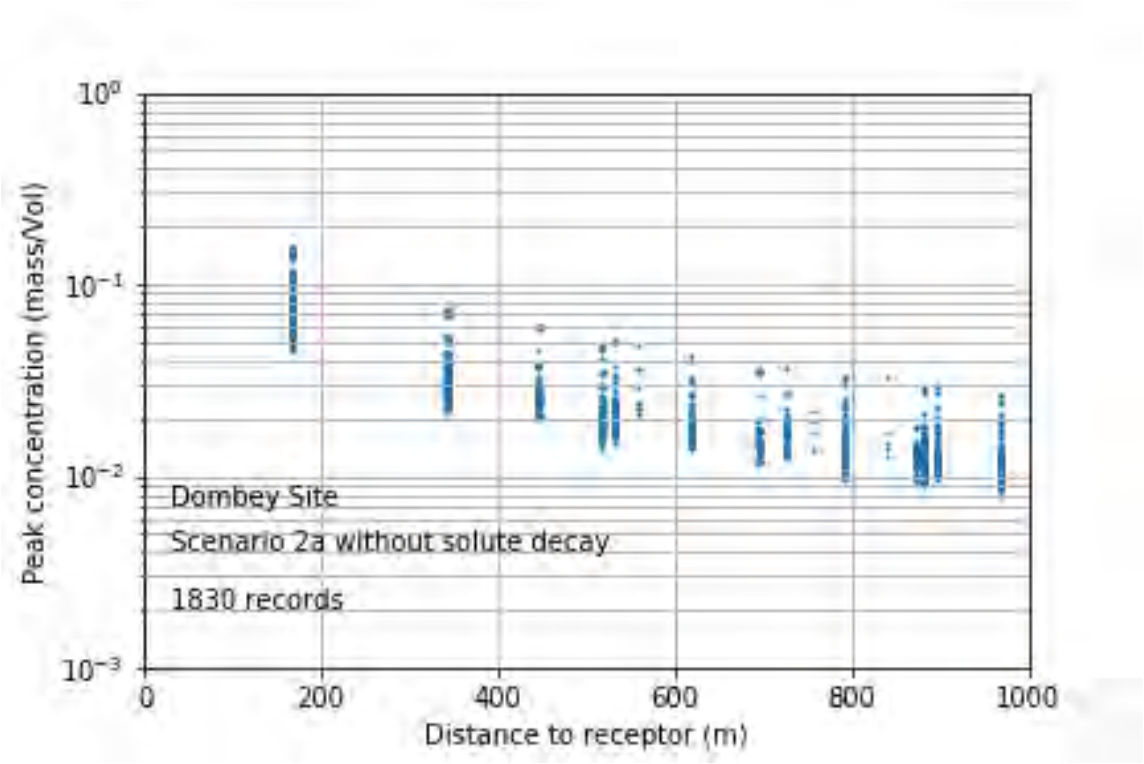

Figure 44: Peak concentrations (without solute degradation) versus distances to receptors (up to 1000 m) for Scenario 2a at Dombey site

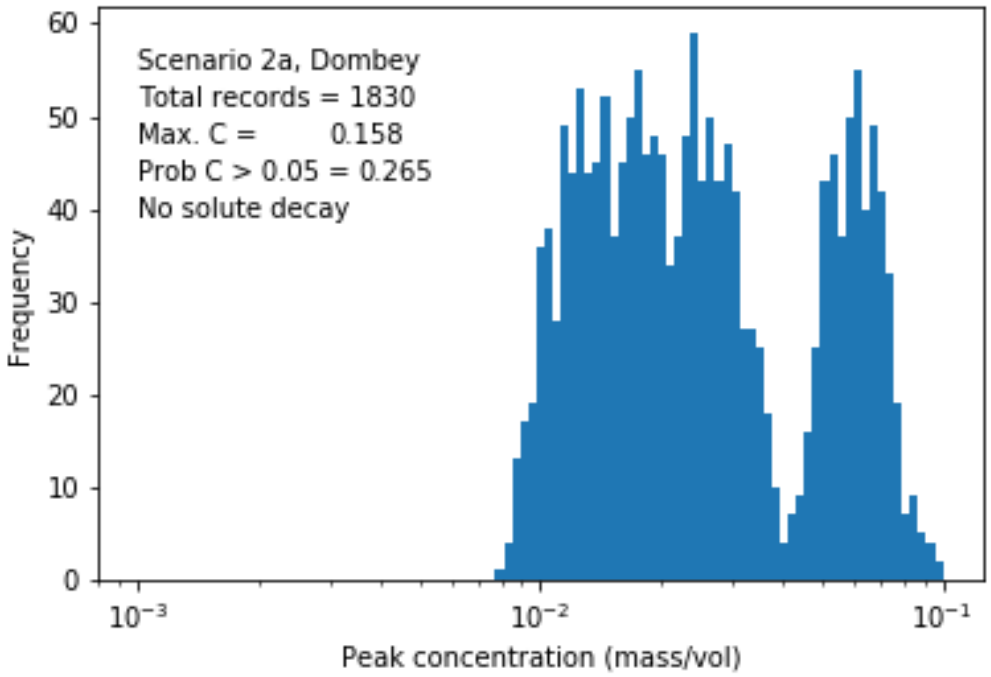

Figure 45: Distribution of peak concentrations (without solute degradation) for Scenario 2a at Dombey site

Dombey 1 well site; with solute degradation

As previously discussed, assets within a 1 km distance were included in this analysis. However, the number of stochastic simulations was maintained over 1000 while keeping the observed distribution of distances to receptors identified by the spatial analysis. Note that the distinct vertical groups of concentrations correspond to specific receptor locations (nearest located at 167 m).

Figure 46 shows a very significant drop in solute concentrations of up to 24 orders of magnitude relative to the unit input concentration, which is much higher than that observed for the case without solute degradation. The spread of the stochastic solute concentrations increases with distance as larger residence times significantly increases the mass of degraded solutes. Figure 47 shows a steep drop in peak concentration as distance to receptor increases.

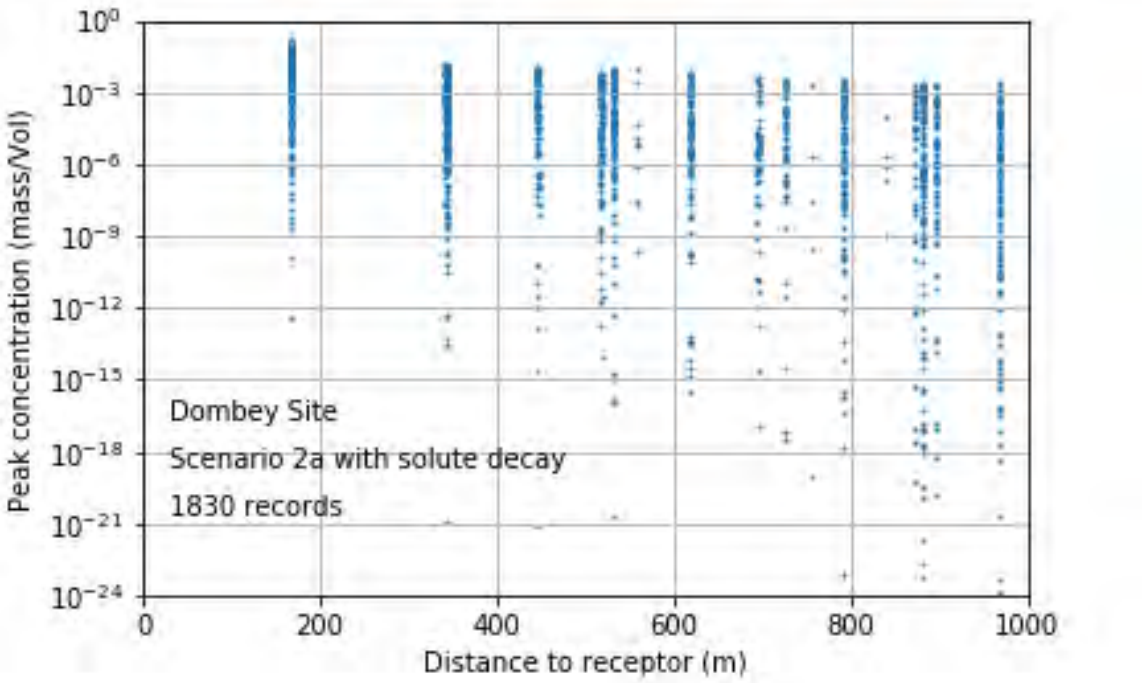

Figure 46: Peak concentrations (with solute degradation) versus distances to receptors (up to 1000 m) for Scenario 2a at Dombey 1 site

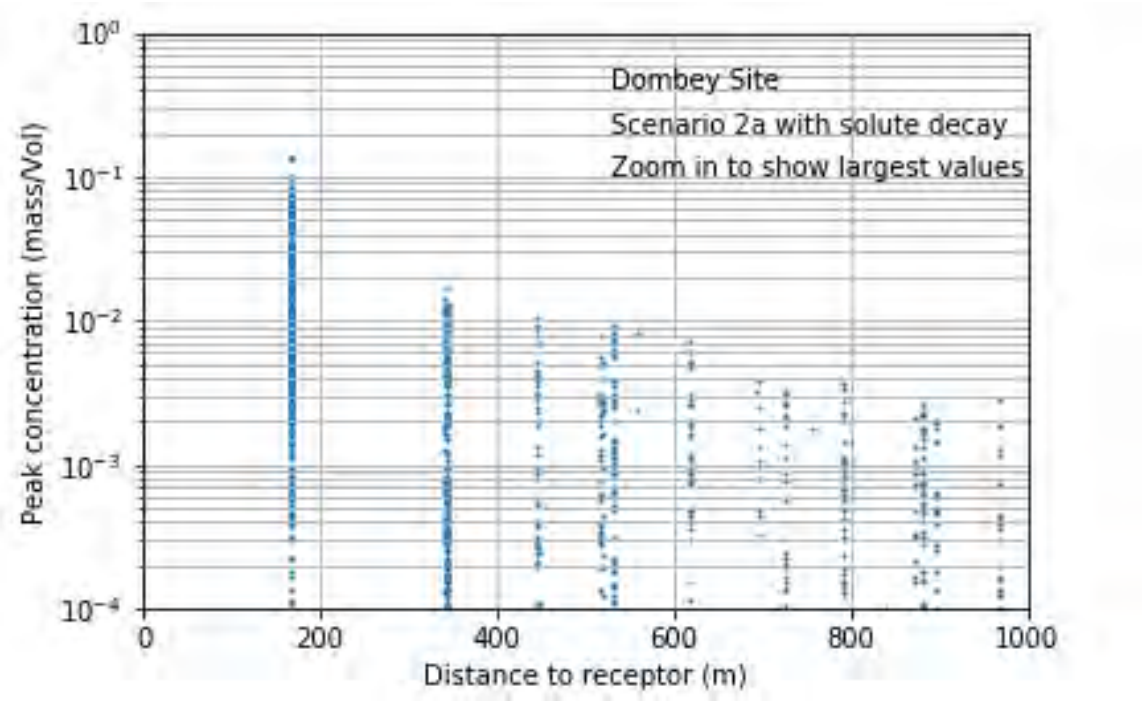

Figure 47: Peak concentrations (with solute degradation) versus distances to receptors (up to 1000 m) for Scenario 2a at Dombey site showing the higher concentration range

Figure 48 shows the distribution of concentrations across the stochastic simulations. The maximal peak concentration was 13.4% of the input unit concentration, which is higher than that observed for Scenario 1 owing to the lack of attenuation in the unsaturated zone. A peak concentration of 1% of the input unit concentration at the source occurred in 12.1% of the stochastic simulations.

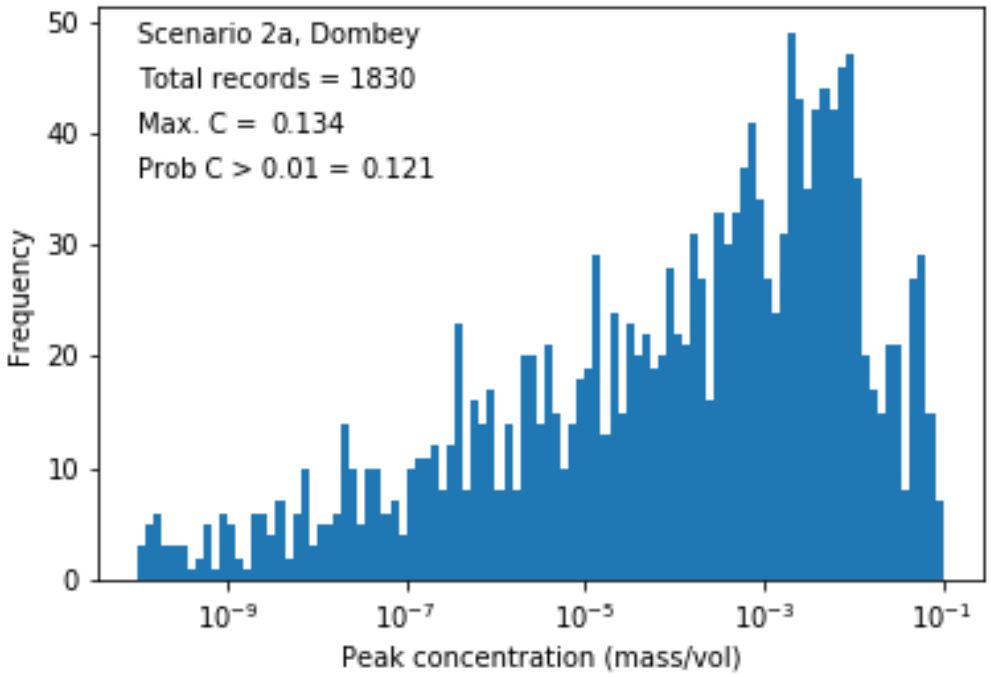

Figure 48: Distribution of peak concentrations (with solute degradation) for Scenario 2a at Dombey site

Figure 49 shows the effect of solute degradation on concentrations where a shorter half-life (higher degradation coefficient) leads to much lower concentrations. Note that the spread of concentrations significantly increases with higher degradation. As the degradation process is exponential, it is very sensitive to residence times, varying the dispersion coefficient and flow rate greatly influences residence times; higher solute dispersion reflects a wider distribution of residence times.

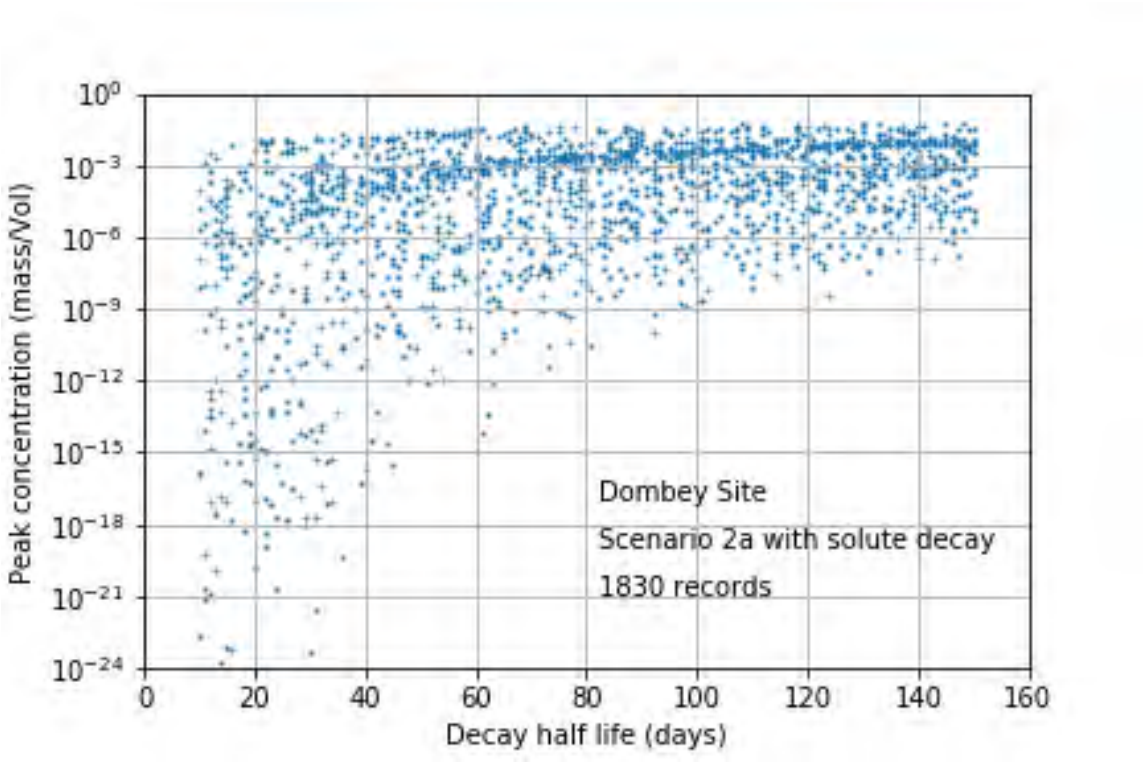

Figure 49: : Peak concentrations versus degradation half-life for Scenario 2a at Dombey site

Haselgrove 4 site; without solute degradation

The results for Haselgrove 4 site without solute degradation are shown in Figure 50 where solute concentrations decrease exponentially as distances to receptors increase as longer travel paths lead to higher solute dispersion. The distribution of peak concentrations is shown in Figure 51. The maximal peak concentration across the entire stochastic analysis amounted to only 32.2% of the input unit concentration at the source, with 31.2% of the simulations having a peak concentration of 5% of the input unit concentration at the source. These values are higher than those reported for Scenario 1, due to absence of solute attenuation in the unsaturated zone. They are the highest concentrations reported in this study due to the facts that there was no attenuation in the unsaturated zone, no solute degradation, and the shortest distance to receptor.

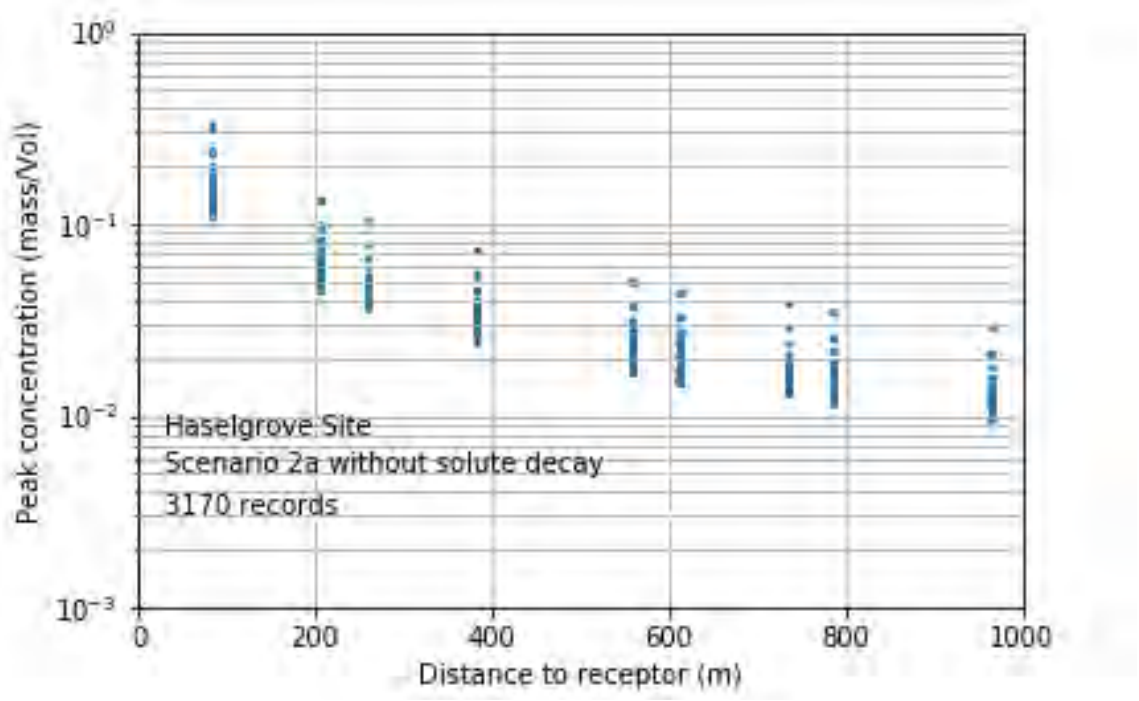

Figure 50: Peak concentrations (without solute degradation) versus distances to receptors (up to 1000 m) for Scenario 2a at Haselgrove 4 site

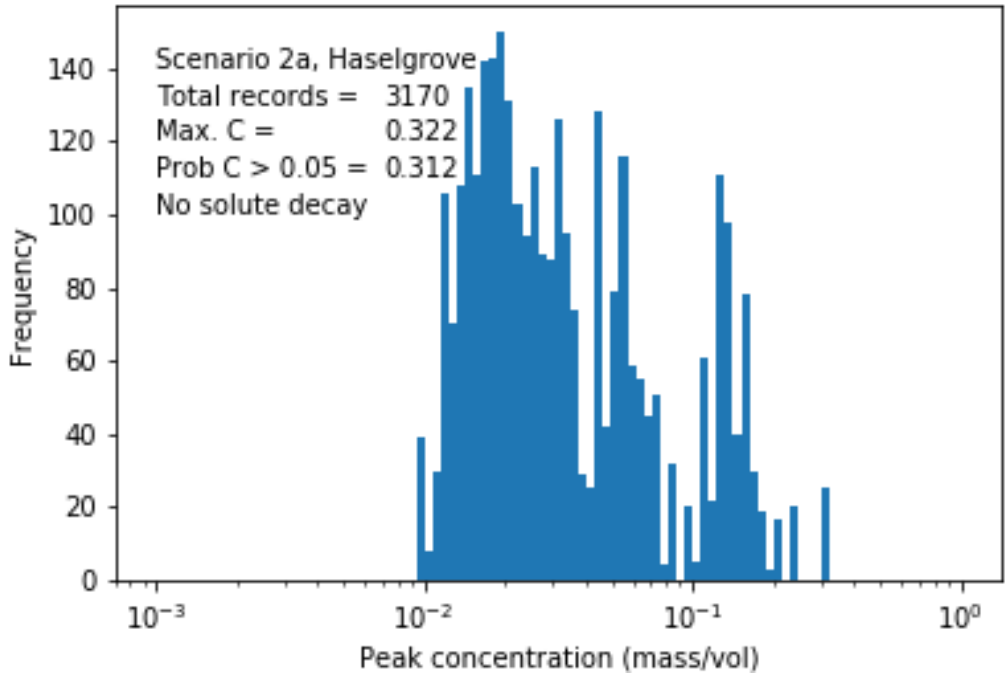

Figure 51: Distribution of peak concentrations (without solute degradation) for Scenario 2a at Haselgrove 4 site

Haselgrove 4 site; with solute degradation

Figure 52 shows a very significant drop in solute concentrations of up to 28 orders of magnitude relative to the unit input concentration, which is much higher than that observed for the case without solute degradation. The spread of the stochastic solute concentrations increases with distance as larger residence times significantly increases the mass of degradationed solutes. Figure 53 shows a steep drop in peak concentration as distance to receptor increases.

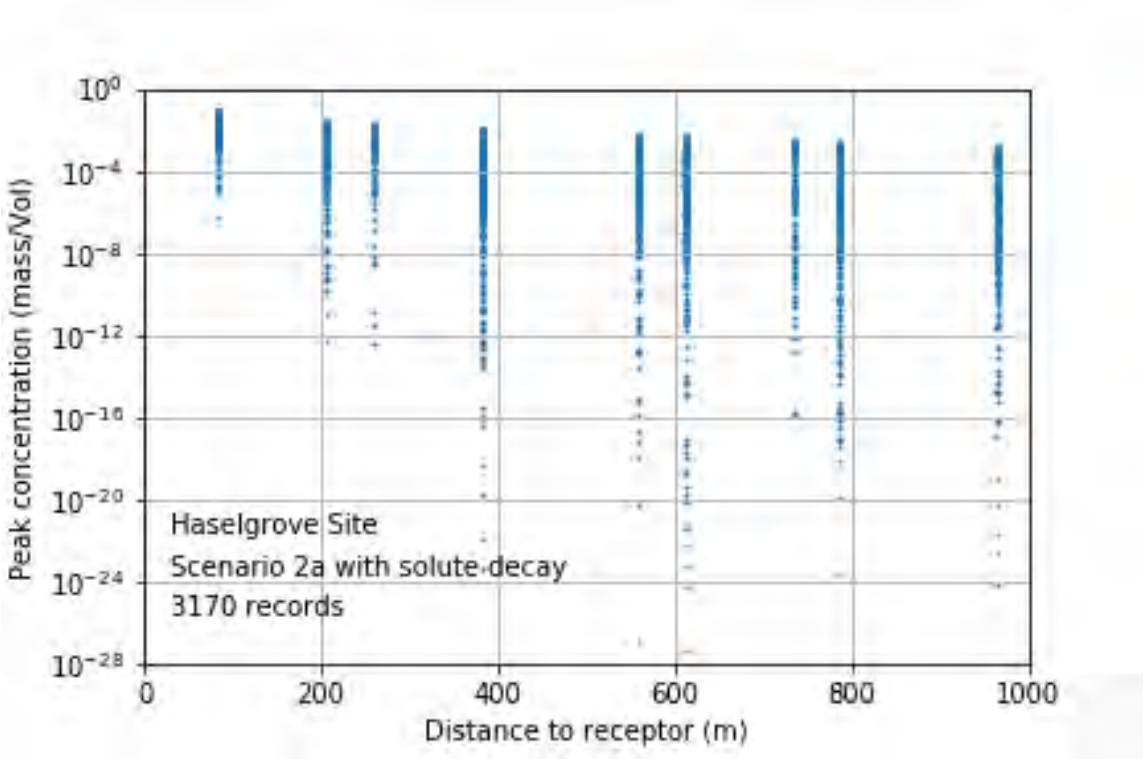

Figure 52: Peak concentrations (with solute degradation) versus distances to receptors (up to 1000 m) for Scenario 2a at Haselgrove 4 site

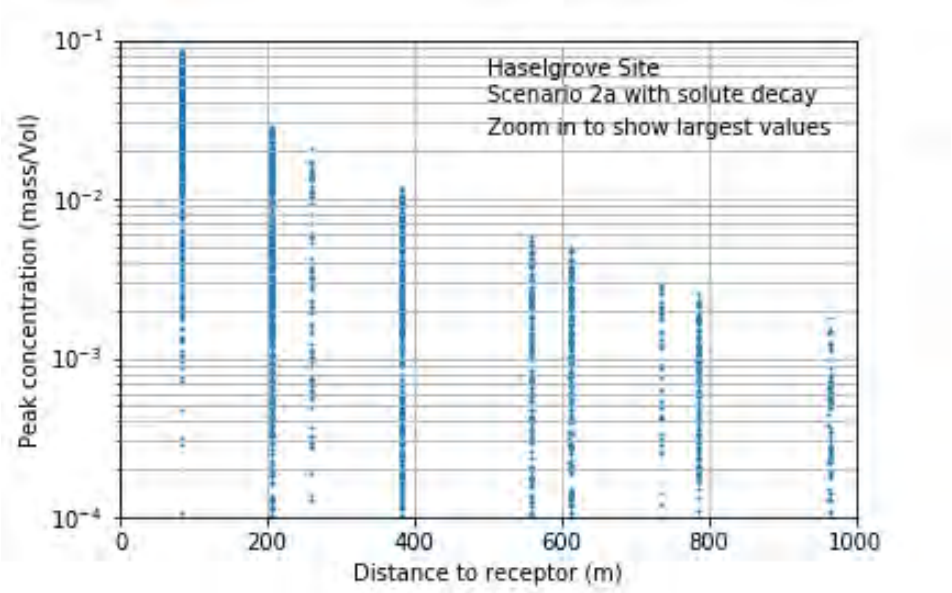

Figure 53: Peak concentrations (with solute degradation) versus distances to receptors (up to 1000 m) for Scenario 2a at Haselgrove 4 site showing the higher concentration range

Figure 54 shows the distribution of concentrations across the stochastic simulations. The maximal peak concentration was 8.6% of the input unit concentration, which is higher than that observed for Scenario 1 owing to the lack of attenuation in the unsaturated zone. A peak concentration of 1% of the input unit concentration at the source occurred in 16.6% of the stochastic simulations.

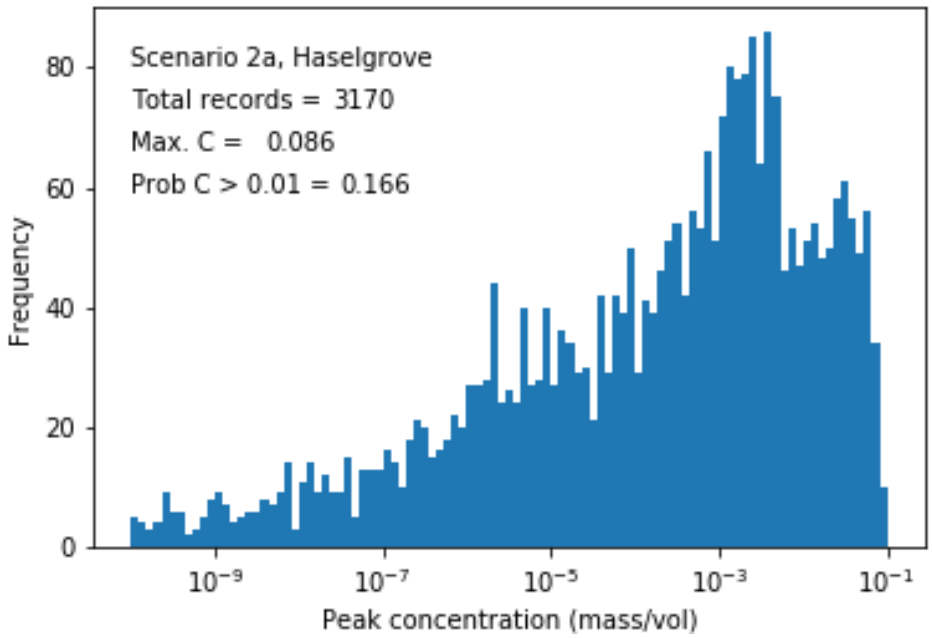

Figure 54: Distribution of peak concentrations (with solute degradation) for Scenario 2a at Haselgrove 4 site

Figure 55 shows the effect of solute degradation on concentrations where a shorter half-life (higher degradation coefficient) leads to much lower concentrations. Note that the spread of concentrations significantly increases with higher degradation. As the degradation process is exponential, it is very sensitive to residence times, varying the dispersion coefficient and flow rate greatly influences residence times; higher solute dispersion reflects a wider distribution of residence times.

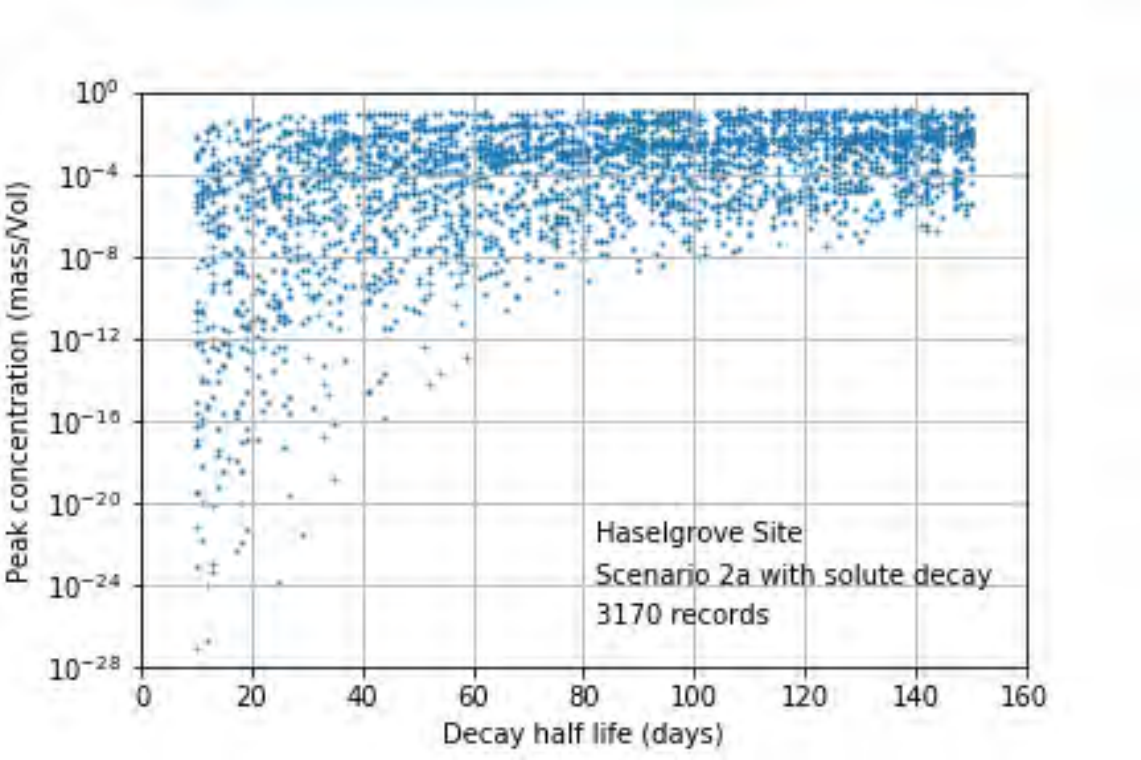

Figure 55: Peak concentrations versus degradation half-life for Scenario 2a at Haselgrove 4 site

5.2.2 Scenario 2b: Leakage into confined aquifer

The GIS spatial analysis has shown that there are no groundwater dependent assets within the vicinity of groundwater flow paths resulting from particles released into the tertiary confined sands aquifer. Hence, no further analysis was warranted.

5.3 Scenario 3: Spill at the surface or sub-surface

This is like scenario 1 with respect to flow and transport modelling considerations in that it is a leakage from near the surface into the unsaturated zone. There are two sub-scenarios considered for this case – 3a) surface spill and 3b) sub-surface spill. The simulations below were carried out for the Dombey site (Table 5).

5.3.1 Scenario 3a: Surface spill

This scenario involves a potential surface spill of 1000 L of a fluid having a unit solute concentration that spreads over a 10 m^2 area and is assumed to be controlled within 1 day. Since the surface spill occurs in an open area, solute movement will be influenced by rainfall and evaporation. Figure 56 shows a time series for rainfall for the 10-year simulation period used by HYDRUS-1D in conjunction with spill scenario.

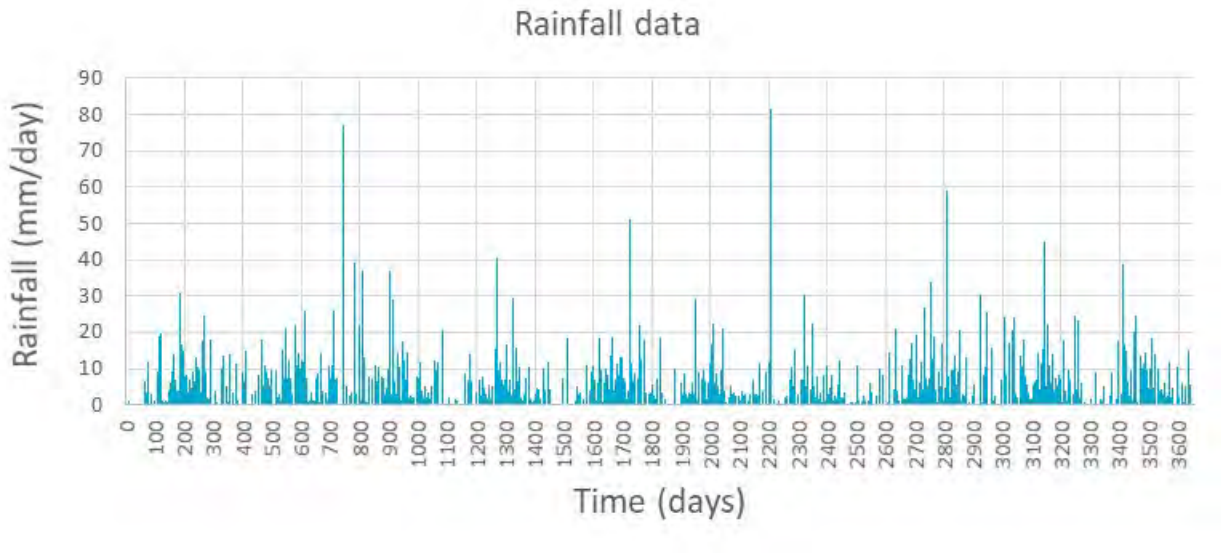

Figure 56: Rainfall data used to constrain the infiltration rate and solute concentration for scenario 3a at Dombey site

Figure 57 shows that concentration (relative to input) observed at the interphase with the water table is 0.18% of the input concentration without taking into account solute degradation. This is attributable to the dilution effect of solute-free rainwater infiltrating the soil profile. During no-rainfall conditions, the profile drains slowly hence solute flux become slow as well. Hence, no further modelling in the saturated zone is warranted.

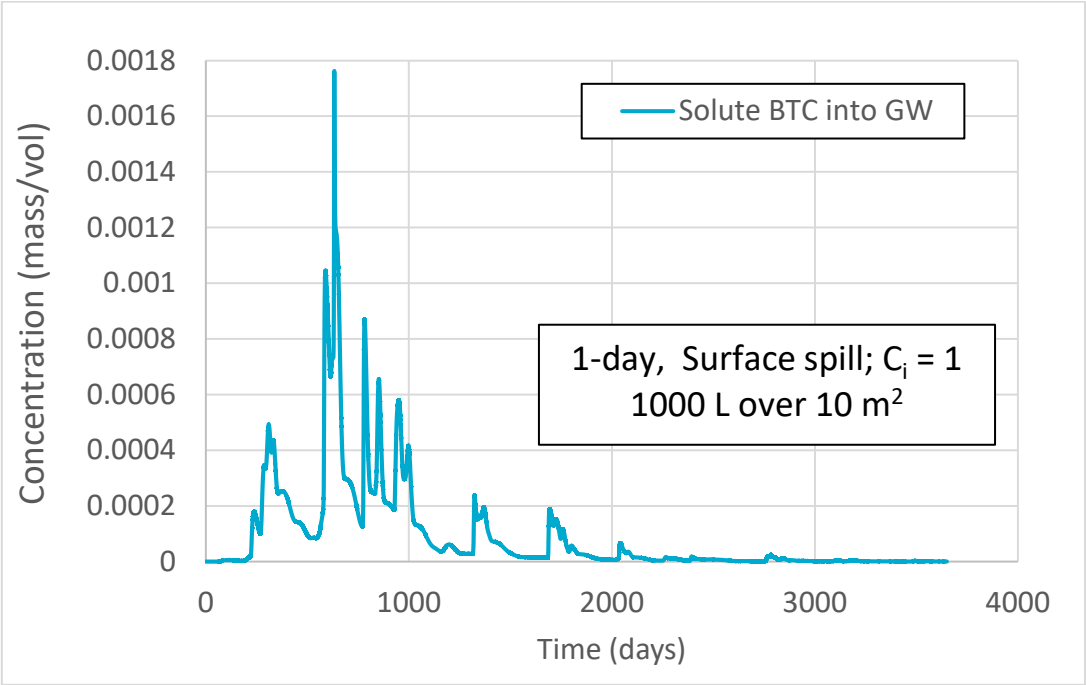

Figure 57: Breakthrough curve (BTC) into groundwater

The maximum concentrations reaching the groundwater table are much smaller those corresponding to scenario 1. So further transport modelling in groundwater was not warranted.

5.3.2 Scenario 3b: Sub-surface flow line leakage

This scenario considers a flow line leaking near the facility and going undetected for a period of 90 days; the flow line is located some 700 mm from the surface. A fluid volume of 5000 L with a unit solute concentration is assumed to be released over a 30 m^2 area. As there is no LDPE lining at the surface as in the case of drilling sump, the vertical movement of the fluid through the soil column will be mainly influenced by rainfall and evaporation.

Figure 58 shows that concentration (relative to input) observed at the interphase with the water table is 0.3% of the input concentration without taking into account solute degradation. This is attributable to the dilution effect of solute-free rainwater infiltrating the soil profile. During no-rainfall conditions, the profile drains slowly hence solute flux become slow as well. Hence, no further modelling in the saturated zone is warranted.

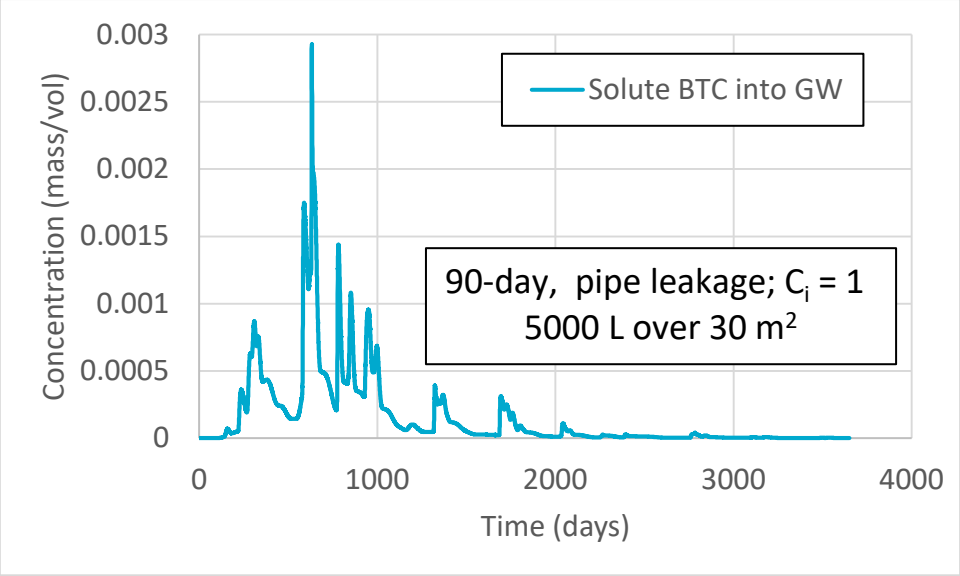

Figure 58: Breakthrough curve in the groundwater for scenario 3b.

The maximum concentrations reaching the groundwater table is much smaller than that corresponding to scenario 1. So further transport modelling in groundwater is not warranted.

5.4 Potential application of the method for informing management or regulatory decisions

The solute transport modelling presented in the previous sections resulted in identifying the level of natural attenuation that solutes undergo in the unsaturated and saturated zones. The analyses identified peak concentrations (C_{peak}; Figure 15) at explicit receptor locations for a range of hydraulic and solute transport parameters resulting from a unit input concentration (C_i) at the source. The degree of natural attenuation is quantified by the ratio C_i/C_{peak}, which reflects the dilution level of a solute, termed herein the Dilution Factor (D.F.). Since the input concentration used in this work was unity, then the D.F. is simply the reciprocal of the reported concentration (e.g., Figure 27). The integrated method developed in this study for computation of D.F. across saturated and unsaturated zones have potential applicability in informing management or regulatory decisions. For example, it can be used to infer management strategies for attaining safe levels of natural attenuation for potable water quality or to avoid aquatic toxicity for target organisms. In this section we illustrate this by computing distances beyond which aquatic toxicity is extremely unlikely to occur from each of the organic and inorganic chemicals used in the drilling fluid considering the composition used at the Haselgrove-3 well site and aquatic toxicity levels for an indicator aquatic crustacean genus, Daphnia.

Natural attenuation is impacted by a number of factors, including the length of the flow path with longer paths associated with greater dilution and dispersion while greater residence times enhance biochemical degradation and mass removal through adsorption processes. Hence, the solute modelling results were re-analysed to derive 50^{th} (median) and 95^{th} percentile dilution factors for each receptor location, i.e., for every unique flow path length (e.g., shown as discrete vertical lines in Figure 31, which represent the explicit location of receptors identified by the particle tracking analysis). Note that the 95^{th} percentile dilution factors represent a smaller dilution relative to the 50^{th} percentile (it was calculated on the 95^{th} percentile highest peak concentration). This was carried out for the Dombey 1 and Haselgrove 4 sites for Scenario-1. As some chemical degrade and others don't (inorganics and potentially some organics if the appropriate biogeochemical conditions for degradation do not exist), the analysis was separately carried out for both cases.

Results for the no-degradation case (Figure 59) show that the dilution factors vary linearly with the length of the flow path. The analysis showed that the concentration versus distance relationship was in the shape of a power function with an exponent very close to (-1), with the dilution factor being the reciprocal of concentration (C^{-1}); D.F. versus L ended up being almost perfectly linear. Equations for the 50^{th} (median) and 95^{th} percentile were derived for Dombey ($D.F._D$) and Haselgrove ($D.F._H$) as shown in Figure 59. Note that the relationships for both gas wells were very similar as the model that was used had the same depth to groundwater table, similar soil horizons, and similar groundwater flow rates. The different points (x-axis) at each site represent different receptors that have intercepted the flow path for each gas well site.

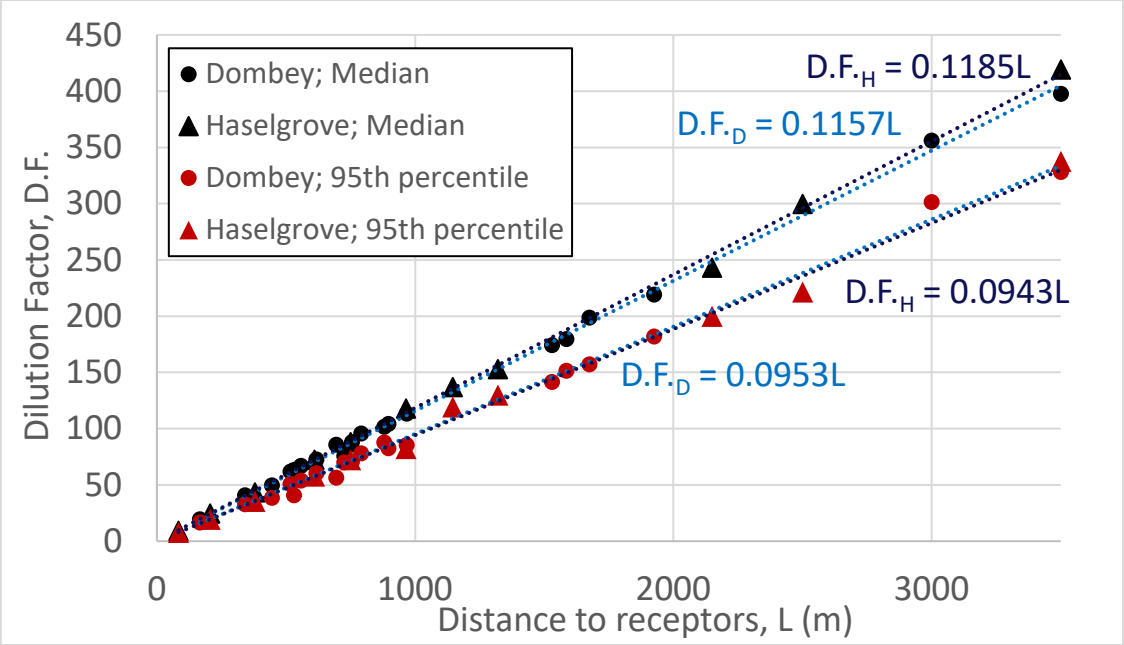

Figure 59: Median and 95th dilution factors (without degradation) at various distances for Dombey ($D.F._D$) and Haselgrove ($D.F._H$)

The process was repeated for degradable solutes with results shown in Figure 60. The relationships were exponential, which is the result of the exponential decay process modelled, note that they appear as straight lines as they are plotted on a semi-logarithmic scale.

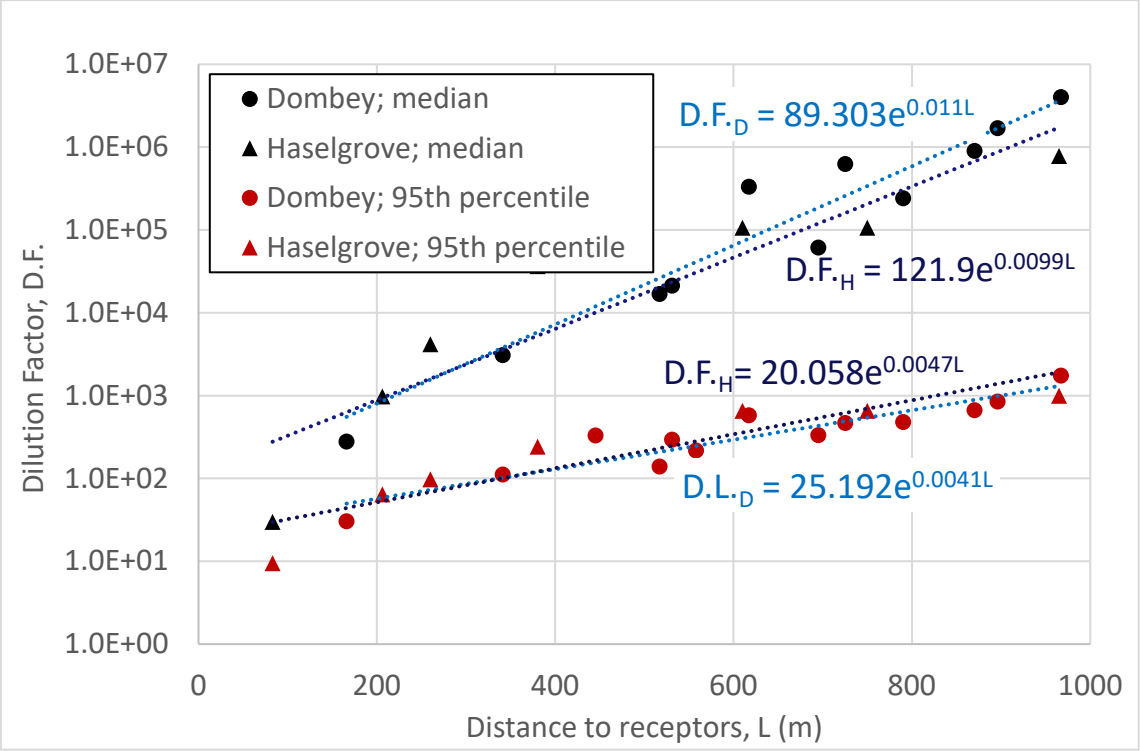

Figure 60: Median and 95th dilution factors (with degradation) at various distances for Dombey ($D.F._D$) and Haselgrove ($D.F._H$)

A variety of chemicals are used during gas production activities. These chemicals are used in different concentrations and have different toxicity levels. As a chemical naturally attenuates, its concentration decreases until it reaches an acceptable concentration for a specific ecotoxicity endpoint (e.g. fish or daphnia), this is termed the predicted no-effect concentration (PNEC). The dilution factor required to achieve this concentration ($D.F._{min}$) is the ratio of the input concentration at source to the predicted no-effect concentration (C_i/PNEC). Values of $D.F._{min}$ for various chemicals used in gas production activities (here drilling chemicals only) are listed in Appendix III; values for four sample chemicals are shown in Table 9.

Having identified mathematical functions that relate dilution factors to travel path length, one can use them to define the minimum flow path length (L) required to achieve the minimum dilution factor $D.F._{min}$. Table 10 shows sample estimates for one degradable (organic) and one non-degradable (inorganic) chemicals. Obviously, the lengths required to achieve $D.F._{min}$ is larger for the latter. This analysis can help regulators to inform management decisions or guidelines, for example, distances around gas well to avoid chronic aquatic toxicity. Similarly, it could also aid in managing concentrations at the source

by defining a maximum concentration to satisfy a minimum dilution factor for a certain target distance. Note that the dilution and dispersion in the saturated and unsaturated zone was calculated with one-dimensional models. These model underestimates the dilution and dispersion, therefore the results shown in Table 9 are conservative especially within proximity of the source (i.e. concentrations and distances would likely be less than the values shown in the table). While the integrated modelling method presented in this study is generic and can be applied for computing Dilution Factors for such applications, the model scales and parameters should be tailored to suit the individual application, source-receptor combinations and chemical species of interest. The saturated zone models we developed in this study has a regional focus with the objective of simulating Dilution Factors for a broad range of plausible parameter combinations and considering 3 gas wells and potential receptors across the region.

Table 9: Estimates of safe distances required for natural attenuation of two sample chemicals obtained using the 1D model and considering the chronic aquatic toxicity level of Daphnia

	Chemicals and minimum dilution factors ($D.F._{min}$)	Distance Dombey 1 (m)		Distance Haselgrove 4 (m)	
		50^{th}	95^{th}	50^{th}	95^{th}
Degradation	Citric acid (186)	67	488	43	474
No degradation	Potassium chloride (18)	156	189	152	191

6 Summary and Conclusions

This report examined plausible pathways for groundwater contamination risk from conventional gas development in the southeast SA considering three gas wells – Dombey 1, Haselgrove 4 and Nangwarry 1 that were recently drilled. The study also undertook vulnerability and modelling analysis to provide an overarching assessment of water quality (concentration) changes should a plausible contamination event happens.

Physiographic and aquifer characteristics in the study area was systematically analysed to quantify the natural vulnerability of the aquifer systems for contamination risks. Six characteristics were considered for vulnerability analysis. These are depth to groundwater table, topographic slope, internal drainage area height, groundwater velocity, recharge potential, and soil clay content. Each of these characteristics has the potential to affect the movement of any contaminant appearing at the land surface towards or within the aquifer. For example, contaminants can reach the aquifer faster if the water table is shallow. On the other hand, contaminant movement towards the aquifer will be slower if there is higher clay content in the soil column. A spatially explicit weighted summation of these characteristics was used in this study to quantify the natural vulnerability of the Gambier Limestone Aquifer and Teritiary Confined Sands aquifer for contamination risks. A similar approach was used to quantify the density of water dependent assets in the study area considering environmental, economic and sociocultural assets. The vulnerability and asset density analyses provide a preliminary and relative assessment of whether physiographic characteristics are conducive for contaminant migration should a contamination event happens and density of assets in the vicinity. The vulnerability analysis showed that there are areas of relatively high vulnerability within the study area and warranted more detailed analysis for modelling-based contaminant transport simulations.

Particle tracking analysis was undertaken as an intermediary step of contamination transport simulation. The particle tracking analysis provides a useful tool for computing and visualising groundwater travel paths, travel times and distances from the gas well using the analogy of a particle moving along with the groundwater flow. Particle tracking was undertaken for a time period of 100 years. A probabilistic approach was used for this simulation to account for prediction uncertainties. The analysis showed that groundwater travel path is predominantly in the northwest direction from the Haselgrove 4 and Nangwarry 1 well locations and towards east from the Dombey well location. The travel distances along these directions ranged from 8 to 20 km over the 100-year simulation period. Locations of receptors (water bores, water bodies, drains and water courses) in relation to particle tracks and gas well locations were recorded to provide distances at which concentrations would be calculated corresponding to relevant contamination scenarios. A spatial analysis has shown that 18%, 67%, and 71% of the flow path tracks have actually intercepted groundwater-dependent assets resulting from particles released from the Dombey 1, Haselgrove 4, and Nangwarry 1 site, respectively.

Following the identification of flow paths, groundwater flow rates along these paths, and their potential interception with groundwater dependent assets, solute modelling was conducted in two stages, the unsaturated and saturated zones. For the former, HYDRUS-1D was used to model coupled transient flow and solute transport, and for the latter stage, an analytical solution of the advective-dispersive equation under steady state flow conditions was adopted. The two models were loosely coupled where the output from stage 1 was used as input to stage 2.

Unsaturated flow and transport modelling for Scenario 1 (leakage from liner) in the has resulted in solute breakthrough curves at the water table that showed a delay in solute arrival and a significant reduction in solute concentration when solute degradation was taken into consideration, with a 35% and 55% reduction rates for the Dombey and Nangwarry 1 sites, respectively. Unsaturated modelling for Scenario 3 (surface spill and leakage from subsurface flow line) has shown that recharge from rainfall, which drives the leaking fluids, lead to significant dilution of up to three orders of magnitudes, thus deeming modelling in the saturated zone unnecessary. Scenario 2 (compromised well integrity) did not involve modelling in the unsaturated zone.

Scenario 1 (leakage from liner): Coupled unsaturated-saturated solute transport modelling for Dombey site has shown a significant reduction in solute concentration from unity to 0.045 and 0.07, with and without solute degradation, respectively. Analysis of the stochastic modelling results had shown that 91.2% and 79.8% of the simulations has concentration of less than 1% of the input concentration with and without solute degradation, respectively. Coupled unsaturated-saturated solute transport modelling for Haselgrove 4 site has shown a significant reduction in solute concentration from unity to 0.129 and 0.143, with and without solute degradation, respectively. Analysis of the stochastic modelling results has shown that 91.6% and 85.7% of the simulations had concentration of less than 1% of the input concentration with and without solute degradation, respectively. The Haselgrove 4 site exhibited higher maximal concentrations due to a closer proximity to groundwater dependent assets.

Scenario 2a (compromised well integrity): Saturated solute transport modelling for Dombey site has shown a significant reduction in solute concentration from unity to 0.134 and 0.158, with and without solute degradation, respectively. Analysis of the stochastic modelling results has shown that with solute degradation, 87.9% of the simulations had concentration of less than 1% of the input concentration; without solute degradation, 73.5% of the simulations had concentration of less than 5% of the input concentration. Saturated solute transport modelling for Haselgrove 4 site has shown a significant reduction in solute concentration from unity to 0.086 and 0.322, with and without solute degradation, respectively. Analysis of the stochastic modelling results has shown that with solute degradation, 84% of the simulations had concentration of less than 1% of the input concentration; without solute degradation, 68.8% of the simulations had concentration of less than 5% of the input concentration. The Haselgrove 4 site exhibited higher maximal concentrations due to a closer proximity to groundwater dependent assets.

Scenarios 3a (surface spill) and 3b (subsurface flow line leakage): Unsaturated flow and transport modelling for both scenarios has shown that when a unit concentration is applied at the source, solute concentrations observed at the water table interphase were equal to 0.0017 and 0.0028, for scenarios 3a and 3b, respectively. This attributable to the dilution effect of rainwater infiltrating the exposed soil surface.

A 2-dimensional MT3D model was also developed for the study area to investigate the flow and transport processes considering advection and dispersion processes in two dimensions. The solute concentrations resulting from the coupled 1-dimensional modelling approach were within the same order of magnitude of those resulting from the 2-dimensional MT3D model described in Appendix III.

The overarching results of simulation of realistic scenarios of contamination events at all the three well locations indicated that the solute concentrations would decrease exponentially with time and distance in the direction of flow from the gas well sites. Probabilistic simulation analysis considering probable range of values for soil and aquifer characteristics and available chemical degradation characteristics indicated that it is highly likely that the concentrations decrease to less than 1% of the input concentration within short distances from where the incident could happen near the gas well head and other facilities. Given that most of the chemical constituents constitute only a small mass fraction of the drilling fluid (<1%), it implies that they would dilute down to very small concentrations before reaching receptor locations, especially those that are located far from the gas well sites.

A generic approach was used in this study whereby transport modelling is applied to quantify the maximum concentration in the aquifer and concentration at the receptor locations as a percentage of the concentration at the source. This generic approach of modelling the dilution and attenuation of contaminant before reaching a water-dependent receptor and in the aquifer would enable the regulator to quantify the residual contamination risk given the concentration of contaminants at the source. The method has potential applicability in informing regulatory and management decisions. For example, it can be used to infer management decisions for attaining safe levels of natural attenuation for potable water quality or to avoid aquatic toxicity for target organisms. We illustrated the applicability of this method for such purposes by computing distances beyond which aquatic toxicity is unlikely to occur from one each of the organic and inorganic chemicals used in the drilling fluid (considering the drilling fluid composition used at one of the sites) and aquatic toxicity levels for an indicator aquatic crustacean genus, Daphnia. The example application for one organic (citric acid) and one inorganic (Potassium Chloride) chemicals considering the concentrations used for drilling one of the wells in the region showed that median distances of 67 and 156 m respectively from the Dombey 1 well could ensure that the concentrations of these chemicals are below the chronic aquatic toxicity levels for the indicator crustacean genus of daphnia. The corresponding 95^{th} percentile values for the distances are 488 m and 189 m respectively. Similar values were calculated for the Haselgrove 4 well as well. Alternatively the simulated dilution levels can also be used to inform the concentration levels used at the source to ensure that concentrations are below prescribed levels within target distances.

While the integrated modelling method presented in this study is generic and can be applied for computing attenuation levels for such applications as described above, the model scales and parameters should be tailored to suit the individual application, source-receptor combinations and chemical species of interest. The saturated zone models we developed in this study has a regional focus with the objective of simulating concentration changes and attenuation levels for a broad range of plausible parameter combinations and considering three gas wells and potential receptors across the region. One-dimensional solute transport models are used in this study due to their simplicity, amenability to stochastic modelling framework and more importantly because they don't underestimate concentrations and thus provide a conservative estimate of concentration changes (worst-case). Two- or three-dimensional modelling of the solute transport processes are warranted if the method is to applied for informing management decisions and those models need to be tailored for individual applications. Rates of dilution and attenuation when transport processes are simulated in 2-d flow field is illustrated in Appendix 1.

The scope if this study is limited to providing a screening analysis to evaluate groundwater contamination risks as relative concentration at spatial locations in comparison to source strength for a broad range of soil, aquifer and chemical characteristics and plausible scenarios of contamination events to provide information to the regulators and other stakeholders an overview of residual risks when standard management and clean up procedures are performed for indicative contamination scenarios. Hence the findings of this study do not preclude the requirement to have stringent monitoring, management procedures to avoid and management contamination events. It does not predict groundwater contamination anywhere in space and time for any specific future event or chemical and such analysis is beyond the scope of this study. Site-specific and species specific modelling an assessments are warranted should such incidents occur.

APPENDIX I: Advection-dispersion transport 2D MT3D model

The regional MODFLOW model developed for the study region has shown that overall groundwater heads on the eastern side are higher than those on western side with the exception of the south west corner that looks like a high recharge area. The petroleum well under investigation is located in an area where groundwater flows from east to west. This risk-based assessment investigates the likelihood of contaminant particles reaching receptors using a 2D cross-sectional conceptual model. The potential contaminant pathways included a surface pathway in relation to surface handling and a deeper groundwater pathway. The surface spills in oil and gas operation are very common issue due to the large amounts of different fluids being handled at or near the well site.

In currently developed child model covering the south eastern part of South Australia, the average distance from source to receptor was around 3 km. This distance was used as the length of 2D cross-sectional model. The geological unit of the child model included the first layer of Gambier limestone, the second layer of Ettrick Formation aquitard, and the third layer of Dilwyn Sand. As the aquitard obstructs the hydraulic connection between the first and third layer, the 2D model only included the first layer with a depth of 100 m aiming to investigate the impact of contamination in relation to the surface contaminant pathway. According to the investigation of South East Regional Water Balance model (Morgan, 2015), Gambier limestone belongs to karstic geology that has not been completely developed. In the 2D cross-sectional model, this karstic characteristic was described by two high permeability zones. Most of the petroleum wells are located between the Penola and Nangwarry, so that site was picked to implement our groundwater reactive transport model. The elevations of ground surface are 2 and 5 m, respectively, for west and east boundary of the 2D cross-sectional model. This conceptual model is shown in Fig. S1.

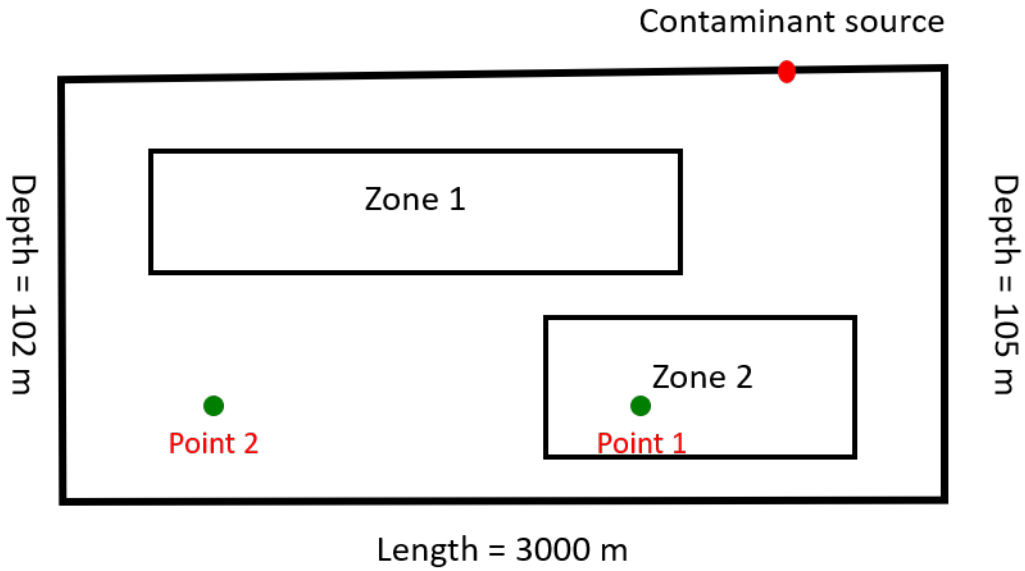

Fig. S1. 2D cross-section conceptual model of an unconfined aquifer located in southeast South Australia. The elevations of ground surface are 2 m and 5 m, respectively, for west and east boundary. Zone 1 and Zone 2 are the high permeable zone. The red dot is the hypothetical contaminant source on ground surface. The green dots are the hypothetical observation points.

Transient boundaries on the eastern and western sides of the model domain were controlled by time-varying groundwater heads during the 50-year simulation period. The data was acquired from WaterConnect website (https://www.waterconnect.sa.gov.au/Systems/GD/Pages/Default.aspx). 20 years observations were found from the nearby observation wells for the two sides of 2D conceptual model. We extended the head variation to 50 years by copying the same downtrend with a period of 20 years (Fig. S2a). The temporal variation of recharge and evapotranspiration were acquired from the WAVES data and further adjust to the proper data for this model. The local recharge and evapotranspiration data of the calibrated child model with steady boundary conditions were used as the mean value for the temporal data. The stress period of all transient data was 30 days. Boundary conditions used in the 2D groundwater transport model are shown in Fig. S2. In addition, the contaminant source was set at the upstream with a unit concentration.

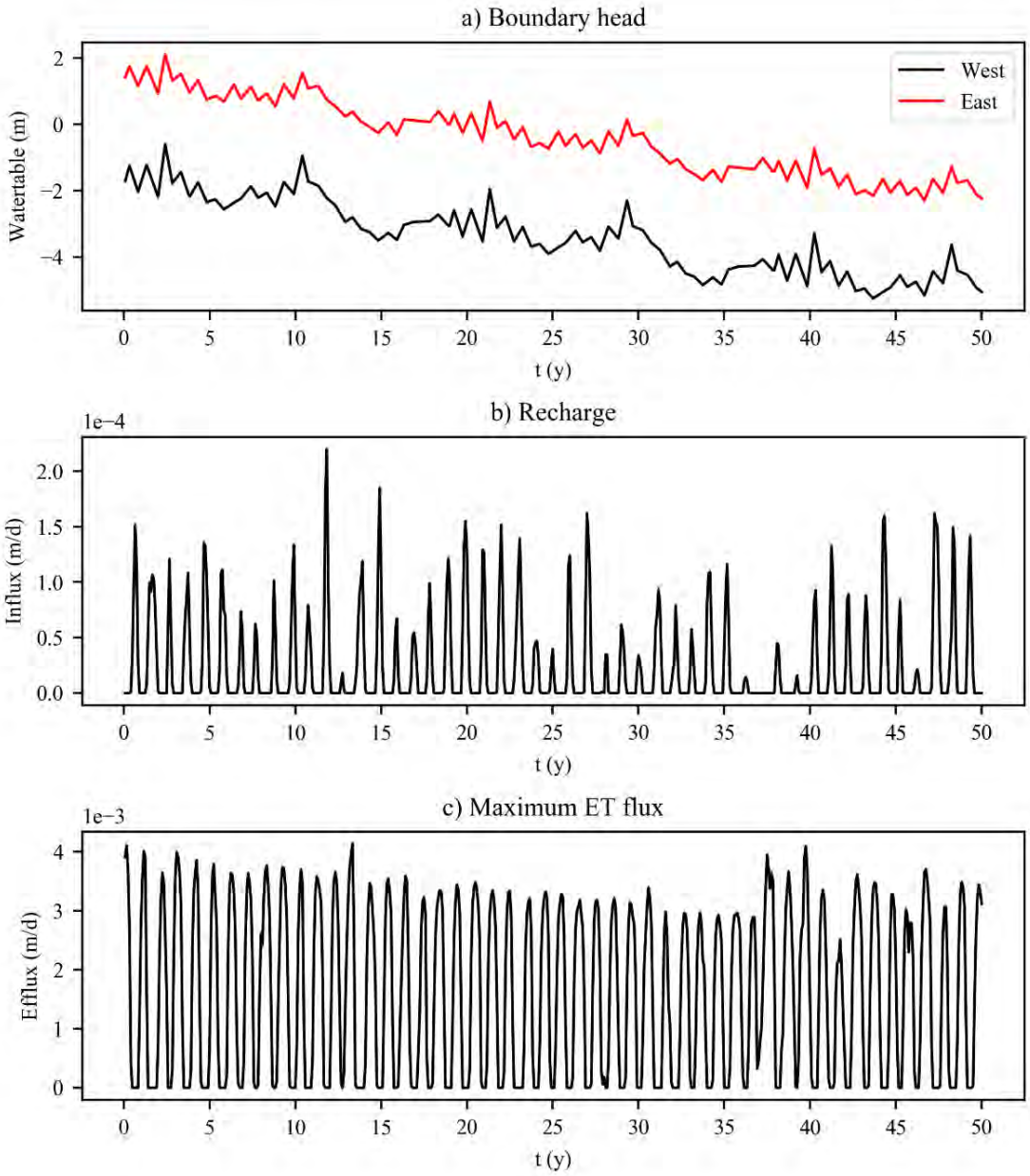

Fig. S2. Transient boundary conditions used in the 2D transport model. (a) Watertables of west and east boundaries. (b) Recharge from the top surface. (c) Maximum evapotranspiration flux.

MODFLOW-NWT (Niswonger, Panday, & Ibaraki, 2011) and MT3D-USGS (Bedekar, Morway, Langevin, & Tonkin, 2016) were selected to conduct the numerical experiment for groundwater flow and contaminant transport simulations, respectively. The Upstream Weighting Package and the Newton Solver were adopted for simulating the drying and wetting processes of the unconfined aquifer in MODFLOW-NWT. The Time-Variant Specified-Head package, Recharge package and Evapotranspiration package were used to implement the flow boundary condition. In MT3D-USGS, the DST and RCT package were used to implement solute diffusion and reaction mechanisms. The contaminant was introduced into the aquifer with recharge using the DRYCELL key-word option, this operation was implemented in the SSM package.

Advection, diffusion and reaction were considered in the transport model. Ten parameters from MODFLOW-NWT and MT3D-USGS were selected to analyse the sensitivity of contaminant concentration at receptors to aquifer properties. based on a prior investigation (Morgan, 2015), the calibrated horizontal hydraulic conductivity was 60 m/d in the study area. The global horizontal hydraulic conductivity (K_{h0}) was set in the range from 20 to 100 m/d for the entire karstic aquifer in the 2D model; the horizontal hydraulic conductivities in the high permeability zones 1 and 2 (K_{h1} and K_{h2}) were set in the same range from 100 to 200 m/d. Aquifer anisotropy was represented by the ratio of horizontal hydraulic conductivity to vertical hydraulic conductivity (K_{h0}/K_{v0}, K_{h1}/K_{v1} and K_{h2}/K_{v2}) with ranges from 5 to 15. The porosity of the karst limestone ranged from 0.05 to 0.5 (Zheng & Bennett, 2002). In this model, the effective porosity was set from 0.1 to 0.35 as this karstic aquifer have not completely matured; specific yield (S_y) in the flow model was assigned the same value as effective porosity. The longitudinal dispersivity (α_L), and the ratio of transverse dispersivity to longitudinal dispersivity (α_T/α_L) was set in the range from 15 to 60 m, and from 0.02 to 0.2, respectively. The distribution coefficient (K_d, used to describe linear sorption) was set in the range from 0.001 to 0.1 m^3/kg (note that no specific chemical was modelled, and this range was deemed to be a suitable distribution coefficient in limestone).

Latin hypercube sampling was used to generate 2700 parameter sets, which were used to run the model 2700 times to acquire the distribution of contaminant concentrations at receptors. Two observation points were selected 500 m and 2000 m downstream of the contaminant source located at a depth of 75 m.

2. Sensitivity results for aquifer properties

The contaminant concentration at observation point 1, which is 500 m away, was in the range from 1.10×10^{-7} to 1.58×10^{-4} for continuously leaking source at unit concentration. The median concentration was 5.78×10^{-5} and the 5th percentile was 9.88×10^{-6}. The concentration at the other receptor was in the range from 1.76×10^{-8} to 1.70×10^{-4}. The median concentration was 6.88×10^{-5} and the 5th percentile was 2.10×10^{-5}. The contaminant concentration exists the wide range for further receptor and the mean value of this receptor is larger than the close receptor in this context (Fig. S3).

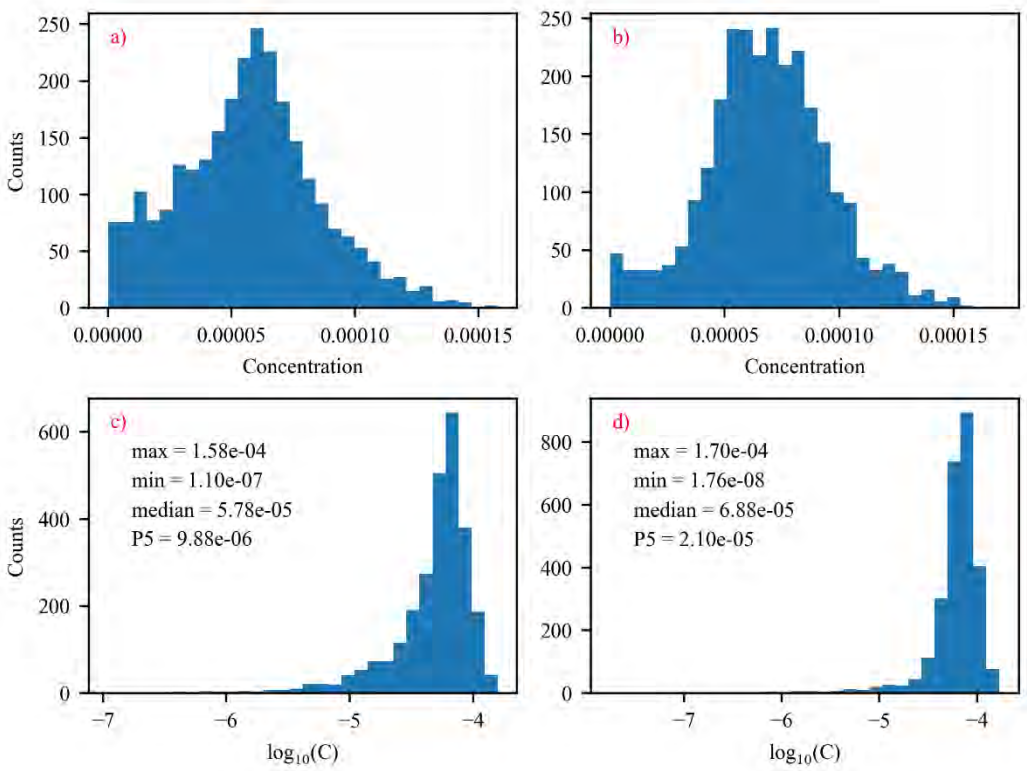

Fig. S3. Concentration distribution of two receptors. (a) and (c) are the contaminant concentration for the receptor with a horizontal distance of 500 m to contaminant source. (b) and (d) are the contaminant concentration for the receptor with a horizontal distance of 2000 m to contaminant source.

Scatterplots relating contaminant concentration and model parameters were constructed to further investigate the impact of aquifer properties on receptor concentration. The close receptor was slected to present the correlation between simulated concentration and model parameters. The competing effects of model parameters on the contaminant concentration are obvious that K_{h0}, α_L and α_T/α_L play the key role in receptor concentration (Fig. S4). Specifically, larger K_{h0} increased groundwater flow and carried more contaminants to the downstream so that the apparent downtrend was captured between concentration and K_{h0} (Fig. S4a). Also, the slight downtrend was observed when K_{h1} and K_{h2} increased (Fig. S4b and S4c). The influence of aquifer anisotropy was relatively less in this context. The effect of S_y (porosity) was also not large. It is interesting to note that smaller receptor concentrations are concentrated in the range of smaller α_L and α_T/α_L and larger K_d, different pattern with advection parameters (Fig. S4h, S4i, and S4j). That means the smaller diffusion and larger sorption greatly aggravate the decrease of contaminant concentration. This phenomenon is the most obvious in the correlation to α_T/α_L among all factors and demonstrate the vertical transverse is very important for the concentration of receptor in this aquifer.

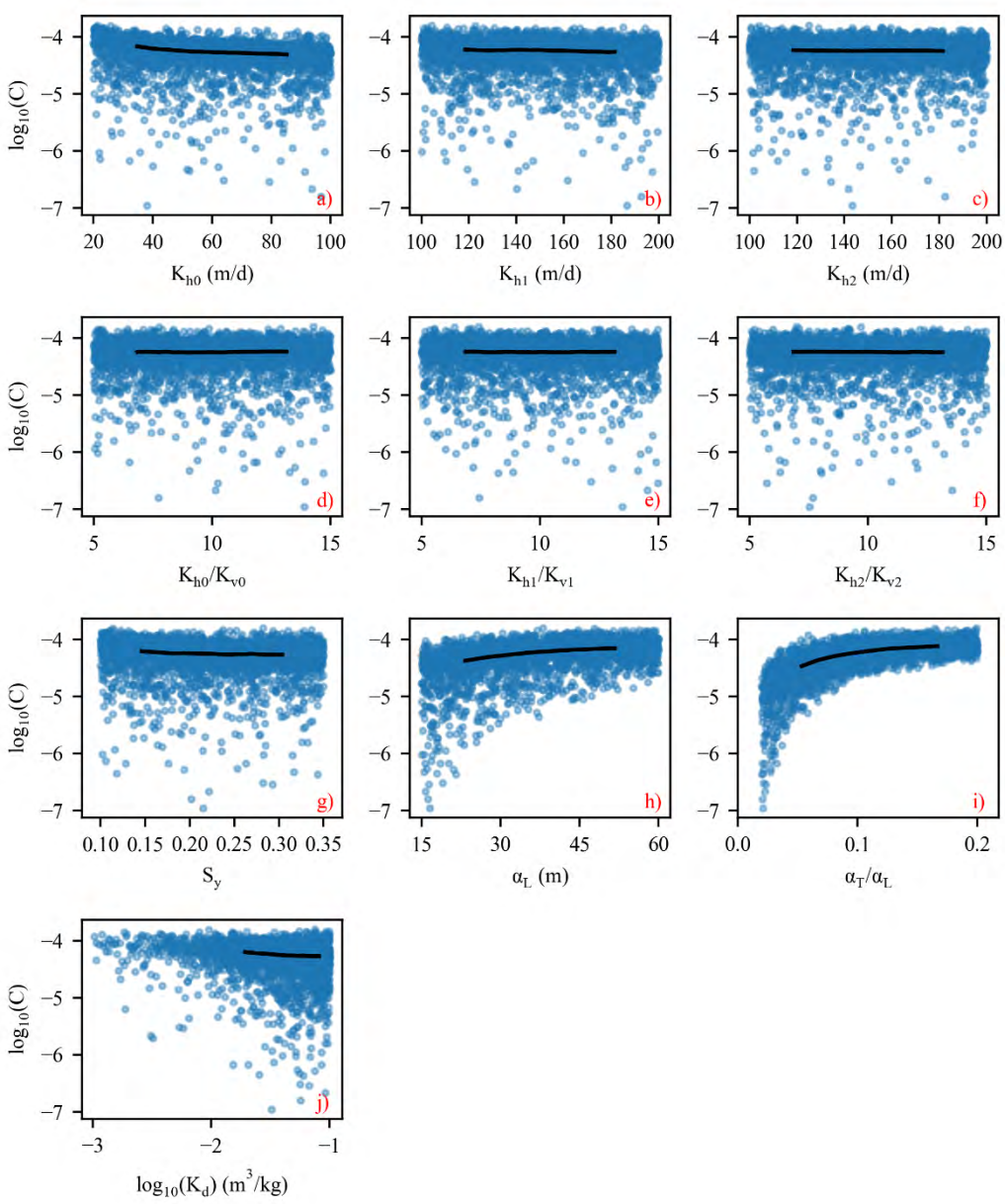

Fig. S4. Scatterplots between the contaminant concentration and model parameters used in MODFLOW-NWT and MT3D-USGS. The model parameters are given in the x-titles. Black lines are the moving average of concentration.

Appendix II: Adsorption isotherm

In groundwater sediments and interburden rocks, chemicals are temporarily removed from the water phase by an interaction with the solid matrix by chemical, physical or electrostatic forces. This process is generally called sorption (US EPA, 1999b), and is referred-to here as geological attenuation. Two sorption phenomena are typically distinguished: adsorption/desorption and absorption. Adsorption refers to the processes in which the chemical accumulates on the surface of a solid particle (i.e. grains, organic matter). Desorption is the reverse of adsorption - chemicals are released from the solid particles back into the porewater. Absorption describes processes in which the contaminant becomes incorporated into the surface layer of a mineral structure.

Geological attenuation determines a chemical's mobility and requires estimation of the sorption or retention behaviour. The Freundlich equation or sorption isotherm is the simplest conceptualisation to quantify the behaviour of retention of reactive solutes with the soil or rock matrix. It has been used widely to describe solute retention by soils and aquifer sediments (Helfferich, 1962; Sposito, 1984; among others). The Freundlich equation is expressed as:

$$C_{ads} = K_d C_{liq}^b \quad (1)$$

where Cads is the concentration of solute retained by the sediment (mg/g of dry sediment), Cliq is the solute concentration in solution (mg/ml), Kd is the solid-liquid partition coefficient (L/kg), and the parameter b is dimensionless and typically has a value of b < 1.

For b = 1, the (nonlinear) Freundlich equation reduces to a linear sorption equation. The Kd parameter then quantifies instantaneous, linear and reversible sorption, and depends on the type of porous medium and on the chemical element (Thibault et al., 1990). It describes the capacity of a solid to remove a dissolved chemical from the liquid phase to the solid phase. If sorption is fast compared to the groundwater flow velocity, the element will reach an equilibrium condition between liquid and solid phase. In other words, sorption is almost instantaneous and thus time-independent. This is called equilibrium sorption.

Inherent in the Kd – type 'linear isotherm' is the assumption that the Kd of the element of interest is independent of its concentration in the aqueous phase. In other words, Kd is a constant accounting for solute uptake processes that are kinetically fast and reversible. Linear sorption generally takes place at a low solute concentration where the sorption capacity of the sorbing solid is large relative to the available chemicals for sorption. Linear isotherms have been widely used as an approximation of the dilute end of the adsorption isotherm (US EPA, 1999b). It has been used widely to describe solute retention by soils and aquifer sediments (Helfferich, 1962; Sposito, 1984; among others).

At low concentrations, sorption of most elements can indeed be described by means of the linear equilibrium sorption approach Figure 61). At higher concentrations, the sorption sites become saturated and non-linear sorption isotherms such as the Freundlich equation with b

≠ 1 may need to be considered. Further increasing the liquid phase concentrations does no longer increase the concentration on the solid phase. At a given point, the solubility limit of the element in the liquid phase is reached, and a precipitate (inorganics) or insoluble phase (organics) is formed. The maximum concentration in the liquid phase beyond which precipitation occurs is called the solubility limit, Cs. The solubility of organic and inorganic compounds may be affected (e.g. decrease) as a result of presence of certain chemicals in hydraulic fracturing fluids.

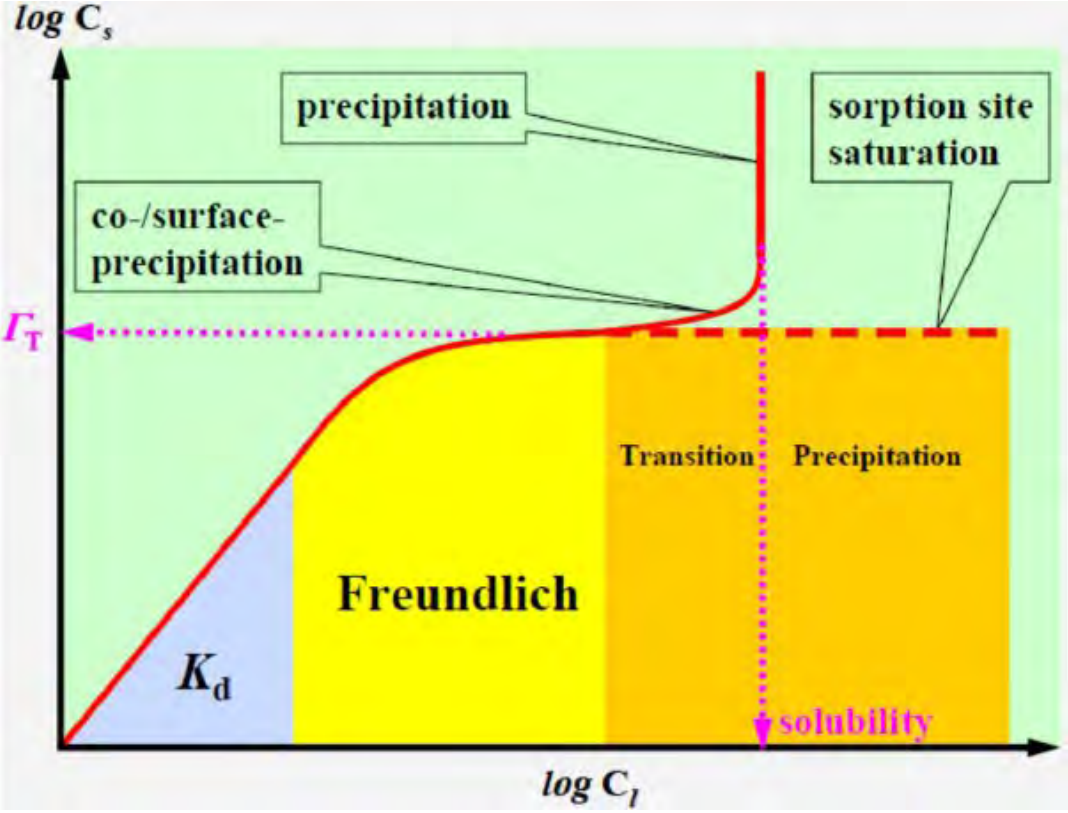

Figure 61 General sorption isotherm representation, showing differences between linear (indicated as "K_d" region) and non-linear sorption (indicated as "Freundlich" region), a transition period left of the precipitation threshold, and solute precipitation (indicated as "precipitation" region). Vertical axis (C_s) and horizontal axis (C_l) are, respectively, the sorbed concentration (on solid phases) and the dissolved concentration (in the liquid phase). Source: Wang et al. (2009).

The K_d is used together with the rock bulk density, ρ_b (g/cm^3), and porosity, η (cm^3/cm^3), to calculate the retardation coefficient R_f (dimensionless)

$$R_f = 1 + \frac{\rho_b K_d}{\eta} \quad (2)$$

The retardation factor R_f defines the transport velocity of a retarded chemical relative to the transport velocity of a water molecule; for instance, a chemical substance with an R_f value of 10 will have a ten times slower transport velocity than a water molecule.

For organic compounds sorption and retardation will be determined from the fraction of organic carbon, f_{OC} (g/g), within geological formations available to adsorb organic compounds and the organic carbon partition coefficient K_{OC} (L/kg):

$$K_d = f_{OC} K_{OC} \quad (3)$$

Where experimental values of K_{OC} are not available, estimation methods based on the octanol-water partition coefficient K_{OW} (L/kg) have been used (e.g., using the US EPA EPI-Suite – US EPA 2012).

Alternative strategies can be developed for inorganic chemicals. Possible interactions will geogenic components will be explored, as the hydrochemical background conditions may affect mobility and persistence.

Given the extreme conditions of temperature, pressure and redox, auxiliary determinations will be explored to establish any potential temperature, pressure and redox effects on chemical persistence and mobility.

Appendix III: Attenuation parameter for drilling chemicals

A total of 24 drilling chemicals provided by Beach Energy Limited (2017) have been analysed here. The chemicals were first screened to assess if they are of low concern for the environment and human health. This was done by considering previous investigations such as the National Chemicals Assessment (DOEE, 2017; NICNAS, 2017a). These investigations (DOEE, 2017; NICNAS 2017b) previously found that 7 chemicals were found of low concern for both environment and human health (Table 10); these chemicals are not further considered in the current quantitative risk assessments.

For the remaining 17 chemicals, the following assumptions were made"

- Inorganic compounds do not degrade but may adsorb; however, for all compounds zero sorption is conservatively assumed;
- Organic compounds may degrade (if sufficiently known, then the half-life is given in Table 10) and may adsorb (if sufficiently known then, logKOC is given in Table 10). When no data are available they are assumed not biodegradable (infinitely large half-life) and not to adsorb.

For the purpose of sensitivity analyses, a probability distribution function (pdf) is assumed for each non-zero parameter. Either a triangular or log-uniform pdf is used.

Log-uniform pdf

The simplest way of representing uncertainty about model parameters is by means of the uniform distribution (Figure 62). Its use is recommended when we can identify a range of possible values, but unable to decide which values within this range are more likely than others. When the uncertainties are large, a log-uniform distribution may used to better describe the data.

The probability density is given as:

$$f = \frac{1}{b - a}$$

where a and b are the observed or calculated minimum and maximum values, respectively. The mean for a uniform or log-uniform distribution is obtained from (a+b)/. Where a log-uniform pdf was selected in

Table 10, the parameters a and b were put equal to the reported minimum and maximum value, respectively.

Triangular pdf

For some model parameters, it is more likely to have values close to the middle of the range of possible values than values near either extreme. In such case, a triangular distribution may be used to represent the data (Figure 62). When the uncertainties are large, a log-triangular distribution may be more appropriate. The pdf is defined by three parameters: minimum (*a*), mode (*b*), and maximum (*c*). We fix the minimum and maximum to the observed minimum and maximum values. This has the advantage that at the time of generation of random samples for use in stochastic calculations, no values larger (or smaller) than the maximum (or minimum) observed value will be generated. In this way unrealistically high (or low) values will be avoided, which would otherwise lead to nonconservative parameter estimates. Values in Table 10 are given as {*a, b, c*}, where *b* is the reported value and a and c are obtained by assuming an overall two-order of magnitude uncertainty, i.e. $a = b/10$ and $c = 10*b$. While such a range is defined arbitrarily here, similar ranges have been observed (see e.g. Mallants et al., 2017).

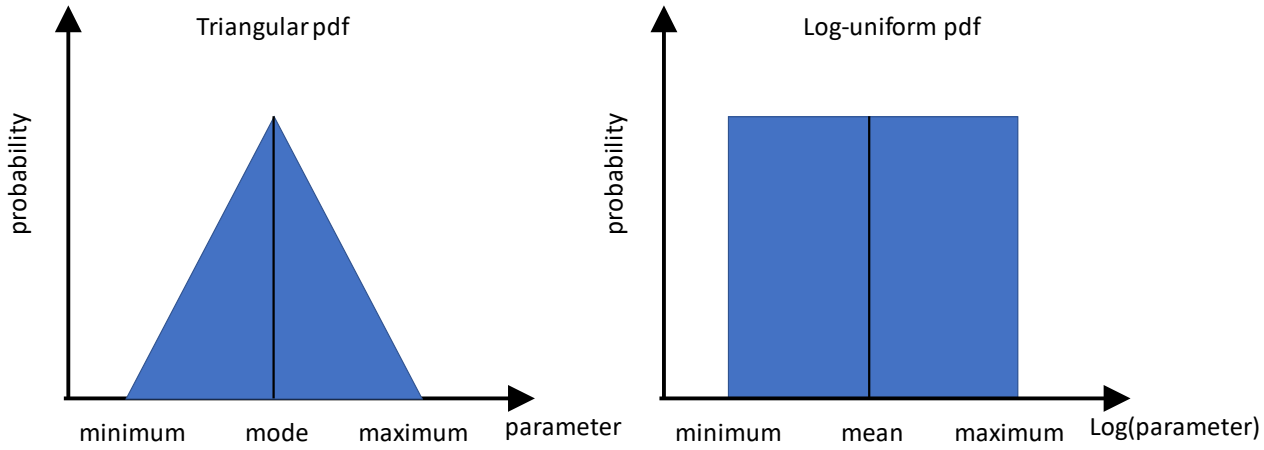

Figure 62 Triangular and log-uniform pdfs used to represent uncertainty around attenuation parameters.

Table 10 Attenuation parameters half-life ($T_{1/2}$) and sorption constant (log K_{OC}) for drilling chemical chemicals. {T} = triangular pdf; {LU} = log-uniform pdf. (A) = DOEE 2017; (B) = Van Ginkel and Gayton, 1996; (C) = https://echa.europa.eu/registration-dossier/-/registered-dossier/15014/5/3/2; (D) = EPI Suite 2012; (E) = based on (B); (G) : based on log K_{OC} = -1.367.

- biodegradable (infinitely large half-life) and do not sorb

#	Compound	CAS	Of low concern	Half-life (days)	Sorption of organics: logKOC	Sorption of inorganics: Kd	Ecotoxicity value ([NCA - report 14] Table 3.3)	Concentration at source (mg/L)	Minimum DF for PEC<=PNEC	Criterion fulfilled?
1	Citric Acid	77-92-9	Y	NA	NA		Chronic Daphnia PNEC=15.3 mg/L	2853	186	
2	Crystalline Silica, Quartz (impurity in cellulose fiber)	14808-60-7	Y	NA	NA					
3	Glyoxal (ethanedial)	107-22-2	Y	NA	NA		Acute fish PNEC = 2.15 mg/L	2853	1327	
4	Potassium chloride	7447-40-7	N	NA	NA	0	PNEC = 3.73 mg/L daphne chronic	68	18	
5	Sodium Carbonate	497-19-8	N	NA	NA	0	Chronic daphnia PNEC = 4.24 mg/L	570	135	
6	Sodium Hydroxide (caustic sodium)	1310-73-2	N	NA	NA	0	Chronic daphnia PNEC = 2.4 mg/L	570	238	
7	Water	7732-18-5	Y	NA	NA	0				
8	Xanthan Gum	11138-66-2	N	[15, 150, 1500]	No data [0]		Acute fish PNEC = 0.42 mg/L	2583	6793	

9	Barite	7727-43-7	Y	NA	NA	0	chronic fish PNEC=100 mg/L	42800	428	
10	Sodium bicarbonate	144-55-8	Y	NA	-3.959		Chronic daphnia PNEC = 5.76	713	124	
11	Bentonite	1302-78-9	Y	NA	NA	0				
12	Carboxymethylsodiumcellulose salt	9004-32-4	N	[28, 280, 2800]	No data [0]					
13	Hexahydro-1,3,5-tris(2-hydroxyethyl)-sym-triazine	4719-04-4	N	[1.217, 12.17, 121.7]	[1, -2.667] => KOC = [10, 0.0021]					
14	Polyetheramine (Diaminopolypropylene glycol)	9046-10-0	N	Assume not biodegradable	No data	0				
15	Ammonium hydrogensulfite	10192-30-0	N	Assume not biodegradable	No data	0				
16	Calciumcarbonate	471-34-1	N	NA	No data	0				
17	Cellulose	9004-34-6	N	(28, 280, 2800]	No data [0]					
18	Copolymer of acrylamide/sodium acrylate	25085-02-3	N	Assume not biodegradable	Strong sorption to organic matter [0]					
19	polyoxypropylene diamine, acetic acid salt	NA	N	Assume not	no conclusive results [0]					

				biodegradable						
20	Polypropylene	9003-07-0	N	[169, 1690, 16900]	no data					
21	Antimony trioxide	1309-64-4	N	NA	NA	0				
22	Cellophane	9005-81-6	N	Assume not biodegradable	no data [0]					
23	2-amino ethanol	141-43-5	N	[3, 30, 300]	-1.367 => KOC = 0.043 sample from [0.0043, 0.043, 0.43]		PNEC = 0.09 mg/L chronic Daphnia	?		
24	Sulfur dioxide	7446-09-5	N	[9, 90, 900]	-1.699 => KOC = 0.02 sample from [0.002, 0.002, 0.2]	0				

References

AE (2012). Stygofauna Assessment. Prepared by 4T Consultants for URS Australia Pty Ltd on behalf of Arrow Energy Pty Ltd (AE), Brisbane, Queensland.

Aller, L., Lehr, J.H., Petty, R., Bennett, T. (1987). DRASTIC: a standardized system to evaluate groundwater pollution potential using hydrogeologic settings. National Water Well Association, Worthington

Beach Energy Limited (2017). Haselgrove 3 disclosure report. RPT-49832.

Beach Energy Limited, 2019), Environmental Impact Report, Drilling, Completion and Well Production Testing in the Otway Basin, South Australia. https://sarigbasis.pir.sa.gov.au/WebtopEw/ws/samref/sarig1/image/DDD/PGER000082019.

Benson, C.H. (2001). Waste containment: strategies and performance. *Aust. Geomech. J.* 36 (4), 1–24 (December 2001).

BOM (2019). Gridded long term mean annual rainfall for Australia. Commonwealth of Australia (Bureau of Meteorology) 2019. http://www.bom.gov.au/jsp/ncc/climate_averages/rainfall/index.jsp Accessed 10/07/2019.

Bonaparte, R., Daniel, D., Koerner, R.M. (2002). Assessment and recommendations for improving the performance of waste containment systems. In: EPA Report EPA/600/R-02/099. U.S. Environmental Protection Agency (US EPA), Washington DC, US.

Boronina, A., Renard, P., Balderer, W., and Stichler W (2005). Application of tritium in precipitation and in groundwater of the Kouris catchment (Cyprus) for description of the regional groundwater flow. *Applied Geochemistry* 20: 1292–1308. doi:10.1016/j.apgeochem.2005.03.007.

Brantley, S.L., Yoxtheimer, D., Arjmand, S., Grieve, P., Vidic, R., Pollak, J., Llewellyn, G.T., Abad, J., Simon, C. (2014). Water resource impacts during unconventional shale gas development: the Pennsylvania experience. *Int. J. Coal Geol.* 126: 140–156.

CAPAD (2016). Collaborative Australian Protected Areas Database (CAPAD) 2016, Commonwealth of Australia. http://www.environment.gov.au/fed/catalog/search/resource/downloadData.page?uuid=%7B4448CACD-9DA8-43D1-A48F-48149FD5FCFD%7D Accessed 18/06/2019.

Carey, J.W., Svec, R., Grigg, R., Zhang, J., Crow, W. (2010). Experimental investigation of wellbore integrity and CO2-brine flow along the casing-cement microannulus. *Int. J.Greenh. Gas Control* 4: 272–282.

Carsel, R.F., and Parrish, R. S. (1988). Developing joint probability distributions of soil water retention characteristics, *Water Resources Research 24*: 755-769.

Chapuis, R. P. (2002). The 2000 RM Hardy Lecture: Full-scale hydraulic performance of soil bentonite and compacted clay liners. *Canadian Geotechnical Journal*, *39*(2), 417-439.Council of Canadian Academies (2014). Environmental Impacts of Shale Gas Extraction in Canada.

Department of Mines and Petroleum (2013). Resources Type Fact sheet.

DERM (2010). Guideline: Approval of Coal Seam Gas Water for Beneficial Use. Queensland Department of Environment and Resource Management (DERM).

DITR (2007). Tailings Management. Handbook prepared by the Department of Industry, Tourism and Resources (DITR) as part of the Leading Practice Sustainable Development Program for the Mining Industry, Canberra, pp. 79.

Doble, R.C., Pickett, T., Crosbie, R.S., Morgan, L.K., Turnadge, C., Davies, P. J. (2017). Emulation of recharge and evapotranspiration processes in shallow groundwater systems. *Journal of Hydrology 555:* 894–908.

Rebecca Doble, Trevor Pickett, Sreekanth Janardhanan, Russell Crosbie, Dennis Gonzalez, Xiayang Yu (2020), Potential impacts on groundwater resources from conventional gas in the South East of SA, CSIRO Land and Water

DOEE (2008). Register of the National Estate (RNE) - Spatial Database (RNESDB). Commonwealth of Australia, Heritage Division of the Australian Government Department of the Environment and Energy, 2008. Accessed 17/06/2019.

DOEE (2017). Environmental risks associated with surface handling of chemicals used in coal seam gas extraction in Australia, Project report prepared by the Chemicals and Biotechnology Assessments Section (CBAS), in the Chemicals and Waste Branch of the Department of the Environment and Energy as part of the National Assessment of Chemicals Associated with Coal Seam Gas Extraction in Australia, Commonwealth of Australia, Canberra.

DOEE (2018). Species of National Environmental Significance Database (Public Grids). Commonwealth of Australia, Department of the Environment and Energy, 2018. http://www.environment.gov.au/fed/catalog/search/resource/downloadData.page?uuid=%7B337B05B6-254E-47AD-A701-C55D9A0435EA%7D Accessed 17/06/2019.

DPTI (2016). Statewide Road Network including sealed and unsealed roads. South Australian Department of Planning, Transport and Infrastructure. http://www.dptiapps.com.au/dataportal/Roads_shp.zip Accessed 24/06/2019.

Folkes, D.J. (1982). Control of contaminant migration by the use of liners. *Can. Geotech. J.* 19 (3): 320–344.

Gelhar, L.W., Welty, C., Rehfeldt, K.R. (1992). A critical overview of data on field-scale dispersion in aquifers. *Water Resources Research* 28: 1955–1974.

Goodwin, K.J., Crook, R.J. (1992). Cement sheath stress failure. *SPE Drill. Eng*. 7 (4): 291–296.

Gusyev, M.A., Abrams, D., Toews, M.W., Morgenstern, U., and Stewart, M.K. (2014). A comparison of particle-tracking and solute transport methods for simulation of tritium concentrations and groundwater transit times in river water. *Hydrology and Earth System Sciences* 18: 3109–3119.

Harbaugh, A.W. (2005). MODFLOW-2005: the U.S. Geological Survey modular ground-water model - the ground-water flow process. Book 6: Modeling techniques, Section A. Groundwater.

Harrington, N. and Lamontagne, S. [eds.] (2013). Framework for a regional water balance model for the South Australian Limestone Coast region, Goyder Institute for Water Research Technical Report Series No. 13/14.

Helfferich, F. (1962). Ion exchange. McGraw-Hill Book Co., New York.

Jacobs (2016). Hydrogeological risk assessment – unconventional gas well – South East, Department of State Development

Kissinger, A., Helmig, R., Ebigbo, A., Class, H., Lange, T., Sauter, M., Heitfeld, M., Klunker, J., Jahnke, W. (2013). Hydraulic fracturing in unconventional gas reservoirs: Risks in the geological system, part 2. *Environ. Earth Sci.* 70 (8): 3855–3873.

Kutchko, B.G., Strazisar, B.R., Dzombak, D.A., Lowry, G.V., Thaulow, N. (2007). Degradation of well cement by CO2 under geologic sequestration conditions. *Environ. Sci. Technol*. 41 (13): 4787–4792.

Lucas (2008). Review of environmental factors for exploration boreholes and production evaluation testing. Document #G-STP-L-AP-A-080818-REF. Lucas Energy Pty Ltd.

McGuire, K.J. and McDonnell, J.J. (2006). A review and evaluation of catchment transit time modelling. *Journal of Hydrology* 330: 543–563. doi:10.1016/j.jhydrol.2006.04.020.

Mallants, D., Bekele, E., Schmid, W. and Miotlinski, K. (2017a). Human and environmental exposure conceptualisation: Soil to shallow groundwater pathways, Project report prepared by the Commonwealth Scientific and Industrial Research Organisation (CSIRO) as part of the National Assessment of Chemicals Associated with Coal Seam Gas Extraction in Australia, Commonwealth of Australia, Canberra.

Mallants, D., Apte, S., Kear, J., Turnadge, C., Janardhanan, S., Gonzalez, D., Williams, M., Chen, Z., Kookana, R., Taylor, A., Raiber, M., Adams, M., Bruce, J., Prommer, H. (2017b). Deeper groundwater hazard screening research, prepared by the Commonwealth Scientific and Industrial Research Organisation (CSIRO), Canberra.

Mallants, D., Bekele, E., Schmid, W., Miotlinski, K., Taylor, A., Gerke, K. (2017c). Human and environmental exposure assessment: Soil to shallow groundwater pathways – A study of predicted environmental concentrations, Project report prepared by the Commonwealth Scientific and Industrial Research Organisation (CSIRO) as part of the National Assessment of Chemicals Associated with Coal Seam Gas Extraction in Australia. Commonwealth of Australia, Canberra.

Mallants, D., Šimůnek, J., van Genuchten, M.Th., Jacques, D. (2017d). Using hydrus and its modules to simulate the fate and transport of coal seam gas chemicals in variably saturated soils. *Water* 9 (6): 385–418. http://dx.doi.org/10.3390/w9060385.

Mallants, D., Jeffrey, R., Zhang, X., Wu, B., Kear, J., Chen, Z., Wu, B., Bekele, E., Raiber, M., Apte, S. and Gray, B. (2018). Review of plausible chemical migration pathways in Australian coal seam gas basins. *Int. J. Coal Geol*. 195: 280 -303.

Malczewski, J. (1999). GIS and Multicriteria Decision Analysis; John Wiley & Sons: New York, NY, USA, 1999.

Moore, T.A. (2012). Coalbed methane: a review. *International Journal of Coal Geology* 101: 36–81.

Morgan, L.K., Harrington, N., Werner, A.D., Hutson, J., Woods, J. (2015). South East Regional Water Balance Project – Phase 2, Development of a Regional Groundwater Flow Model. Goyder Institute for Water Research Technical Report Series No. 15/38, pp. 138.

Mount, R.E., Mitchell, P.J., Macfarlane, C., Marston, F.M., McNamara, J.M., Raisbeck-Brown, N., O'Grady, A.P., Moran, B.T., Wang, J. (2015). Compiling water-dependant assets. A sub-methodology from the Bioregional Assessment Technical Programme. Department of the Environment, Bureau of Meteorology, CSIRO and Geoscience Australia, Australia.

Mustafa, S., & Lawson, J. S. (2011). *South Australia-Victoria border zone groundwater investigation: Results of the pumping test program*. Science, Monitoring and Information Division, Department for Water.

NCGRT(2016). Quantitative assessment of the likelihood of adverse water resource impacts from gas production from unconventional reservoirs, National Centre for Groundwater Research and Training.

NICNAS (2017a). Identification of chemicals associated with coal seam gas extraction in Australia, Project report prepared by the National Industrial Chemicals Notification and Assessment Scheme (NICNAS) as part of the National Assessment of Chemicals Associated with Coal Seam Gas Extraction in Australia, Commonwealth of Australia, Canberra.

NICNAS (2017b). Chemicals of low concern for human health based on an initial assessment of hazards, Project report prepared by the National Industrial Chemicals Notification and Assessment Scheme (NICNAS) as part of the National Assessment of Chemicals Associated with Coal Seam Gas Extraction in Australia, Commonwealth of Australia, Canberra.

Origin 2008, JPMorgan CSG Corporate Access Day. CSG comes of age. 28 October 2008.

Pollock, D. (2012). User Guide for MODPATH Version 6—A Particle-Tracking Model for MODFLOW. Chapter 41 of Section A, Groundwater Book 6, Modeling Techniques and Methods 6–A41.

Reagan, M.T., Moridis, G.J., Keen, N.D., Johnson, J.N. (2015). Numerical simulation of the environmental impact of hydraulic fracturing of tight/shale gas reservoirs on near surface groundwater: Background, base cases, shallow reservoirs, short-term gas, and water transport. *Water Resour. Res.* 51: 2543–2573.

Renpu, W. (2011). Advanced well completion engineering, Third ed. Gulf Professional Publishing, Houston, TX.

Rowe, R.K. (2012). Short- and long-term leakage through composite liners, The 7th Arthur Casagrande Lecture. *Can. Geotech. J.* 49: 141–169.

RPS (2011). Onshore co-produced water: extent and management. In: LTD, R. A. P. (ed.) Waterlines Report Series No.54, Canberra: National Water Commission.

SA EPA (2020) Bunding and spill management, South Australia Environmental Protection Agency, https://www.epa.sa.gov.au/files/47717_guide_bunding.pdf.

Sanford, W. (2010). Calibration of models using groundwater age. *Hydrogeology Journal* 19: 13–16. doi:10.1007/s10040-010-0637-6.

Schinteie, R., Tran-Dinh, N., Vergara, T. J., & Midgley, D. J. (2019). An estimation of chemical compound concentrations used in onshore gas production, a review of their degradation, and associated policy frameworks in South Australia.

Scow, K.M. and Johnson, C.R. (1997). Effect of sorption on biodegradation of soil pollutants. *Advances in Agronomy* 58: 56.

Šimůnek, J., van Genuchten M.T., Šejna, M. (2016). Recent developments and applications of the HYDRUS computer software packages. *Vadose Zone J.* 15:25.

Šimůnek, J., van Genuchten M.T., Šejna, M., N. Toride, and F.J. Leij (2009). Studio of Analytical Models for Solving the Convective-Dispersive Equation (STANMOD). www.hydrus3d.com

Skaggs, T.H. and Leij, F.J (2002). Solute Transport: Theoretical Background. Materials Science , DOI:10.2136/sssabookser5.4.c56

Sposito, G. (1984). The surface chemistry of soils: Oxford University Press, New York, 234 pp.

Taylor, A., Pribilovic, D., Carr, J., Bindinganaville, B. (2007). Petroleum Production Licence No. 62, 168 & 202 (Katnook & Ladbroke Grove Complex) Development Plan And 2006 Operational Review - Otway Basin, South Australia, http://energymining.sa.gov.au/__data/assets/pdf_file/0012/250041/annual_development_plan_and_operational_review_2007_www.pdf

The Royal Society and Royal Academy of Engineering (2012). Shale gas extraction in the UK: a review of hydraulic fracturing.

Thibault, D.H., Sheppard, M.I. and Smith, P.A. (1990). A critical compilation and review of default soil solid/liquid partition coefficients, Kd, for use in environmental assessments. Atomic Energy of Canada Limited. Whiteshell Nuclear Research Establishment Pinawa, Manitoba, Canada.

Todd, D. K., & Mays, L. W. (1980). Groundwater hydrology. John Willey Sons. *Inc., New York*, *535*.

Tran-Dinh, Vergara, T.J., Schinteie, R., Mariani, C. and Midgley, D.J. (2019). Microbial degradation of chemical compounds used in onshore gas production in the SE of South Australia, CSIRO, Australia.

US EPA (1994). Handbook of Ground Water and Wellhead Protection, US Environmental Protection Agency, Report EPA/625/R-94001, 288 p.

US EPA (1998a). Technical Protocol for Evaluating Natural Attenuation of Chlorinated Solvents in Ground Water. EPA/600/R-98/128 September 1998.

US EPA (1998b). Reregistration Eligibility Decision (RED) Methylisothiazolinone. United States Environmental Protection Agency. Prevention, Pesticides and Toxic Substances (7508C), EPA738-R-98-012 October 1998.

US EPA (1999a). Understanding variation in partition coefficient, Kd values. Volume II: Review of geochemistry and available Kd Values for cadmium, caesium, chromium, lead, plutonium, radon, strontium, thorium, tritium (3H), and uranium. US Environmental Protection Agency report EPA 402-R-99-004B, 341 pages.

US EPA (1999b). Understanding variation in partition coefficient, Kd, values. Volume 1: The Kd model, methods of measurement, and application of chemical reaction codes. *Washington, DC: US Environmental Protection Agency*.

US EPA (2012). The Estimation Programs Interface (EPI) Suite. ECOSAR.

Van Genuchten, M. T. (1980). A closed-form equation for predicting the hydraulic conductivity of unsaturated soils 1. *Soil science society of America journal*, *44*(5), 892-898.

Van Ginkel, C.G. and Gayton, S. (1996). The biodegradability and nontoxicity of carboxymethyl cellulose (ds 0.7) and intermediates. *Environmental Toxicology and Chemistry* 15: 270–274.

Viscarra Rossel, R., Chen, C., Grundy, M., Searle, R., Clifford, D., Odgers, N., Holmes, K., Griffin, T., Liddicoat, C., Kidd, D. (2014): Soil and Landscape Grid National Soil Attribute Maps - Sand (3" resolution) - Release 1. v5. CSIRO. Data Collection. https://doi.org/10.4225/08/546F29646877E

Wang, L., Martens, E., Jacques, D., De Canniere, P., Berry, J.A., and Mallants, D. (2009). Review of sorption values for the cementitious near field of a near-surface radioactive waste disposal facility, NIROND-TR 2008-23 E.

White, J.T. (2018). A model-independent iterative ensemble smoother for efficient history-matching and uncertainty quantification in very high dimensions. *Environmental Modelling & Software 109*: 191–201.

Wu, B., Doble, R., Turnadge, C., Mallants, D., (2016). Well Failure Mechanisms and Conceptualisation of Reservoir-Aquifer Failure Pathways. Society of Petroleum Engineers Asia Pacific Oil & Gas Conference and Exhibition. SPE-182460182460-MS. OnePetro.org. http://dx.doi.org/10.2118/182460-MS.

Wu, B., Doble, R., Turnadge, C., Mallants, D. (2018). Bore and well induced inter-aquifer connectivity: a review of literature on failure mechanisms and conceptualisation of hydrocarbon reservoir-aquifer failure pathways, prepared by the Commonwealth Scientific and Industrial Research Organisation (CSIRO), Canberra.

CONTACT US

t 1300 363 400

+61 3 9545 2176

e csiroenquiries@csiro.au

w www.csiro.au

FOR FURTHER INFORMATION

CSIRO Land and Water

AT CSIRO, WE DO THE
EXTRAORDINARY EVERY DAY

We innovate for tomorrow and help improve today – for our customers, all Australians and the world.

Our innovations contribute billions of dollars to the Australian economy every year. As the largest patent holder in the nation, our vast wealth of intellectual property has led to more than 150 spin-off companies.

With more than 5,000 experts and a burning desire to get things done, we are Australia's catalyst for innovation.

CSIRO. WE IMAGINE. WE COLLABORATE.
WE INNOVATE.